A THESIS

FOR THE DEGREE OF DOCTOR OF PHILOSOPHY

Fabrication and Analysis of Stretchable Films on Rough Ultra-low Modulus Polydimethylsiloxane Using Non-vacuum Techniques

Syed Murtuza Mehdi

Department of Mechatronics Engineering

GRADUATE SCHOOL

JEJU NATIONAL UNIVERSITY

2015. 02

Fabrication and Analysis of Stretchable Films on Rough Ultra-low Modulus Polydimethylsiloxane Using Non-vacuum Techniques

Syed Murtuza Mehdi

(Supervised by Doctor Professor Kyung Hyun Choi)

A thesis submitted in partial fulfillment of the requirement for the degree of Doctor of Philosophy

2015.02

The thesis has been examined and approved by.

Thesis Director, Kyung Hyun Choi, Professor, Department of Mechatronics Engineering

---

Kyung Ho Cho, Professor, Department of Mechatronics Engineering

---

Chang Nam Kang, Professor, Department of Mechanical Engineering

---

Ki Rin Kwon, Professor, Department of Mechanical Engineering

Dr. Jae Bum Kim, Korea Institute of Industrial Technology

Date

Department of Mechatronics Engineering
GRADUATE SCHOOL
JEJU NATIONAL UNIVERSITY
REPUBLIC OF KOREA

Read! In the name of your Lord (Cherisher and Sustainer)”

(Quran 96:1)

Acknowledgments

Deepest thanks and praise to the Almighty Allah, the supreme authority, for He has blessed me with the dignified cause of acquiring and delivering knowledge and made me capable of achieving the goals. I am greatly thankful to the Holy Prophet (peace be upon him) and all the purified members of his Holy family for their continuous guidance and blessings.

I extend my gratitude to Khurshid Fatima, my mother and Iftikhar Mehdi, my father for their eternal love, prayers and sacrifice. Without their presence I would have achieved nothing. It's truly a blessing having them in my life. No matter how kind I can be towards you people, it can never be enough. God bless you both for being such loving and caring parents.

I am extremely thankful to my PhD supervisor Prof. Dr. Kyung Hyun Choi for providing the opportunity of pursuing my research studies at the Advance Micromechatronics Lab. I really appreciate his unwavering trust, support and motivation over all these years. I would also like to convey my kindest regards to all the committee members for managing their precious time to read this thesis and for providing their suggestions. I would also like to thank Prof. Dr. Sin Kim for his sincere cooperation.

I will always remember Dr. Ahmar Rashid, Dr. Anil Khambampati, Dr. Wang Rongli, Dr. Ko Min Seok, Dr. Boan Lee Dr. Nauman Malik, Dr. Ahsan Rehman, Dr. Khalid Rehman, Arshad Khan and Saleem Khan for being like a family to me in Jeju. I really acknowledge Dr. Nauman Malik for his special cooperation and for being a remarkable friend. I express my thanks to colleagues like Dr. Adnan Ali, Dr. Navaneethan Duraisamy, Dr. Muhammad Naeem, Dr. Maria Mustafa, Dr. Muhammad Zubair and Dr. Konstantin Lyakhov for their sincere suggestions regarding my research. I would like to express my thanks to Kamran Ali for managing his busy schedule and providing timely cooperation during the course of my research work. I am also thankful to rest of my lab mates which includes, Junaid Ali, Shahid Aziz, Ghayas Uddin Siddiqui, Memoon Sajid, Hyun woo, Hyeon Beom, Bong Su, Soo Wan, Young-Jin, Gobum and Lim Ji Eun for their friendly cooperation and assistance. I really enjoyed the pleasure of their company during my stay at the Jeju National University and I wish happiness and success to all my friends and colleagues.

Thank you, Dr. Anis Fatima for being such a nice and caring sister. Even though, you were miles away, but always there in my support. Dear Mustafa thanks a lot for managing all the responsibilities back at home while I was away. I wish you blessings, success and happiness forever. I would also like to take the opportunity to express thanks to my aunts Shereen Rizvi, Kaneez Fatima, Yasmeen Jafry, Shaheen Fatima, my Uncles Syed Ali Haider Jafry, Syed Ali Akbar Jafry, Qamar Abbas and Zafar Abbas for their trust, support and prayers.

As for you Weera, I can never stop thanking you for your exceptional love and prayers. Your wonderful companionship is truly a source of endless happiness in my life. Thanks for being with me as a loving and caring companion. Your presence in my life is my real treasure.

Syed Murtuza Mehdi, November 2014

Contents

List of Figures

List of Tables

ABSTRACT

Fascinating ideas like electronic skin, stretchable and flexible energy harvesting devices, biomedical sensors, stretchable and foldable displays, artificial muscles and many more have made stretchable electronics an interesting and challenging engineering domain which also amalgamates different sciences like electronics, materials, fabrication, surface sciences, numerical computations and mechanics.

In stretchable electronics the presence of a thin film on a compliant substrate as an electrode or any other functional layer is inevitable and therefore, plays a significant role in the device functionality. Conventional fabrication technique such as chemical vapor deposition (CVD), physical vapor deposition (PVD) and photolithography that has long been used for the realization of such intricate devices are costly and requires complex accessories and procedures that usually operates under high vacuum and temperatures. Unlike these conventional techniques the advent of printed electronics has revolutionized the industry. Printed electronics is actually a collection of simple, cost effective, non-vacuum based fabrication techniques. Printed electronics has an added advantage of being acquiescent towards the material usage. For instance, use of solution based direct writable inks that can even consist of nano or micro structures of different materials like micro and nanoparticles, nano wires, flakes and whiskers are common in printed electronics, making it a promising alternative over existing technologies.

Stretchable behavior of thin films of both metallic and nonmetallic materials on compliant substrates, for instance polydimethylsiloxane (PDMS), polyimide (PI) and polyethylene terephthalate (PET) have been extensively studied in the past. However, these films were mostly fabricated using vacuum based techniques that require intermediate metallic adhesive layers. On the other hand, a majority of the research work regarding thin films on PDMS has utilized high or the conventional value for the Young's modulus which is approximately 1 MPa and having a thickness that is 1 or 2 mm. It is to be noted that even though the stiffer substrates can better delocalize the strains within the films, the usage of ultra-low modulus PDMS (120-140 kPa) and sub millimeter thicknesses can be of vital importance in applications like bio medical sensing, artificial skin and epidermal electronics.

Therefore, the main focus of this thesis is to investigate the stretchable and flexible resistive behaviors of silver (Ag) nanoparticles and poly(3,4-ethylenedioxythiophene) polystyrene sulfonate (PEDOT:PSS) based films on rough ultra-low modulus PDMS substrates. However, in certain cases films on the conventional modulus ($\approx$1MPa) PDMS has also been studied. All the films studied in this thesis were fabricated by simple, cost effective and non-vacuum based techniques like spin coating, blade coating, rod coating and electrospray deposition (ESD). The intentionally generated roughness patterns were introduced for the purpose of enhancing the adhesion between the film and the hydrophobic PDMS surface. New models that relate the change in resistance as a function of applied strain on these rough PDMS substrates have been presented. The research results forms an important database on the stretchable behavior of Ag and PEDOT:PSS films on rough PDMS substrates fabricated by simple, cost effective and non-vacuum based techniques. Different laminates studied in this research work have shown intriguing results that can be used in applications like stretchable and flexible electronics and energy harvesting devices, microfluidics and microelectromechanical systems.

1. Introduction

Thin films are widely used in various engineered devices for instance, thin film solar cells, artificial muscles, thin film thermoelectric generators, thin film fuel cells, heating elements, thin film optical devices and many other like light emitting diodes, thin film transistors, transparent electrodes, temperature sensors, thin film antenna and piezoresistive strain sensors. It is to be noted that the word “thin” however, is a relative term and depends on the device characteristic dimension. For example in a typical thin film on a compliant substrate, the film thickness remains of order of few hundreds of nanometer to several tens of micrometers as compared to the thickness of the substrate.

1.1 Thin films in stretchable electronics

An interesting application of thin films has appeared in form of stretchable and flexible electronic devices. Fascinating ideas like stretchable batteries, stretchable and flexible energy harvesting devices, biomedical sensors, stretchable capacitors and many more has made stretchable electronics an interesting and challenging engineering domain. Stretchable electronics is a versatile field that amalgamates different engineering aspects like design optimizations, materials, fabrication, simulations and finally methods of characterization (Bossuyt et al. 2011; Bossuyt et al. 2013; Gonzalez et al. 2008). It also combines different sciences like mechanics, electronics, surface sciences, and studies related to micro and nano structured materials (Renault et al. 2003; Rogers et al. 2010; Lu et al. 2007; Wei & Zhao 2012; Davis & Crosby 2011; Hay et al. 2008; Bayati et al. 2014; Aricò et al. 2005; Schoonman 2000). In stretchable and flexible electronics entire electronic circuits or devices are deposited onto a stretchable substrate or completely embedded inside it. In stretchable electronics a thin film (metallic or nonmetallic) can act as an electrode or other functional layer under the action of a particular mechanical load which can be of bending nature, repeated nature or tensile nature. Therefore, tremendous research efforts have been devoted in this field for instance (Lipomi et al. 2011) fabricated stretchable organic solar cell using PEDOT:PSS thin films, (J.-H. Lee et al. 2014) using graphene nanosheets and carbon nanotubes fabricated stretchable nanogenerator, (Xu et al. 2013) fabricated stretchable

batteries using gel electrolyte and other materials like aluminum, copper, polyimide and silicone, (Niu et al. 2013) fabricated stretchable supercapacitors using thin film based on carbon nanotubes, (J. Lee et al. 2014) fabricated Ag nanoparticles based strain gage, (White et al. 2013) fabricated stretchable light emitting diode and (Kim et al. 2007) fabricated electro active paper actuator using cellulose and thin gold films. It is worth mentioning that the performance of a thin film considerably relies on factors like fabrication technique, choice of materials, relative film and substrate properties and the adhesion between the film and the underlying substrate (Hamasha et al. 2011; Li & Suo 2006; Chung et al. 2011). Figure 1-1 shows few stretchable electronic devices

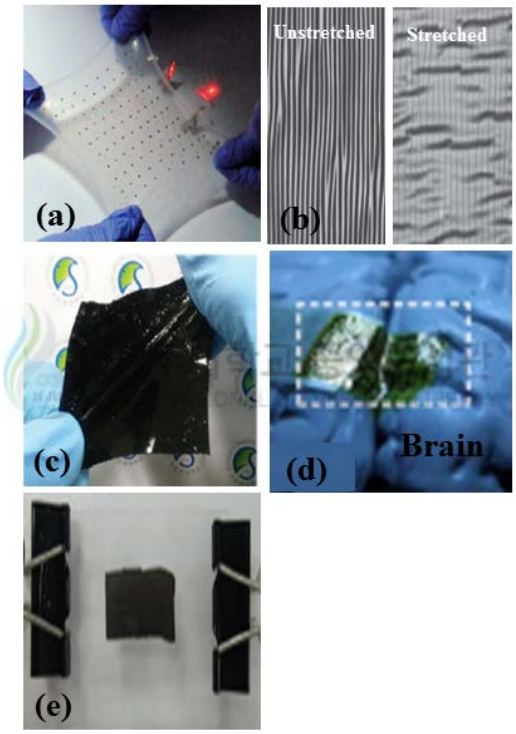

Figure 1-1 Photographs of stretchable devices. (a) Stretchable batteries, (b) stretchable polymer solar cell, (c) stretchable Nanogenerator, (d) biomedical sensor and (e) stretchable supercapacitor.

Realization of devices like bionic skin, epidermal electronics, artificial muscles, strain gages, smart textiles, flexible and foldable displays and, stretchable light emitting diodes are not possible with the conventional rigid electronics. These features unavoidably demand the use of thin film technology combined with the stretchable and flexible substrates that can offer the desired flexibility during extreme working conditions. Figure 1-2 shows few such devices.

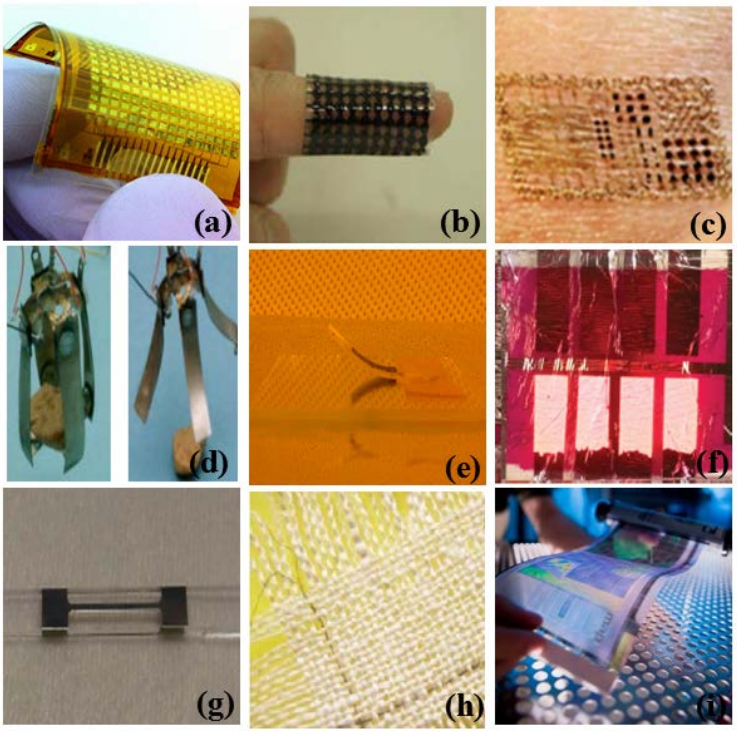

Figure 1-2 Photographs of stretchable devices. (a) and (b) Electronic skin, (c) epidermal device, (d) and (e) electro active and thermal actuators, (f) Stretchable light emitting diodes, (g) strain gage, (h) smart textile and (i) flexible/foldable display device.

It is to be noted that in almost all the stretchable devices mentioned above thin films of different materials forms an integral and most important part of the device.

1.2 Thin film fabrication

Conventionally, thin films can be fabricated by using technologies like chemical vapor deposition (CVD) (Choy 2003) or physical vapor deposition (PVD) (Helmersson et al. 2006). However, these technologies are expensive, slow and require high vacuum and high temperatures for their processing. Also with these technologies the deposition on complex surfaces is hard to achieve. Beside this, the high temperatures during processing can cause adverse effects on the deposited films such as cracking due to difference in coefficient of thermal expansion between the film and the substrate material. These techniques also pose restrictions on choice of materials that can be used as target and substrate. Since, high energy demands are also involved these systems also require appropriate cooling mechanisms.

Unlike vacuum based technologies, printed electronics is simple, cost effective and can be processed at atmospheric conditions (non-vacuum) (Kim et al. 2013; S. M. Mehdi et al. 2014). Printed electronics groups together simple techniques like spin coating (Hummelgård et al. 2013), roll to plate printing (Jung et al. 2013), gravure printing (Cho et al. 2011), bar or rod coating (Murphy et al. 2011), blade coating (M. Mehdi et al. 2014), and inkjet printing and deposition techniques (Duraisamy et al. 2013). One of the major advantages of printed electronics is its ability to utilize solution based inks that can also contain micro or nanoparticles, flakes, wires and whiskers of different materials (metals and nonmetals). This particular feature of printed electronics has opened a door way for ongoing research in the synthesis of new materials that are based on micro and nanostructured entities of metals and nonmetals to be exploited in future electronics. Due to the use of micro and nanostructured materials the process temperatures can also be reduced as compared to the vacuum based technology which is a vital advantage and therefore, sintering temperature as low as 60 ^{o}C has also been reported (Tokuno et al. 2012).

1.3 Mechanical testing of thin films

With the advent of microelectronics and innovative thin film devices new methods have been devised for the testing of thin films. The wafer curvature method was developed for stress measurement during a temperature change, when difference between the coefficients of thermal expansion exists between the film and the substrate. The radius of curvature of the substrate is used to calculate the stress in the film (Flinn 1989).

Bulge test is also a specialized method to study the elastic and plastic behavior of thin free standing films. Air pressure is supplied from beneath and the corresponding bulge height is used to study the behaviors (Xiang et al. 2005). Microbeam bending (Florando et al. 1999) is used to investigate the elasticity, plasticity and fracture in thin films. In this method a point load can also be repeatedly applied to study the fatigue behavior as well. Nano indentation (Oliver & Pharr 2004) can be used to determine the mechanical properties of the thin film however, inhomogeneous stresses and strains are likely to appear in this method.

In comparison to above mentioned techniques, there exist two more methods to estimate the ductility of thin films. One is to observe the in-/ex-situ the microcracks in the films with the applied strain, e.g., cracks spacing method (Niu et al. 2007) or statistical microcracks density method (Cairns et al. 2000). The cracks spacing method relates the average distance of adjacent cracks to the value of applied strain. The other and the more widely used test is to make real time observations of the change in the electrical resistance of the film as a function of applied strain (Li et al. 2004). The strain can be uniaxial or biaxial. The basis of this test method is that the damage or failure in microstructure could be most sensitively revealed by a macroscopic property such as the electrical resistance. The resistance-strain curve for a particular thin film is of vital importance, since all other characteristics such as crack initiation, crack propagation, crack length, crack width and their spacing are all functions of externally applied strain. The schematic of a typical micro tensile test setup is shown in Figure 1-3.

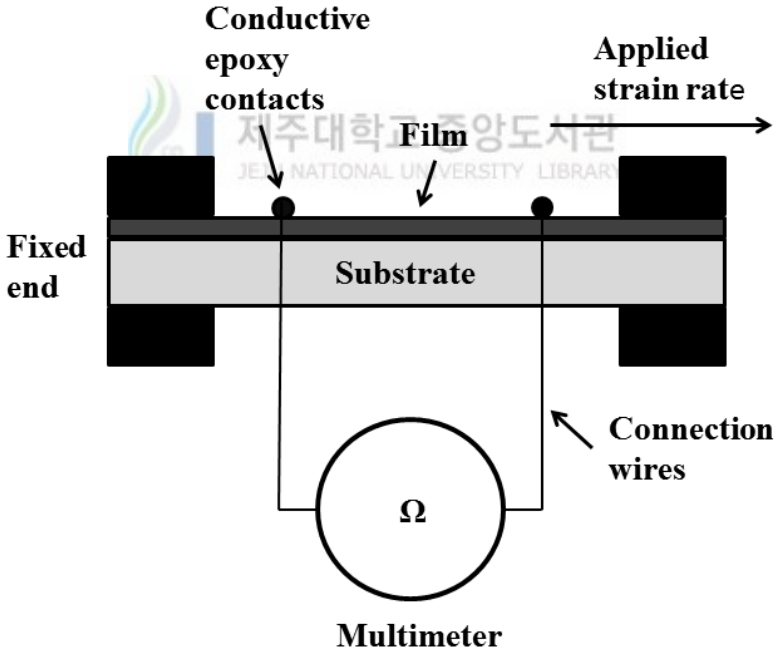

Figure 1-3 Schematic of a typical micro tensile test setup for thin films

1.4 Materials for stretchable films

With the advent of nanostructured materials and solution based inks a wide choice of materials is now available for the realization of stretchable electronics. In fact, in order to achieve desired level of mechanical flexibility in the device an engineered design and choice of material is of vital importance. There exist two broad alternatives to achieve functionally stretchable films on compliant substrates, firstly to use intelligent and innovative designs for electrical interconnections and secondly to use intrinsically stretchable materials and possibly their combinations as nanostructured materials that can offer high mechanical flexibility. Metals can be much more conductive but their ductility is limited, on the other hand conductive polymers are less conductive but they can be much more ductile than metals. According to the literature survey many materials including metallic nanoparticles (Lee et al. 2011), conductive polymers (Syed Murtuza Mehdi et al. 2014) and carbon based materials like carbon nanotubes (Cai et al. 2012) and graphene (Yan et al. 2012) has been used as thin stretchable films on elastomeric substrates. Also interesting composites of these materials, for instance silver nanowires in poly(3,4-ethylenedioxythiophene) polystyrene sulfonate (more popularly known as PEDOT:PSS) matrix (Noh et al. 2013) and composite of nanostructured materials for instance, metallic nanoparticles with nanowires (Lee et al. 2013) and carbon nanotubes are also possible (Ko & Lin 2013). Figure 1-4 depicts micrographs of substrate bonded nanostructured thin films of different materials.

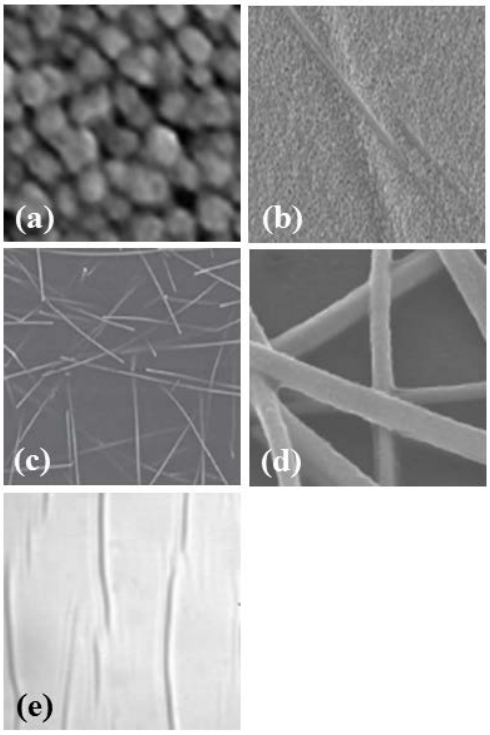

Figure 1-4 Micrographs of thin films of different nanostructured materials. (a) Ag nanoparticles based thin film, (b) Ag nanoparticles and Ag nanowires based thin film, (c) Ag nanowire thin film, (d) Ag nanowire and PEDOT:PSS based thin film and (e) PEDOT:PSS thin film.

In general a thin film on a stretchable substrate can act as a conductor, an insulator or a semiconductor depending on its intended use.

As for the substrate, a variety of materials such as polyimide (PI), polyethylene terephthalate (PET), textiles and paper can be used for the realization of a flexible and stretchable device. The most commonly used material for this purpose is however, polydimethylsiloxane (PDMS) which is both flexible and stretchable. PDMS is inexpensive, biocompatible and chemically nonreactive towards other materials and can also withstand high temperatures up to 230 ^{o}C repeatedly (as noticed in this study). PDMS can also be easily patterned which makes it a useful elastomer for microfabrication.

1.5 Objective of the thesis

The main focus of this thesis is to study and form a comprehensive data base regarding the stretchable and flexible resistive behaviors of Ag nanoparticles based and PEDOT:PSS films

on rough ultra-low modulus (120-140 kPa) PDMS substrates fabricated by cost effective, simple and non-vacuum based techniques. The use of ultra-low modulus PDMS imparts human epidermis like mechanical properties to the substrate and therefore, the results of this study are not only unique but also important for such applications. The film thicknesses and the roughness patterns used in this study remains of order of few micrometers. These micrometer thick films of Ag and PEDOT:PSS on rough ultra-low modulus PDMS shows substantial stretchability and flexibility. It is anticipated that micrometer thick films of metals and nonmetals on rough ultra-low modulus PDMS can be potentially useful in applications like heating elements for microfluidics, microelectromechanical systems (MEMS), thermoelectric generators, thin film fuel cells, electroactive polymer actuators, piezoresistive and capacitive strain gages and pressure sensors, high power applications, biomedical sensors and implants and numerous other stretchable and flexible electronics applications. The research results signifies that the non-vacuum based thin film fabrication techniques on rough PDMS substrates having both high and ultra-low modulus of elasticity can act as a viable choice for the realization of stretchable and flexible electronics.

2. Factors Effecting the Mechanics of Stretchable Films

The mechanics of thin films (nano or micrometer thick) on compliant substrates differ considerably from their bulk material behavior. For instance, a bulk material at a given value of strain breaks with a single crack, on the other hand a thin film of the same material bonded to a compliant substrate breaks with multiple cracks. The mechanical properties of thin films on compliant substrates strongly depend on factors like morphology of the fabricated films, film thickness, fabrication technique and interfacial adhesion between the substrate and the film. For very small grains and film thicknesses dimensional constraints imposed by interfaces can appear. Beside the above mentioned factors the substrate stiffness and its thickness also have strong influence on the ductility of the substrate bonded films. In this chapter important factors that influence the mechanics of thin substrate bonded films are discussed.

2.1 Effect of substrate stiffness and thickness

From past research work (Li et al. 2004; Li & Suo 2006) it has been concluded that films bonded to stiffer substrates (O(10^9 Pa)) elongates more than the films bonded to more compliant substrates (O(10^6 Pa)). This result clearly suggests that as the Young's modulus of the substrate increases the rupture strain of the films also increases. On the other hand, it is worth mentioning that low values of the Young's modulus for the substrate material can be very useful for applications like biomedical implants, electronic skin and epidermal electronics (Kim et al. 2011; Wang et al. 2012).

As tensile strain is applied, tensile stresses are generated in the film which at a certain level can increase the strength of the thin film causing it to rupture (crack formations). After cracking is initiated further increase in the value of the strain causes delamination of the film from the substrate. On the other hand, if the interfacial adhesion between the film and the substrate material is not sufficient the interfacial shear stresses can directly cause the adhesive failure (Chiu et al. 1994). At the site of rupture, strain localization takes place which can be suppressed by the presence of a substrate, thereby increasing the rupture strain of the film (Li et al. 2005).

The effect of substrate thickness has the same nature as the substrate Young's modulus on the bonded films. Li & Suo 2006 has also shown that as the substrate thickness increases the rupture strain of the film also increases. These results are shown in Figure 2-1.

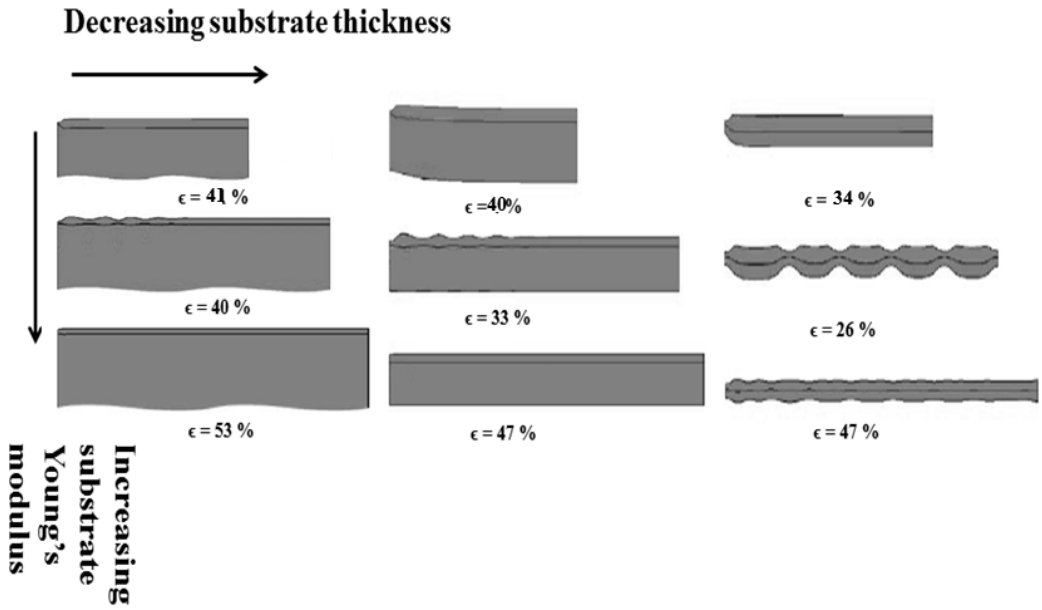

Figure 2-1 Effect of substrate Young's modulus and thickness on rupture strains of thin metallic film. (From Li & Suo 2006)

2.2 Effect of film thickness

The thickness of the substrate bonded thin films has important effects on grain size, fracture behavior and yield strength of the films. It has been investigated by (Lu et al. 2010) that copper films having thicknesses less than 200 nm always fail by intergranular fracture at strains of only a few percent, while thicker films rupture by ductile transgranular fracture and local debonding from the substrate. As the film thickness increases the grain size also increases and therefore the yield stress of the film decreases. This phenomenon makes it difficult for the films to debond from the substrate, since necking and debonding are known to coevolve the rupture strain for thick films therefore, increases. However, when the thickness is further increased (beyond 500 nm) the fraction of (1 0 0) grains in the (1 1 1) textured metallic films increases. The (1 0 0) grains are vulnerable to necking and debonding and causes the rupture strain to reduce. Figure 1-5 quantitatively shows this mechanism.

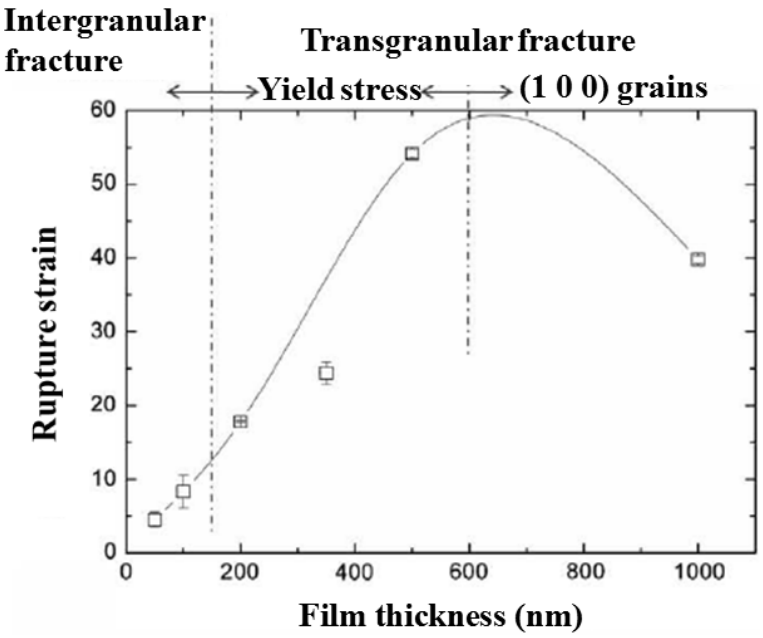

Figure 2-2 Variation of rupture strain with film thickness for copper films. (From Lu et al. 2010)

The work of Chiu et al. 1994 has indicated that the film thickness also plays an important role in the delamination of the films from the substrate. They found that failure strain at the onset of delamination for gold (Au) films increases with the increase in the thickness from 0.25 to 2 μm. They also showed that at a given value of an applied strain the interfacial shear stress decreases as the thickness of the film increases. This effect is shown in Figure 1-6.

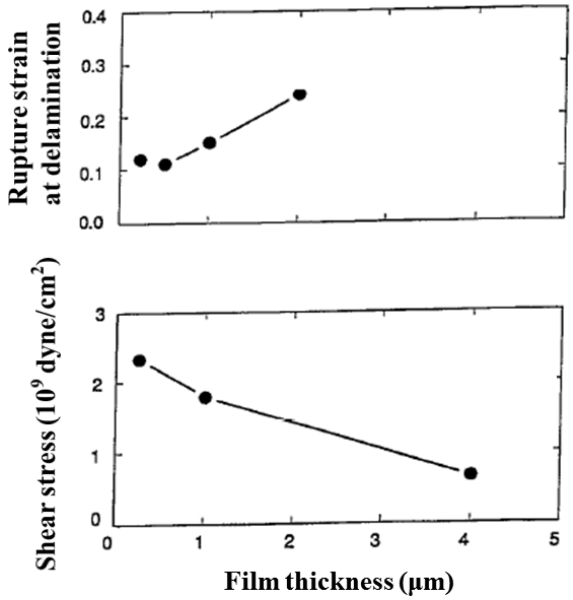

Figure 2-3 Variation of rupture strain at delamination (top) and interfacial shear (bottom) with increasing thickness. (From Chiu et al. 1994)

Beside these results (Gray et al. 2004) has shown that the stretchability of gold wires embedded in PDMS increases as the thickness of the wires is doubled. This discussion eventually concludes that, unless an application really demands a film thickness that remains on order of nanometer, film thicknesses of order of several micrometers are always advantageous in terms of mechanical considerations.

2.3 Effect of substrate roughness

Substrate roughness is also one of the key factors that affect the ductility of thin films. The density of surface cracks in the film, tensile stresses along the film surface, interfacial damage and interface crack length all reduces as the substrate roughness is increased (see Figure 2-4) (Xu et al. 2011). Channel cracking can also reduce with rough (curve) surfaces.

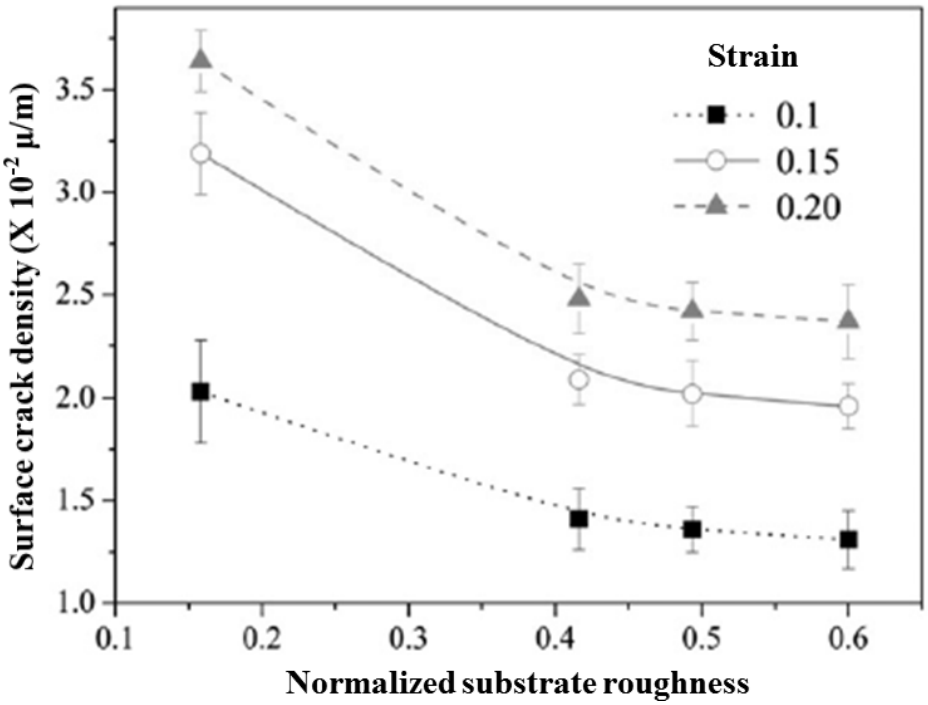

Figure 2-4 Decrease in surface crack density with substrate roughness. (From Xu et al. 2011)

The experimental results of Xu et al. 2011 suggests that the initiation and propagation of surface cracks in a thin metallic film can be retarded by roughening the surface of the underlying substrate (as shown in Figure 2-4) which increases the ductility of the film. On the other hand, a curve rough surface actually obstructs the slipping between the film and the substrate which increases the adhesion and delay interfacial debonding thereby increasing the ductility of the film.

Substrate roughness therefore, plays a key role in stretchable electronic devices. Due to the above mentioned reasons the performance of thin film enhances as the substrate roughness is increased. Consequently, there are studies available that have investigated the stretchability of thin films on rough substrates. For instance, as shown in Figure 2-5, (Lambricht et al. 2013) investigated that the stretchability of gold (Au) films on rough PDMS substrates increases as the substrate roughness is increased.

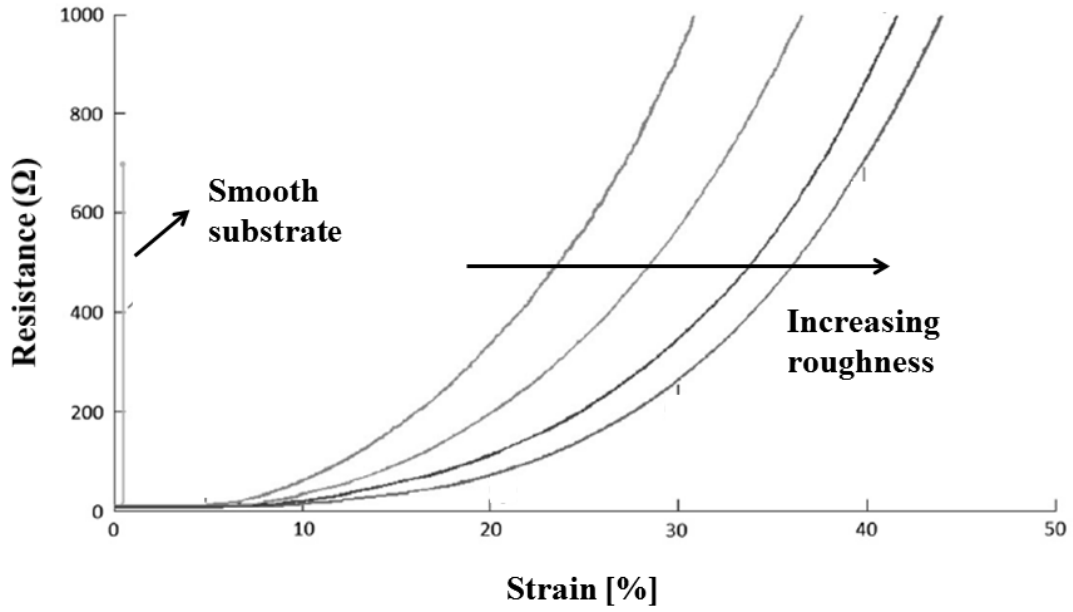

Figure 2-5 Variation of resistance with tensile strain for gold (Au) films on increasingly rough elastomeric substrate. (From Lambricht et al. 2013)

Patterning the PDMS surface actually generates roughness features on the surface and therefore tends to increase the adhesion between the film and the substrate. It is to be noted that roughness patterns in their work was random. (Robinson et al. 2011) showed that patterning the silicone (PDMS) substrates with micrometer size cylindrical features in an organized manner enhances the wettability and pinning of silver films on hydrophobic PDMS. Consequently, they showed that silver films maintained their stretchability up to 20% axial strain for up to 1000 stretching cycles.

Chung et al. 2011 also showed that the stretchability of inkjet printed silver electrodes on rough PDMS substrate having average roughness of 1.05 μm increases up to 13% as compared to 2.5% for smooth PDMS. The roughness in their work was randomly generated using wire EDM (electro discharge machining). This result is shown in Figure 2-6.

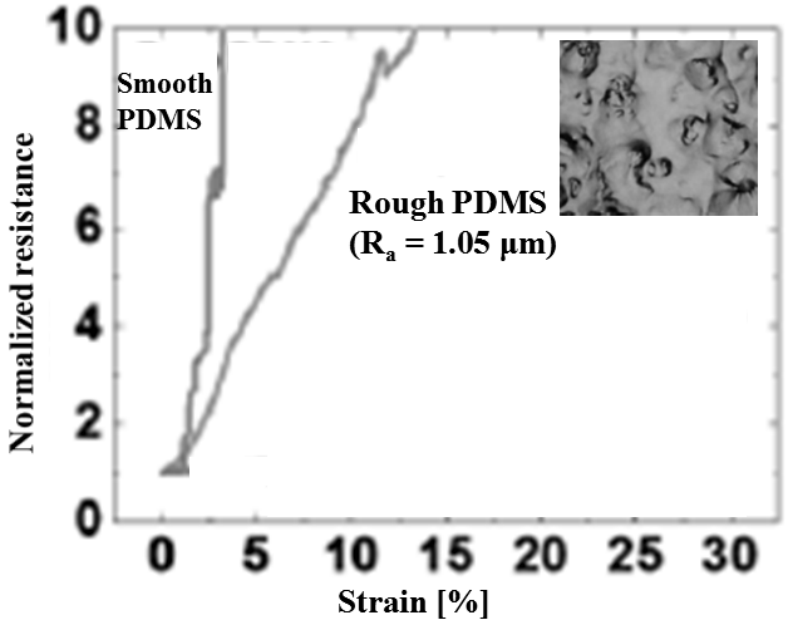

Figure 2-6 Variation of normalized resistance with strain for Ag electrodes on rough and smooth PDSM. The inset shows the rough surface of the PDMS substrate. (From Chung et al. 2011)

Wu et al, designed substrates with strain relief mechanism by roughening the PDMS surface with wavy structure. Their results show that the performance of organic thin film transistors (OTFT) on these wavy PDMS substrates was enhanced compared to flat and smooth substrates (Wu et al. 2013).

The film/substrate adhesion therefore, plays a vital role in enhancing the stretchability of thin films on polymeric substrates. The adhesion can be increased by generating roughness patterns which can either be organized or remain random. Various techniques for instance, sand blasting, wire EDM, micromachining, patterning, oxygen plasma, UVO exposures and photolithography can be used to intentionally roughen the surface of the substrate prior to the film fabrication.

2.4 Effect of fabrication technology

The effect of fabrication technology also plays a crucial role in the ductility of substrate bonded thin films. Generally speaking, the vacuum based fabrication techniques for example thermal evaporation, electron beam evaporation, sputtering and chemical vapor deposition

produces films that show higher morphological quality and performance as compared to non-vacuum based techniques (Kim et al. 2013). Figure 2-7 depicts this comparison.

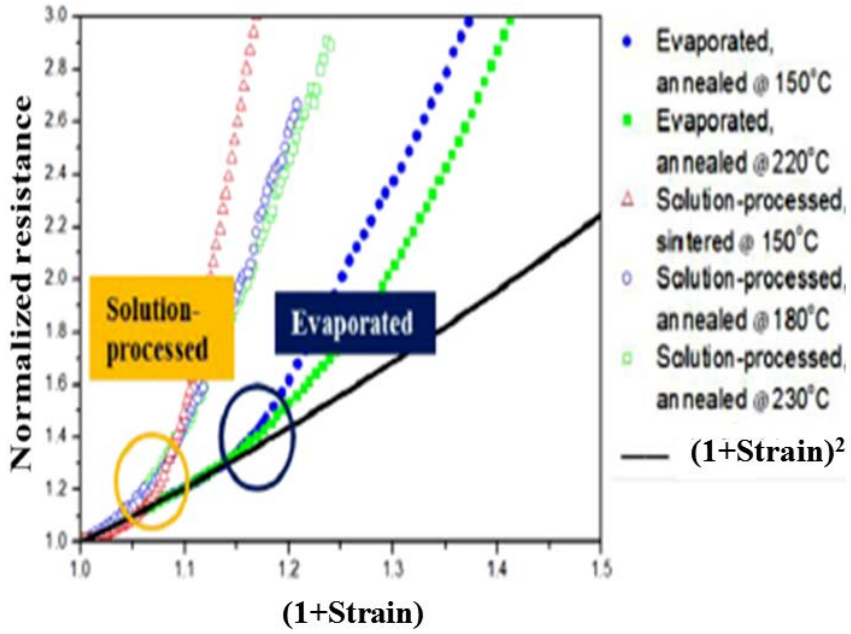

Figure 2-7 Performance comparison of vacuum and non-vacuum based thin film fabrication technologies. (From Kim et al. 2013)

Figure 2-7 highlight an important observation that the performance of thin films fabricated by non-vacuum based techniques is always lower than the performance of the films that are fabricated by vacuum based methods. The cause of this difference is the presence of higher porosity in the microstructure of the films that are fabricated using solution based inks and non-vacuum based techniques as can be seen from Figure 2-8.

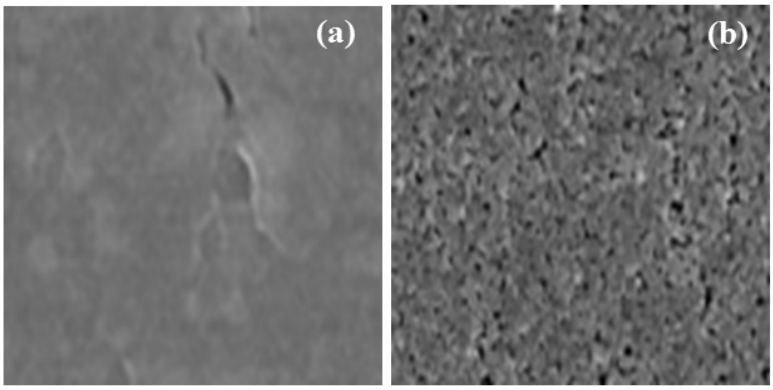

Figure 2-8 Scanning Electron Micrographs of (a) Electron beam evaporated film and (b) Solution based non vacuum deposited film. Note the presence of high amount of pores in (b). (From Kim et al. 2013)

As previously mentioned, non-vacuum based fabrication techniques are not only cost effective, energy efficient and simple, but are also capable of utilizing wide range of micro and nanostructured materials that can tremendously cut down the curing and sintering temperature requirements. Because of these reasons ongoing research is inevitable in improving the performance of solution based thin films mainly fabricated through non-vacuum based techniques.

2.5 Effect of sintering

Films that are fabricated using micro and/or nanostructured materials essentially require sintering process to render them properly functional. For example the deposited nanoparticles based film on any kind of substrate must be sintered, such that the deposited nanoparticles can fuse together to form a continuous solid film. However if there is a difference in the coefficient of thermal expansion (CTE) of the film and substrate material then sintering at higher temperatures can generate thermal stresses within the film material. These thermal stresses are known to degrade the film morphology and cause cracking during sintering process (Fang & Lo 2000). Consequently, the results of Kim et al 2013 (see Figure 2-9) show that sintering the silver nanoparticles based thin films at higher temperatures produces porosity and larger pore sizes in the films which tends to reduce the rupture strains and hence the stretchability of the films.

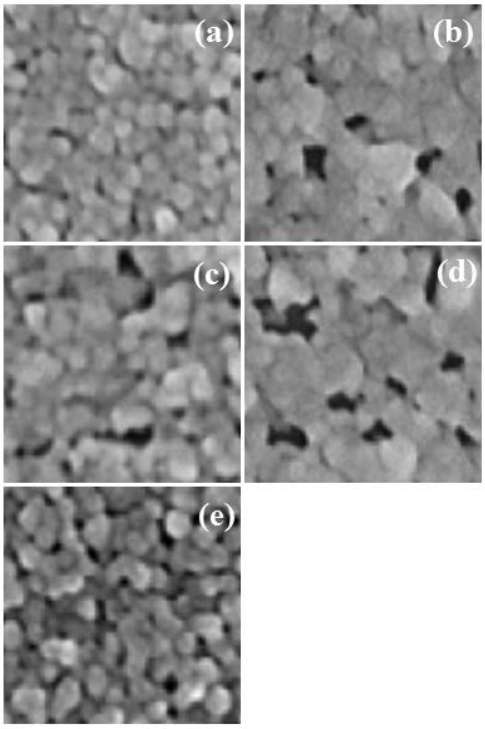

Figure 2-9 Scanning electron micrographs of silver nanoparticles based films at different sintering temperatures and times. (a) 180 ^{o}C for 3 h, (b) 230 ^{o}C for 3 h, (c) 180 ^{o}C for 6 h, (d) 230 ^{o}C for 6 h and (e) 150 ^{o}C for 0.5 h. Note that as the temperature and time of sintering increases from (a) to (d) the porosity and pore size also increases. (From Kim et al. 2013)

The above discussion leads towards the fact that for solution based micro and/or nanostructured thin films that are usually fabricated using non-vacuum techniques, increasing the sintering conditions (i.e. the temperature and time) can result in adverse effects which can limit the stretchability of the films. Consequently need for low temperature sintering options are desirable.

3. Polydimethylsiloxane as a Substrate Material

It has been mentioned in chapter 2 that the choice of substrate material, its stiffness (Young's modulus) and thickness has important effects on the mechanics of substrate bonded thin films. Hence, it is of vital importance to select a proper substrate material for the performance of thin substrate bonded films. From the literature survey it has been found out that PDMS has been extensively used as a substrate material for both stretchable and flexible electronics and also in numerous microfluidics applications. The major cause of its intensive utilization is due to the fact that being an elastomer it is inherently stretchable and flexible, chemically inert, biocompatible, easily moldable and can acquire nano and micro scale details, thermally stable over a wide range of temperature and can be easily tunable in terms of mechanical properties to meet various requirements. In this work only PDMS (Sylgard 184) from Dow Corning (USA) has been used as a substrate material therefore, it is of great importance to shed some light over this useful silicon elastomer.

3.1 Chemical attributes of PDMS

PDMS (Sylgard 184) comes as a two component elastomer kit (i.e. the elastomer base and a silicone cross linker agent). The fragmented formula for Sylgard 184 is shown in Figure 3-1.

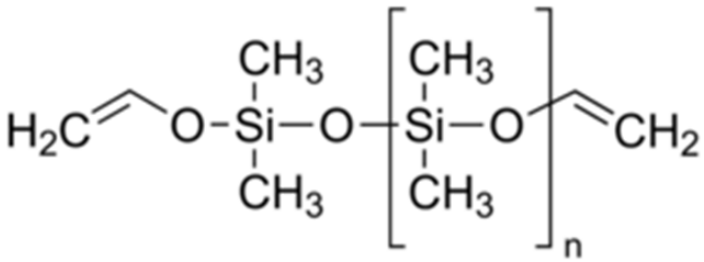

Figure 3-1 Chemical structure of cross linked PDMS (Sylgard 184).

Where n is the number of repetitions of the monomer. Liquid PDMS solution is prepared by thoroughly mixing the two components in a desired concentration either 10 % by weight (recommended) or 3% by weight of the cross linker in the elastomer base. The mixing of the two components and curing (if desired) causes a primary hydrosilylation reaction. The rate of hydrosilylation reaction depends on the terminal groups of the elastomer base and the number

of Si-H groups on the cross linker as well as their concentration and temperature at which the reaction takes place (Esteves et al. 2009). In polymer chemistry, cross linking actually refers to the mixing of two polymers such that the physical properties of the cross linked polymer can be altered. For instance, the work of (Mata & Fleischman 2005), has revealed that increasing the cross linker concentration in the PDMS formulation increases its ultimate tensile strength (UTS) while decreases the thickness of the spin coated PDMS films.

Using PDMS as a substrate material for stretchable and flexible electronics involves various post treatment steps that requires treatment with different chemicals mainly for cleaning or surface modification purposes. Several studies have investigated the effect of chemical treatments on cross linked PDMS samples. For instance, Mata et al. 2005 showed that potassium hydroxide (KOH) (both diluted and concentrated), hydrofluoric acid (HF) (both diluted and concentrated), Nitric acid (NH_3) and sulphuric acid (H_2SO_4) has strong ability to react with the PDMS causing chemical etching. Their result showing the solvent compatibility with the conventional (1 MPa) PDMS is shown in Figure 3-2.

Chemical	Concentration (wt.%)	Time (min)	No	Mild	Medium	Total	Weight gain (%)
Buffered hydrofluoric acid	49.0	10	x				−0.97
Hydrochloric acid	37.9	10	x				−0.34
Potassium hydroxide[a]	86.9	10	x				−0.27
Hydrogen peroxide (H_2O_2)	31.8	10	x				2.01
Piranha	3(H_2O_2) : 1(H_2SO_4)	10, 30	x				0.64
Photoresist developer[b]	100.0	10	x				−0.97
Water (deionized)	100.0	10, 30	x				−0.33
Hexane	99.9	10	x				4.67
Tolueme	99.9	10	x				45.51
Acetone	99.7	10, 30	x				2.78
Methanol	100.0	10	x				−0.34
Isopropanol	100.0	10	x				−0.97
Potassium hydroxide[a]	86.9	60		x			0.75
Buffered hydrofluoric acid	49.0	30			x		1.39
Nitric acid	69.8	10			x		4.13
Hydrofluoric acid	49.0	10				x	−1.38
Sulfuric acid (H_2SO_4)	96.0	10				x	−14.00
Potassium hydroxide[a]	86.9	1620				x	−0.90

Figure 3-2 Solvent compatibility for conventional PDMS. (From Mata et al. 2005)

Also the work of (Lee et al. 2003) indicates that treatment of PDMS with strong acids causes chemical reactions to take place which can dissolve the PDMS into smaller subunits with a white precipitate. Through mass spectroscopy they found that the products of the reaction consisted of oligomers with different numbers of dimethylsiloxane subunits. The effect of

acid treatment of PDMS can be noticed in Figure 3-3. It can be seen from Figure 3-3 that strong acids (as mentioned above) have ability to react with PDMS dissolving it and changing the surface condition considerably.

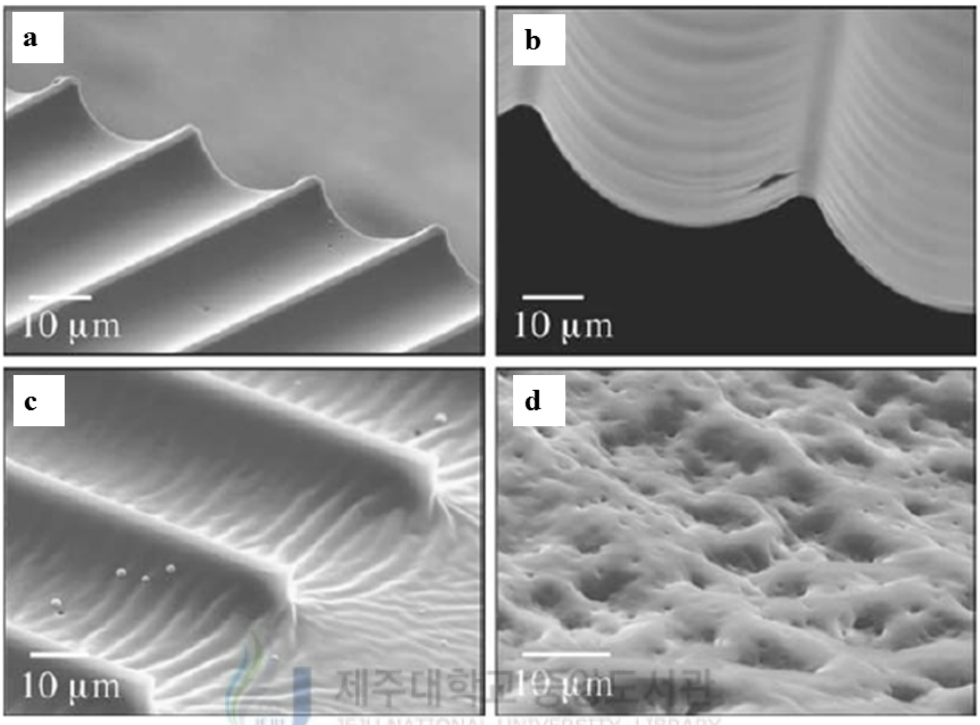

Figure 3-3 SEM images showing the condition of PDMS after chemical immersion (a) no change, (b) mild change, (c) medium change and (d) total change. (From Mata et al. 2005)

Lee et al. 2003 also investigated the swelling of PDMS when treated with different organic solvents. Their result indicates that organic solvents having solubility parameter (δ) similar to that of PDMS have higher ability of swelling the PDMS as compared to solvents that have substantially different values of δ. This is clearly visible in Figure 3-4.

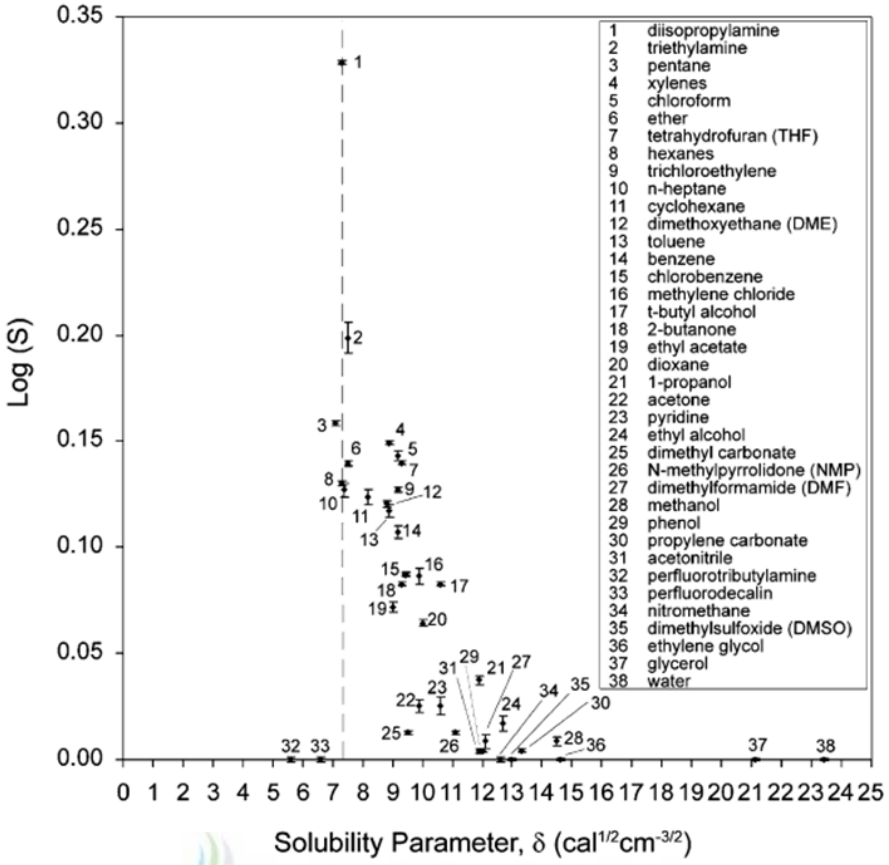

Figure 3-4 Relationship between swelling ratio (S) (shown as Log (S)) of PDMS in various solvents and the solubility parameter (δ) for these solvents. The solvents are numbered in order of decreasing swelling ability. The dashed line indicates the solubility parameter of PDMS = 7.3 $cal^{1/2}$ $cm^{-3/2}$). In general, a greater degree of swelling is observed with solvents that have a value of δ similar to that of PDMS. (From Lee et al. 2003)

Low-solubility solvents generally have $\delta = 9.9$ $cal^{1/2}$ $cm^{-3/2}$. These solvents range from water (38) to 1-propanol (21) (see Figure 3-4) and include most alcohols (1-propanol, ethanol, methanol, phenol, ethylene glycol, glycerol), nitriles (acetonitrile), disubstituted amides (NMP, DMF), and tetrasubstituted ureas (1,1,3,3-tetramethylurea), sulfoxides (DMSO, tetramethylene sulfone), pyridines, and nitro compounds (nitro methane). Fluorocarbons (perfluorodecalin, trifluoroethanol, perfluorotributylamine) also do not swell PDMS. Therefore, Low-solubility solvents can be used with PDMS without swelling.

3.2 Mechanical attributes of PDMS

Since PDMS is inherently stretchable several studied has been conducted in order to investigate its strength and maximum elongation reached before complete rupture. (Han et al.

2012) in their work conducted tensile tests on strip specimen of conventional PDMS. They showed that maximum elongation reached by the specimen increases and therefore, the stiffness reduces as the aspect ratio (L_o/W) decreases. Where L_o is the gage length of the specimen and W is the width of the specimen. On the other hand, the maximum stress was approximately 2 MPa. Figure 3-5 shows this trend.

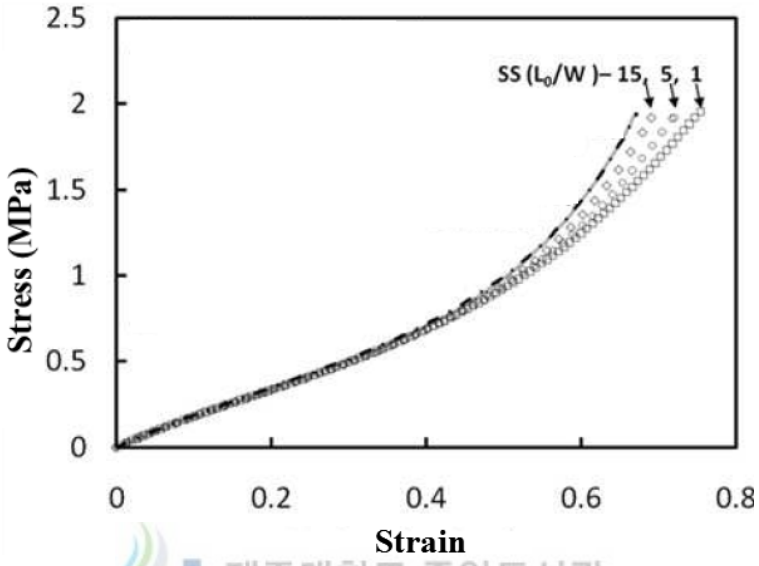

Figure 3-5 Engineering stress-strain curve for high modulus strip specimen (SS) of PDMS with decreasing (L_o/W) ratios. (From Han et al. 2012)

It can be noticed that within the range of the aspect ratios studied the maximum stretchability of the strip specimen changes by less than 10%. From these results it can be concluded that the conventional PDMS can easily reach stretchability levels of above 60% without failure. From their experiments Han et al. 2012 also verified that the Poisson's ratio of the conventional PDMS can be considered to be approximately 0.5 which makes PDMS an incompressible material i.e. the volume of the PDMS specimen remains almost the same before stretching and during stretching.

The mechanical strength and Young's modulus of PDMS is also shown to be thickness dependent. The work of (Liu et al. 2009) has shown that below the thickness of 200 μm PDMS membranes showed increased strength and thus reduced elongations (maximum stretchability). The increase in the strength is attributed to shear stress dependent alignment

of polymer chain coils at reduced thicknesses which increases the strength of the PDMS membranes. Their result indicates that micrometer thick membranes of PDMS can achieve higher stretchability (on average 130%) before complete failure. This is shown in Figure 3-6.

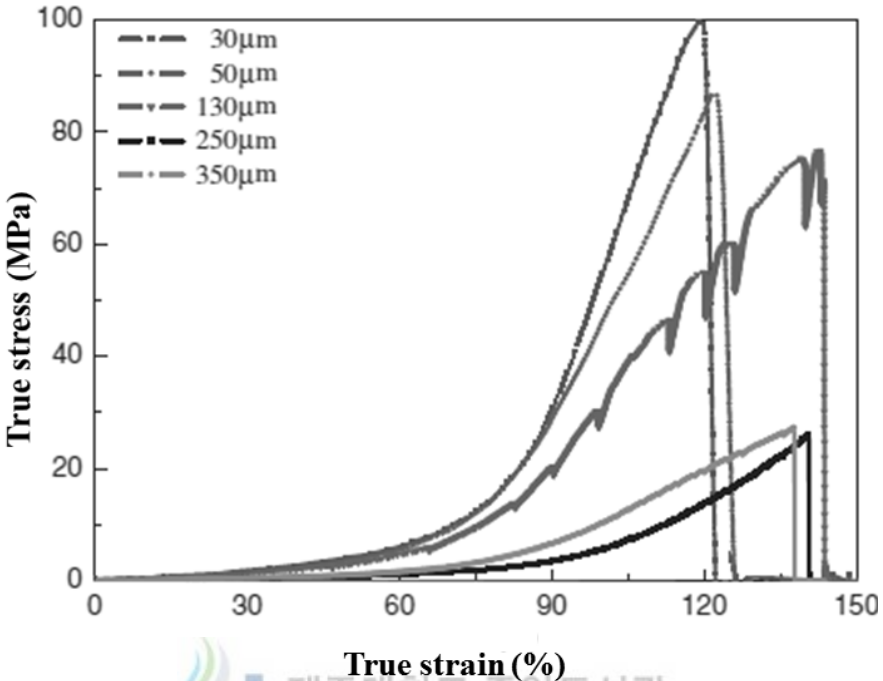

Figure 3-6 True stress-strain curves for micrometer thick conventional PDMS test specimen. (From Liu et al. 2009)

The PDMS membranes in their study were prepared by spin coating which is capable of exerting high shear stresses at the liquid PDMS-substrate interface. From Figure 3-5 and Figure 3-6 it is evident that within the small zone (20 % to 30 % strain) the stress-strain curves for the PDMS can be considered linear however, for high deformation domain the material response is always nonlinear.

For the ultra-low modulus PDMS the maximum elongation reached before complete failure (breaking point) were studied using one point stretching tests. The results are plotted in Figure 3-7 and indicate that by decreasing the thickness and increasing the width of the substrate the maximum strain to failure increases. It is to be noted that only two thicknesses were tested i.e. 725 µm and 420 µm. It can be seen from Figure 3-7 that the ultra-low modulus PDMS substrates have substantial stretchability over the tested dimensions.

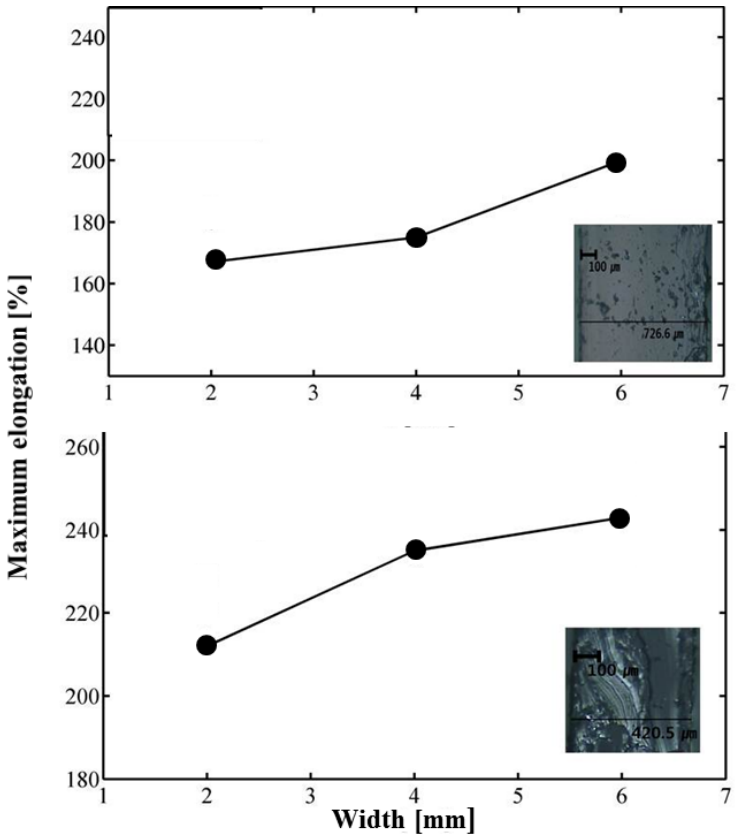

Figure 3-7 Maximum elongation before failure for ultra-low modulus PDMS substrates at various substrate widths for two different substrate thicknesses. The inset shows the cross sectional micrographs showing the thicknesses. Each data point represents a mean of at least three readings. Scale bar given in the inset is 100 μm.

The substrate thicknesses shown in Figure 3-7 can be achieved by spin coating. Figure 3-8 indicates the variation of substrate thickness with the spin speed at a constant time and volume of 30 second and 1 mL, respectively. As can be seen in Figure 3-8 the thickness of the ultra-low modulus PDMS membrane can be correlated with the spin speed by equation (3-1).

$$\text{Thickness} = 1693 \times \text{Speed}^{-0.31} \quad (3\text{-}1)$$

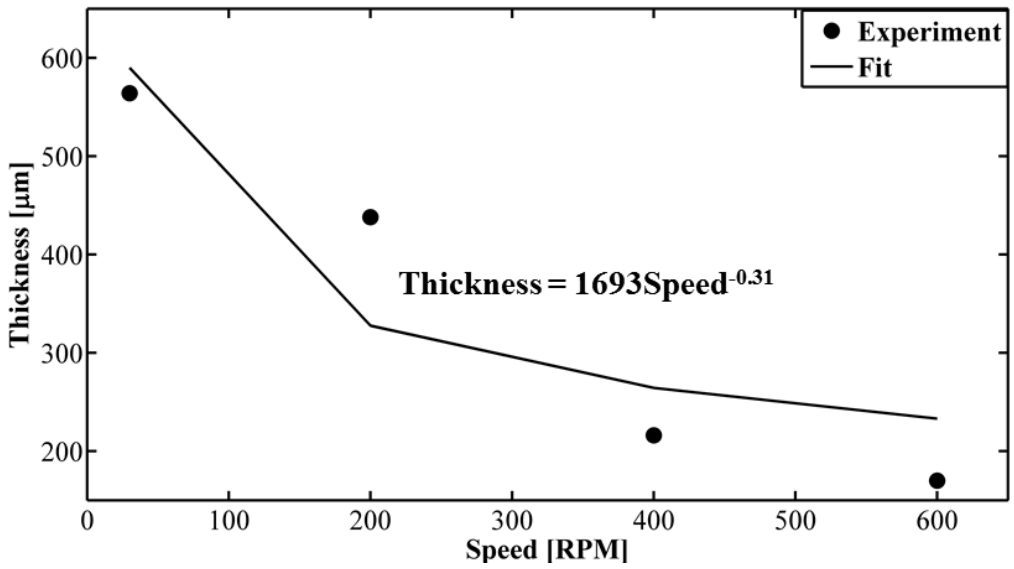

Figure 3-8 Variation of ultra-low modulus PDMS thickness with the spin speed at a constant spin time of 30 seconds. Each data point is an average of three readings. The equation in the figure is a curve fit model.

3.3 Surface modification techniques for PDMS

After cross linking the PDSM converts into a transparent stretchable and flexible solid which can be used for applications like stretchable/flexible electronics, microfluidics and microelectromechanical systems. However, the cross linked PDMS is hydrophobic in nature and can pose obstacles when used as a substrate for stretchable and flexible electronics. This problem can be overcome by number of ways that includes oxygen plasma exposure (Bhattacharya et al. 2005), ultraviolet ozone exposure (Efimenko et al. 2002), chemical treatments (Vickers et al. 2006; Akter & Kim 2012) and intentionally generating micro or nano roughness patterns on its surface (Lambritcht et al 2013; Robinson et al. 2011; Chung et al. 2011). These techniques can convert the PDMS into a hydrophilic surface which can promote adhesion of the deposited material (film or pattern) with the PDMS. It is to be noted that compared to other techniques available, the generation of micro or nano roughness patterns can be a permanent way of imparting tunable adhesion and wettability properties to the PDMS. On the other hand, when ultra-low modulus PDMS was used it was found out that due to low cross linker concentration the surface of the PDMS remains very sticky and enhances the wettability of the deionized (DI) water. From Figure 3-9 it can be seen that the contact angle (CA) of DI water on the UVO treated ultra-low modulus PDMS can be

substantially decreased as compared to both the conventional modulus PDMS ($CA \approx 113.6^{o}$ treated, Mata et al. 2005 and $CA \approx 116^{o}$ untreated, Someya 2012) and ultra-low modulus PDMS without UVO exposure.

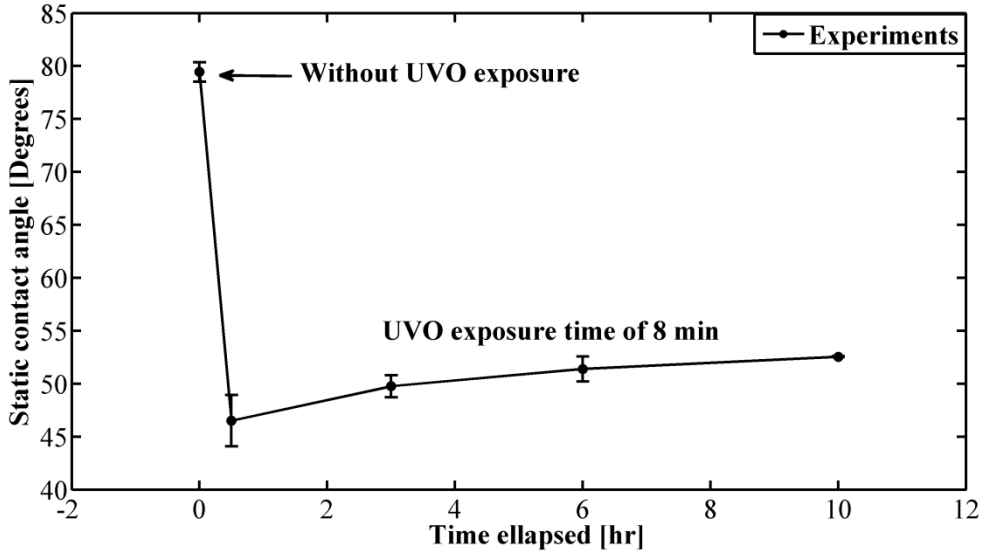

Figure 3-9 Static contact angle of DI water on ultra-low modulus PDMS with and without the UVO exposure.

Also it was found in this study that the wettability of organic solvents like ethylene glycol and isopropyl alcohol on ultra-low modulus PDMS without any UVO exposure can increase significantly. Figure 3-10 depicts this result in which two different synthesized inks containing, isopropyl alcohol, dimethyl sulfoxide and ethylene glycol as a solvent was used respectively, to pattern a thin film on ultra-low modulus PDMS.

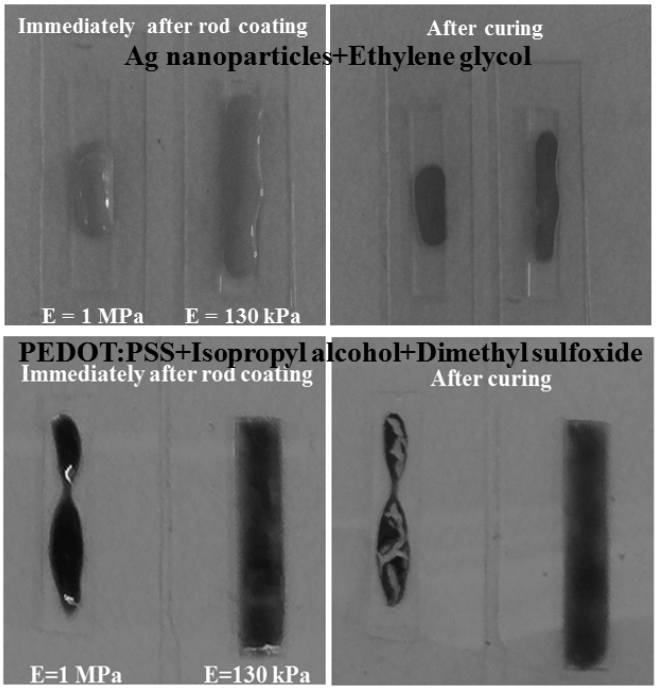

Figure 3-10 Photographs showing the wettability of the inks on high and ultra-low modulus PDMS substrates.

Figure 3-11 shows the contact angles of these inks on ultra-low modulus PDMS. It can be clearly seen that the contact angles are well below the value of 116^{o} for conventional high modulus PDMS.

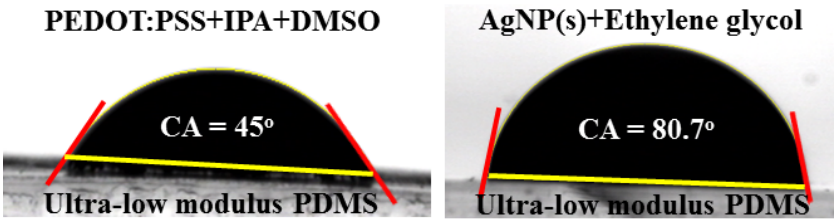

Figure 3-11 Static contact angle of the inks on bare ultra-low modulus PDMS.

Oxygen plasma exposure and UVO exposure both are known to generate brittle silica like layer on PDMS. During this study it was found that for ultra-low modulus PDMS, higher UVO exposure time can generate blister type cracks which were not reported for the high modulus PDMS in spite of the fact that the exposure times were higher than the one used in this study. Figure 3-12 shows typical micrographs of UVO treated ultra-low modulus PDMS

for two different thicknesses. It can be noticed that for thinner substrates these cracks can appear at relatively lower exposure time. Hence, when UVO or plasma exposure of ultra-low modulus PDMS is required, one should use exposure times that can avoid cracking of the silica layer.

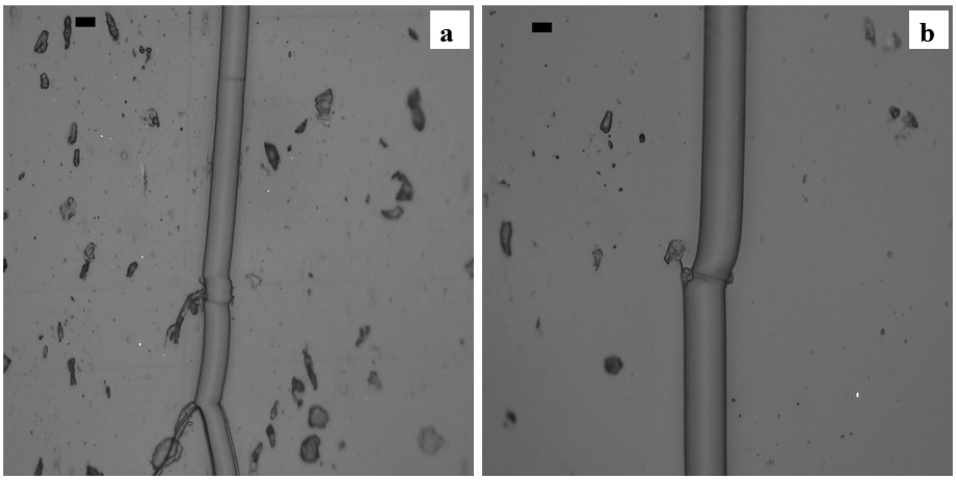

Figure 3-12 Blister type cracks appeared on ultra-low modulus PDMS substrates. (a) Thin substrate with 9 minutes of exposure time and (b) thick substrate with 13 minutes of exposure time. The scale bar in each figure is 25 μm.

The formation of these cracks during UVO exposure is attributed to the difference between the Young's modulus of the silica layer and bulk PDMS which can accumulate stress (Berdichevsky et al. 2004).

3.4 Thermal stability of PDMS

Thin film fabrication requires sintering of films at temperatures that can be in excess of 150^{o}C. It might also require multiple sintering steps for instance when multi layered films are to be fabricated. Therefore, the effect of temperature on PDMS is essential to study. A Review by Rhein 1983 has indicated that thermal stability of an elastomer is the temperature of incipient chemical alteration, such that the mechanical properties have deteriorated to the point where the elastomer is no longer useful. Polmanteer reported in his work that continuous exposure temperature versus service life of silicone elastomers ranges from 15000 hours at 148^{o}C to maximum of 30 minutes at 371^{o}C (Polmanteer 1979). Baney 1968 indicated that high temperature degradation consists of siloxane rearrangements and ring-

chain equilibrium. The silicone-carbon bonds can withstand temperatures up to 600^{o}C but the silicone-oxygen bond rearrangements can take place within 250-350^{o}C. Polydimethylsiloxane therefore, undergo thermal rearrangements with the rupture of the siloxane chain. Also the work of (Norkhairunnisa et al. 2011) showed that initial degradation of PDMS starts at about 258^{o}C and complete degradation takes place at 513^{o}C. They also show that the thermal stability of PDMS and can be increased with filler materials such as multi walled carbon nanotubes and carbon black nanoparticles. Korshak 1971 indicated that among elastomers only silicone rubber retain appreciable mechanical strength above 250^{o}C.

Based on the above mentioned references, it can be claimed that conventional PDMS deteriorate around 250^{o}C. On the other hand, in this study, it was found out that ultra-low modulus PDMS can sustain temperatures up to 230^{o}C. The result is shown in Figure 3-13 where the ultra-low modulus PDMS samples were post baked at different temperatures up to 230^{o}C for 3 hours inside a hot air convection oven. It can be seen that substantial stretchability can still be obtained when post baking temperature of 230^{o}C is used. However, when the ultra-low modulus PDMS samples were post baked at 300^{o}C for 1 hour inside a hot air convection oven severe deterioration (cracking) was observed which ultimately indicates complete failure. Although, no such deterioration was observed when post baking temperature of 250^{o}C was used but the functionality was not such that the PDMS can be utilized. The result can be seen in Figure 3-14. These results suggest that solution based inks containing nano/micro structured materials with sintering temperatures up to 200^{o}C could possibly be used in combination with ultra-low modulus PDMS.

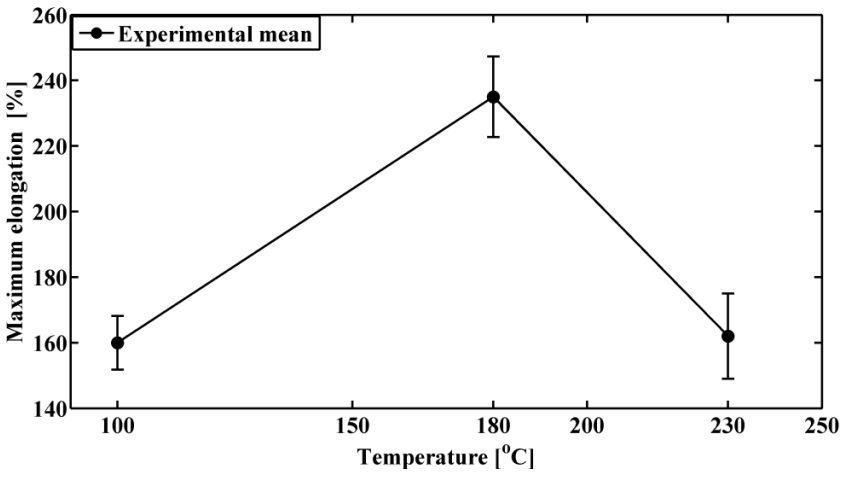

Figure 3-13 Stretchability of ultra-low modulus PDMS at various post baking temperatures.
Each data point represent mean of at least three readings.

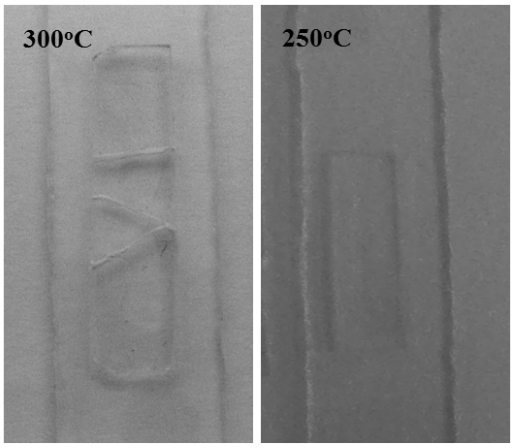

Figure 3-14 Photograph showing the condition of the ultra-low modulus PDMS substrates post baked at 300°C and 250°C.

Also Figure 3-15 indicates that the percentage of the weight loss from the ultra-low modulus PDMS when baked at various post baking temperatures remains negligibly small.

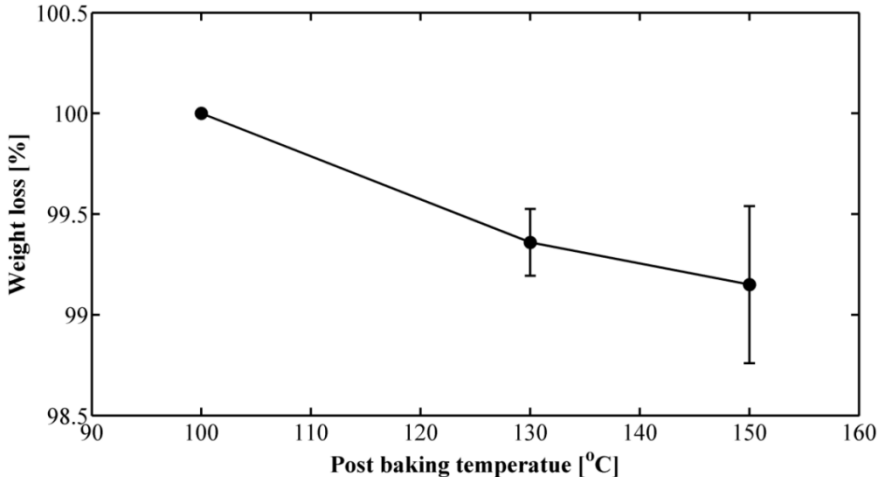

Figure 3-15 Percentage of weight loss as a function of post baking temperature for ultra-low modulus PDMS.
Each data point is an average of at least three readings.

4. Experimental

This chapter presents a brief explanation about the experimental procedures, chemicals and instrumentation utilized in this work.

4.1 Substrate preparation

All PDMS substrates used in this work were either prepared by mixing the base (component A) and the curing agent (component B) as shown in Figure 4-1 in 10:1 or 10:0.3 ratio by weight which corresponds to either 10% concentration of the curing agent or 3% concentration of the curing agent, respectively. 10% concentration was used to have an approximate Young's modulus of 1 MPa for the PDMS substrates. On the other hand, a 3% concentration was used to have ultra-low modulus PDMS substrates (120-130 kPa). As can be seen in Figure 4-1 the PDMS kit was purchased from Dow Corning Corp. (USA).

Figure 4-1 PDMS kit.

After thoroughly mixing the two components together, the solution was degassed inside a vacuum chamber with a capacity of generating a maximum of -0.1 MPa vacuum. The time to remove all the air bubbles depends on the quantity of the solution to be degassed. In this study the degassing time was either 10-15 minutes (for 10 mL of PDMS solution) or 20-25

minutes (for 20 mL PDMS solution). After the removal of air bubbles the clear PDMS solution was deposited over glass substrates in measured volumes of 1 mL using a medical syringe. The glass substrates were either covered with aluminum foils or PET foils. These substrates were then rotated on a spin coater ACE-200 (Dong Ah Tech, Korea) shown in Figure 4-2 at desired speeds and times in order to have required thickness of the PDMS substrates.

Figure 4-2 Photograph of the spin coater.

The PDMS substrates obtained in this way were baked either at 100^{o}C for 35 minutes for 10% concentration of cross linker in order to have approximately 1 MPa Young's modulus or at 100^{o}C for 3 hours for 3% concentration of cross linker in order to have approximately 120-140 kPa Young's modulus. All PDMS castings were baked inside a hot air convection oven SOF-50 (SciLab, Korea).

The PDMS substrates were then cut into desired dimensions using a sharp blade cutter and were bath sonicated in acetone using WiseClean WUC-A02H (Daihan Scientific, Korea) for cleaning purpose. The bath sonication time varies from 2minutes to 20 minutes depending on the condition of the PDMS substrates. In certain cases the cleaned PDMS substrates were also exposed to ultraviolet ozone (UVO) treatment for 9 to 13 minutes using a UVO cleaner which was capable of generating 184.9 nm and 253.7 nm wavelength UV radiations with an

average intensity of 28-32mW/cm^2. The distance between the UV source and the substrates was fixed at 5 mm. Once the PDMS samples were ready, fabrication of either Ag nanoparticles based films or PEDOT:PSS films using various non-vacuum based techniques were done. These non-vacuum based techniques are discussed in the subsequent chapters of this thesis. The fabricated films were either annealed inside the hot air convection oven SOF-50 (SciLab, Korea) or were simply baked on a hot plate NEO HOTPLATE HI-1000 (AS ONE, Japan) in ambient air. It is to be noted that throughout this research work annealing temperatures of $\leq 115^{o}$C were used for the fabricated films with maximum annealing time of 60 minutes.

4.2 Chemicals and synthesis

The nanoparticle paste was purchased from PARU Corp. (Korea), PEDOT:PSS paste was purchased from AGFA Materials (Japan) and rest of the chemicals for instance, Isopropyl alcohol (IPA), ethylene glycol, dimethyl sulfoxide (DMSO), acetone and ethanol were purchased from Sigma Aldrich (USA). All chemicals were used as received. The viscosities of the as synthesized inks were measured using a rotating viscometer VISCOMATE VM-10A (Sekonic Corp. Japan). The densities of the as synthesized inks were calculated by measuring the mass and volume of the inks. In order to determine the wettability of the as synthesized inks on ultra-low modulus PDMS substrates, all static contact angles were measured using a goniometer PHOENIX 3000 (Surface Electro Optics, Korea). All inks in this work were synthesized by precisely adding a particular mass of desired species (either Ag nanoparticles paste or PEDOT:PSS paste) in desired solvents (either ethylene glycol or mixture of IPA and DMSO) of known mass. All measurements regarding mass were done on a precision electronic mass balance KERN KB1200-2 (Germany) having a least count of 0.01 gm.

4.3 Experimental set up for strain measurements

Figure 4-3 depicts the photograph of the experimental setup that was used to perform the stretchability test for all the fabricated films whether metallic or nonmetallic in this study.

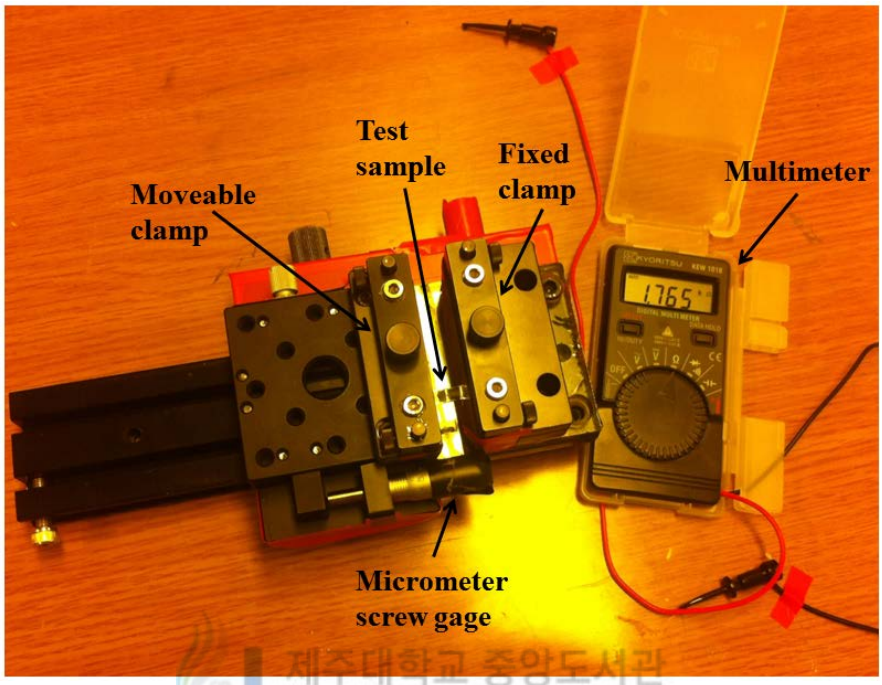

Figure 4-3 Photograph of the experimental setup used for the stretching experiments.

As already explained in chapter 1, in order to investigate the maximum stretchability of the films (metallic or nonmetallic) on rough PDMS substrates, method of electrical resistance was adopted. The reference length for the measurement of strain was either taken to be the distance between the electrical connection points that remained 5 mm or the distance between the clamps that remained 14 mm for each case studied. The axial elongation was applied in step of 30 μm or 50 μm and the strain rate in this work remains of order of 10^{-3} sec^{-1} for each case studied. The resistance was recorded using a multimeter KEW 1018 (Kyoritsu, Japan) having an accuracy of $\pm 1\%$ as shown in Figure 4-3. The electrical contacts were made by embedding 50 μm diameter pure copper wires (Nilaco Corp. Japan) in a silver conductive epoxy CW2400 (circuitworks, USA) and then heating the substrates at 100^{o}C for 10 minutes on a hot plate to secure the connections. Axial strain was applied untill the resistance was

found to abruptly increase due to cracks formation and their propagation eventually resulting in complete rupture of the films and thus the open circuit.

When the bending tests were performed in order to study the flexible nature of the fabricated films, the substrates were bent with conformal contact on circular rods of different diameters. The rod diameter was continuously reduced untill enough bending strain was produced eventually causing the films to rupture and finally results in an open circuit. A typical bending test performed is shown in Figure 4-4.

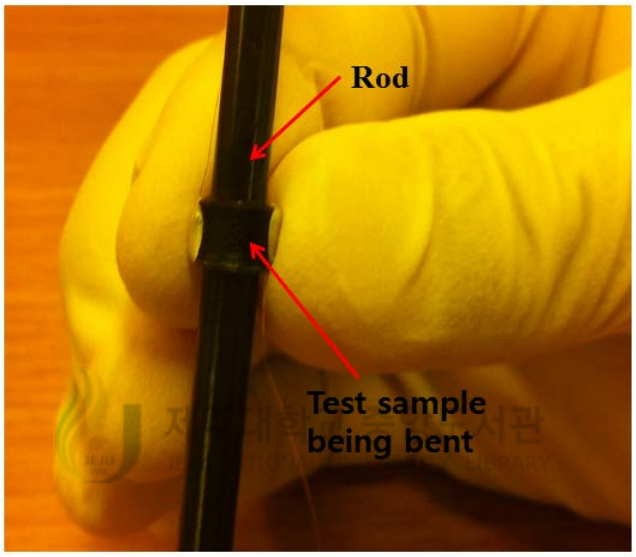

Figure 4-4 Photograph showing a typical test sample being bent on a circular rod.

Scanning electron microscope (SEM) JEOL JSM-6700F (JEOL Ltd. Japan) and optical surface profiler 3D NanoView E-1000 (Nano System Co. Ltd. Korea) was used to characterize and study the roughness patterns on the PDMS substrates. In most of the cases the substrate and film thicknesses were also measured using lateral SEM images at 90 degrees. In few cases the film thicknesses were also estimated using gravimetric analysis by using a precision electronic mass balance AUW220D (shimadzu, Japan) with a least count of 0.01mg. The sintered morphology of the films in certain cases was studied using SEM images. Figure 4-5 shows the photograph of SEM whereas Figure 4-6 depicts the photograph of the optical profiler used in this work.

Figure 4-5 JEOL JSM-6700F scanning electron microscope (SEM).

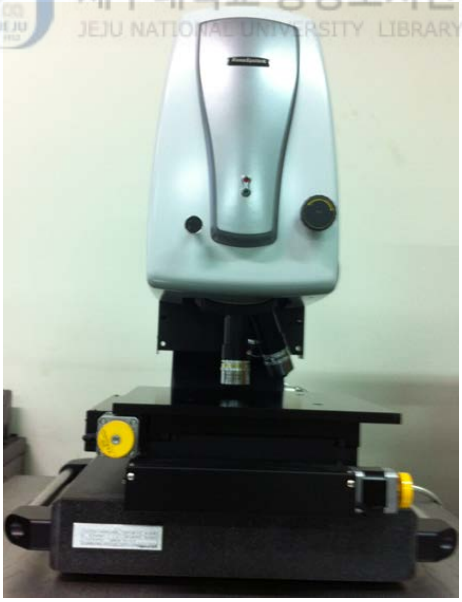

Figure 4-6 Optical surface profiler NanoView E-1000.

Finally micrographs were used in order to study the crack patterns and surface deterioration of the fabricated films before and after the application of axial and/or bending strain. All micrographs were taken from optical microscope OLYMPUS BX51M as shown in Figure 4-7.

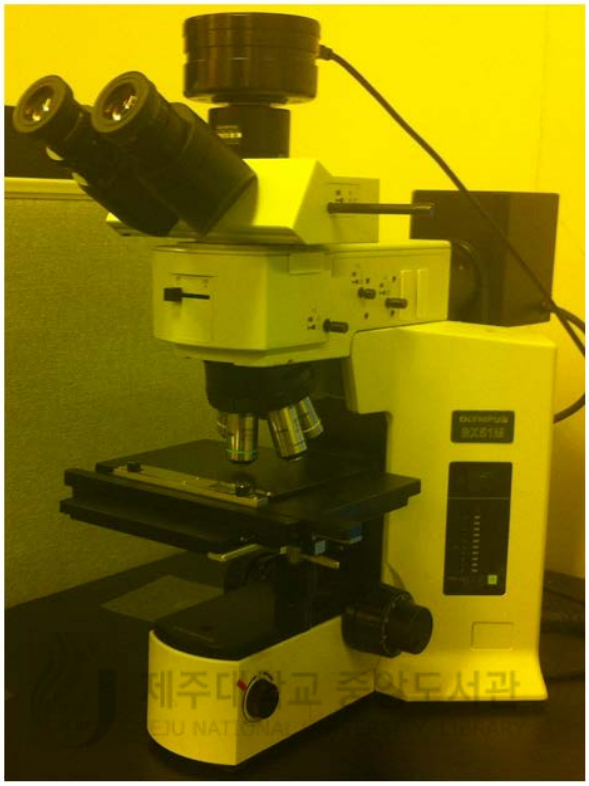

Figure 4-7 Olympus BX51M optical microscope.

5. Stretchable and Flexible Behaviors of Ag Nanoparticles Films on Rough Polydimethylsiloxane Substrates

This chapter presents the film fabrication technique, roughness generation technique and its characterization and finally experimental results regarding stretchable and flexible resistive behaviors of silver (Ag) nanoparticles based films on rough polydimethylsiloxane (PDMS) substrates. In each case different types of roughness patterns were generated on either high modulus PDMS or the ultra-low modulus PDMS with a different non vacuum based film fabrication technique.

5.1 Spin coated Ag nanoparticles films on random micro ridged type PDMS

Spin coating is a simple and cost effective technique to deposit thin films ranging from thicknesses of orders of nanometers to micrometers. It requires some quantity of the solution based ink (metallic or nonmetallic) to be deposited on a flat substrate which is then rotated at desired rpm for a controlled time. The liquid spreads with the help of centrifugal forces which causes the excess liquid to fall off. The film thickness depends on factors like viscosity of the ink, concentration of solute (micro or nanoparticles or nanowires), spin speed, spin time and the type of solvent involved (Bräuer et al. 2006; Fang et al. 1994; Hwang & Kim 1999). After performing the deposition, the films can be sintered or dried using elevated temperature environments. This method of applying films is widely used in microelectronics industry. The schematic of spin coating is shown in Figure 5-1.

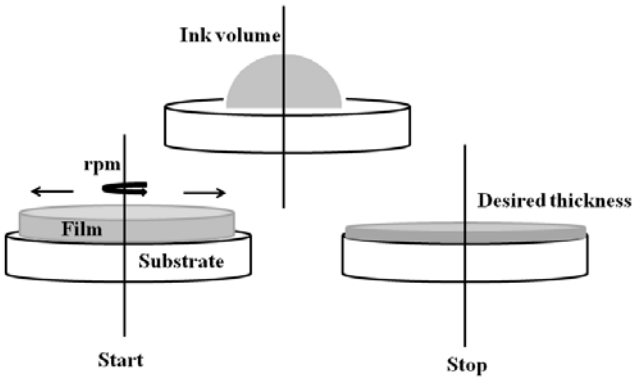

Figure 5-1 Schematic of the spin coating technique.

Ag nanoparticles ink was prepared by diluting the Ag nanopaste (PARU Corp.) by adding ethylene glycol as solvent in a 50% concentration by weight. The solution was mechanically stirred for 15 minutes followed by bath sonication for another 15 minutes. The Ag nanoparticles ink was then spin coated on the PDMS substrates to uniformly cover an area of 10×5mm at a spin speed of 750 rpm for 20 seconds with a 5 second ramp in the beginning and end stages. Figure 5-2 shows the smooth and rough (having micro ridges) PDMS substrates after spin coating and sintering the Ag nanoparticles films on them. It is evident that the micro ridges due to viscous friction helps in retaining the ink on the hydrophobic PDMS surface, while no coating is observed on the smooth PDMS even if the spin coating procedure was repeated at lower spin speeds and times.

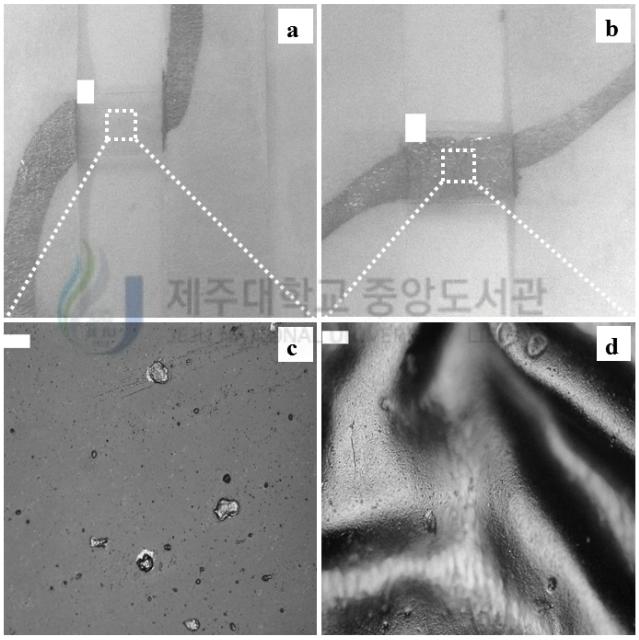

Figure 5-2 Spin coating of Ag nanoparticles based films on rough PDMS substrates. (a) Plain PDMS substrate, (b) rough PDMS substrate, (c) micrograph of plain PDMS substrate indicating no deposition of Ag film and (d) micrograph of rough PDMS substrate showing the spin coated Ag film. Scale bar in (a) and (b) is 2 mm while in (c) and (d) is 50 μm.

This effect can also be explained by observing Figure 5-3 which depicts that PDMS substrate having random micro ridges has resisted the motion of water droplet on its surface after the application of an external force (sudden downward jerk). On contrast, the water droplet has been allowed to spread on the plain PDMS substrate. This simple experiment explains the fact why the Ag nanoparticles ink retained on rough PDMS substrates even after the

application of centrifugal forces that were continuously acting during the spin coating process. Based on this observation, and compared to water, it can be claimed that the presence of nanoparticles in conductive inks must have further increase this effect due to enhance viscous friction.

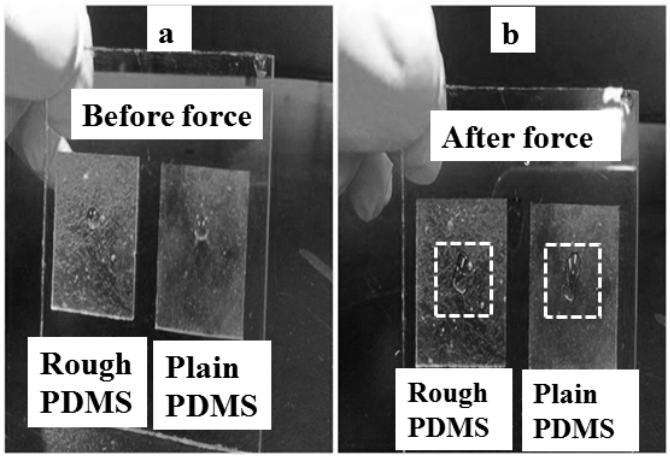

Figure 5-3 Experiments showing the retention and spreading of water droplet on rough and plain PDMS substrates. (a) Before the application of external force (sudden downward jerk) and (b) after the application of the external force. Note that within the dotted region the water droplet on the plain PDMS substrate has spread more compared to the rough PDMS substrate.

Also Figure 5-4 shows that the presence of random micro ridges has assisted the adhesion of the spin coated Ag film on the rough PDMS substrate.

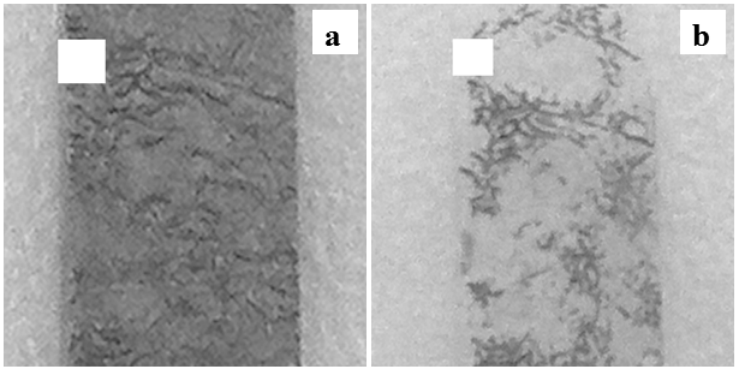

Figure 5-4 Photograph showing the adhesion of Ag nanoparticles based film on rough PDMS substrate. (a) Before tape test and (b) after tape test. Scale bar in each figure is 1 mm.

These results are encouraging in the sense that spin coating (a low cost and non-vacuum based thin film deposition technique) can work well with the hydrophobic PDMS substrates having random micro ridges. However, it was observed that due to the viscous friction of the micro ridges the spin coating procedure has to be repeated several times (3 to 4 times) in order to fully and uniformly cover the substrate area (each time a small volume of ink (5μL) was used). Finally the as fabricated films were sintered at 100^{o}C for 60 minutes and then brought to ambient temperature inside the furnace. It is to be noted that due to the randomness and complexity of the micro ridges the measurement of the film thickness by optical means was difficult therefore the gravimetric analysis (Trifigny et al. 2013) was used to estimate the average film thickness and was found to be 14 μm. The gravimetric analysis requires the measurement of the mass of the substrates with and without the films using a precision mass balance (0.01mg least count). The thickness can then be estimated from $t \approx m_f / \rho_f A_s$ (where t is the thickness of the thin film, m_f is the mass of the thin film, ρ_f is the bulk density of the film's material and A_s is the surface area of the film).

5.1.1 Micro ridged type roughness generation and characterization

The roughness on one surface of the PDMS substrates was generated by patterning the PDMS against sacrificial wrinkled aluminum foils. The wrinkled aluminum foils were prepared by squeezing and unfolding the foils (45 to 50 mm in diameter and 10 μm in thickness) six times as shown in Figure 5-5.

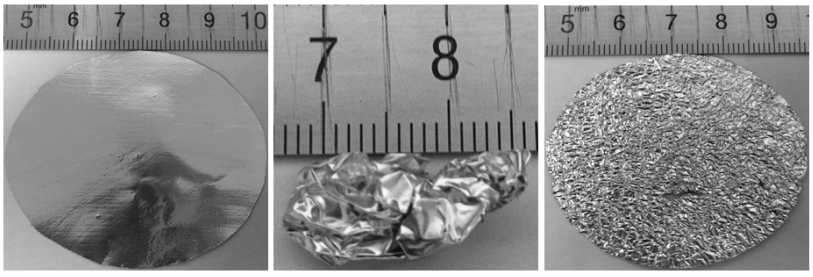

Figure 5-5 Sequence showing the generation of random micro ridges on a sacrificial aluminum foil substrate.

This methodology generates random micro ridges on the aluminum foil which were finally suppressed by using a soft hammer (since large amplitudes of the ridges can severely reduce

the stretchability of the PDMS substrates). These wrinkled aluminum foils were than stick on to the glass substrates using a double sided stick tape. Liquid PDMS was prepared by mixing the base and cross linker agents in 10:1 ratio by weight (10% concentration by weight of the cross linker in base), respectively and were degassed in a vacuum chamber for 20 minutes before casting them on the wrinkled aluminum foils. The casted PDMS was then cured inside an oven at 100^{o}C for 35 minutes and then again brought to room temperature inside the oven. This entire recipe is known to give a Young's modulus value of approximately 1MPa for the prepared PDMS substrates (Fuard et al. 2008). The cured PDMS was then cut into substrate size of 20×5×1mm. Figure 5-6 shows the SEM images of a typical PDMS surface having random micro ridges. From the SEM images a roughness ratio $r = a/b$ (where r is the roughness ratio, a is the average height of the ridges and b is the average peak to peak distance between the ridges) (Lambricht et al. 2013) was defined and was found to be 0.31.

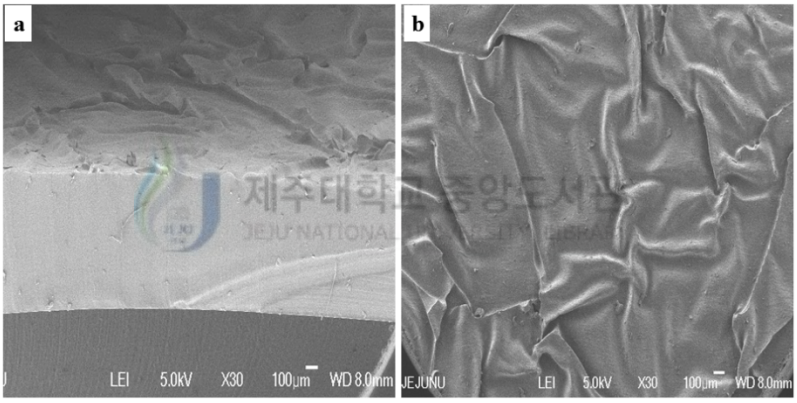

Figure 5-6 Scanning electron microscope (SEM) images of a typical rough PDMS substrate having random micro ridges on its surface. (a) Lateral view and (b) top view. Scale bar in each figure is 100 μm.

5.1.2 Stretchability of spin coated Ag films on random micro ridged type PDMS

Figure 5-7 depicts the variation of the normalized resistance with axial strain for three tested samples.

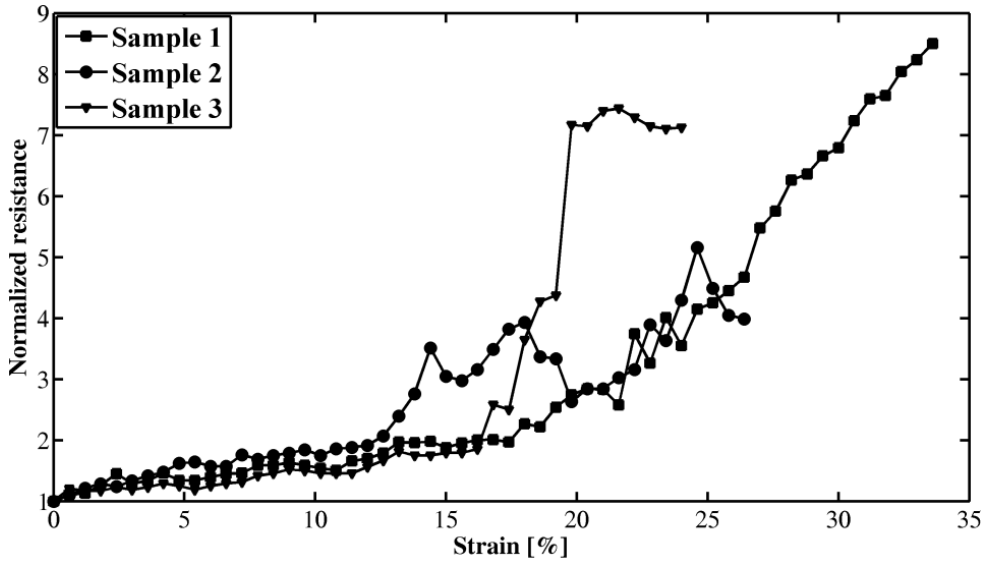

Figure 5-7 Variation of normalized resistance with axial strain for spin coated Ag films on PDMS substrate having random micro ridges. The symbols signify that three samples were tested. All three samples were prepared by following the same experimental protocols.

From Figure 5-7 the maximum average failure strain that resulted in complete rupture of the films and thus open circuit (also known as the maximum stretchability) was found to be 28% for this metal-polymer laminate. It was found that the normalized resistance at this strain increases up to 7 times that of the initial value (on average). It can be observed from the above figure that, as the axial strain exceeds 16% roughly the variation among the curves tend to increases which could be possibly due to the random nature and thus the difference in the roughness patterns on the surface of the samples. Therefore, a suitable model that fits the experimental data with a coefficient of determination (COD) of 0.92 within 16% of the axial strain was finally used and is shown in Figure 5-8 which represents an average of all curves given in Figure 5-7.

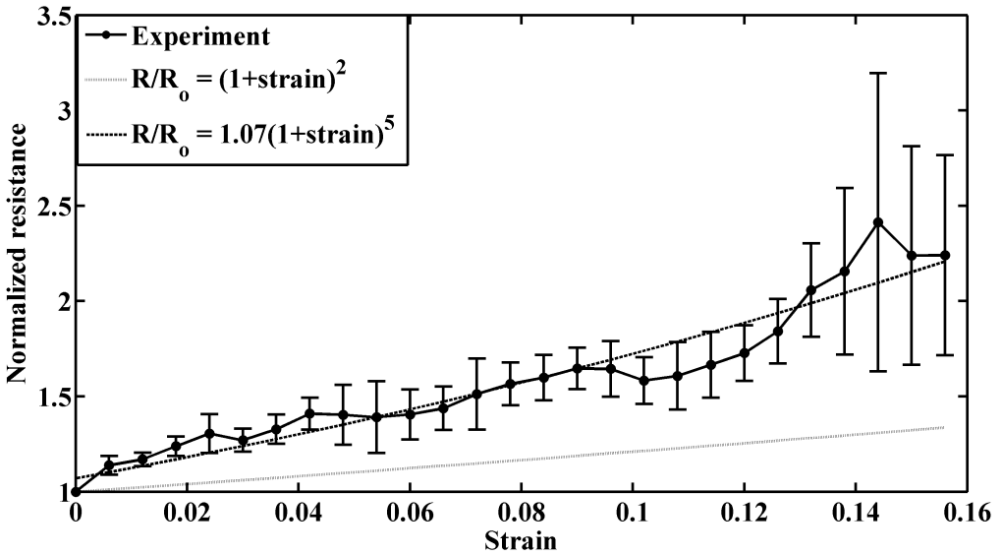

Figure 5-8 Variation of the normalized resistance within 16% axial strain for spin coated Ag films on PDMS substrate having random micro ridges. Error bars represent standard deviations in the experiments.

In Figure 5-8 it can be noticed that the increase in the normalized resistance is less than 2.5 times that of the initial value. A comparison of the reference model ($R/R_o = (1+strain)^2$) (Lu et al. 2007) with the experimental curve is also shown. It can be noticed that the fitted model of the form ($R/R_o=1.07(1+strain)^5$) matches better with the experimental data points. This is due to the fact that the change in resistance of the as-fabricated film actually depends on both the geometric part and the piezoresistive part according to the theoretical expression of the form [$\Delta R/R_o = (1+\nu+\beta)\varepsilon$] where ΔR is the change in resistance of the film, R_o is the initial resistance, ν is the Poisson's ratio of the film material, β is the piezoresistive coefficient and ε is the applied axial strain (Lang, Rust, et al. 2009). In this equation $(1+\nu)\varepsilon$ represents the geometric part whereas $\beta\varepsilon$ represents the piezoresistive part. Since, the reference model ($R/R_o=(1+strain)^2$) ignores the dependency on the piezoresistive part, the deviation with the experimental data points in the above figure suggest that the change in resistance of the spin coated Ag films on PDMS substrates having random micro ridges also depends on the piezoresistive portion. Therefore, the fitted equation models the experimental data with much better accuracy. This discussion leads to the fact that these spin coated Ag films on PDMS substrates having random micro ridges possesses piezoresistive sensitivity. Therefore, based on the statistics of the experiments, the variation of the normalized resistance as a function of

axial strain for the spin coated Ag nanoparticles films on rough PDMS with random micro ridges can be given by equation (5-1).

$$R/R_o = 1.07(1+\text{strain})^5 \quad (5\text{-}1)$$

The evolution of the microcracks with the applied strain explains important facts regarding how these micro ridges enhances the stretchability and preserves the cracking morphology of the film. Figure 5-9 depicts that firstly these randomly connected micro ridges forms multiple interconnected network of conductive paths for the current during stretching.

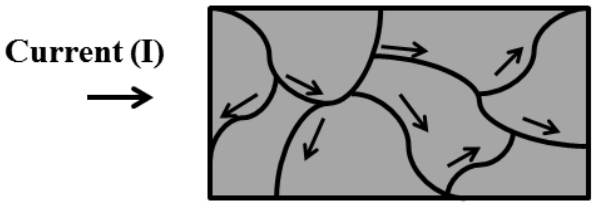

Figure 5-9 Schematic showing micro ridges forming network of interconnected multiple conductive paths.

Secondly Figure 5-10 indicates that these random micro ridges can arrest the cracks within the region between them and therefore reduces the crack propagation and preserve the morphological state of the film.

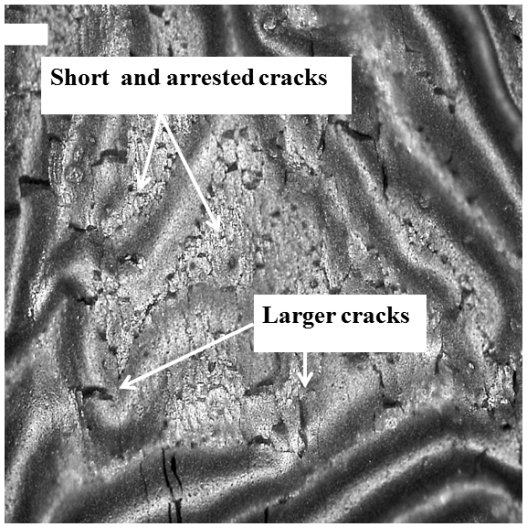

Figure 5-10 Micrograph showing short and arrested cracks in the region located between the micro ridges and few larger cracks on the micro ridges. Scale bar is 100 μm.

An interesting phenomenon was found to exist in this metal-polymer laminate which is attributed to the above mentioned reasons. Once the films were fully stretched to their limit (≈28%) which eventually resulted in an open circuit, the films were found to preserve their crack morphologies as shown in Figure 5-11.

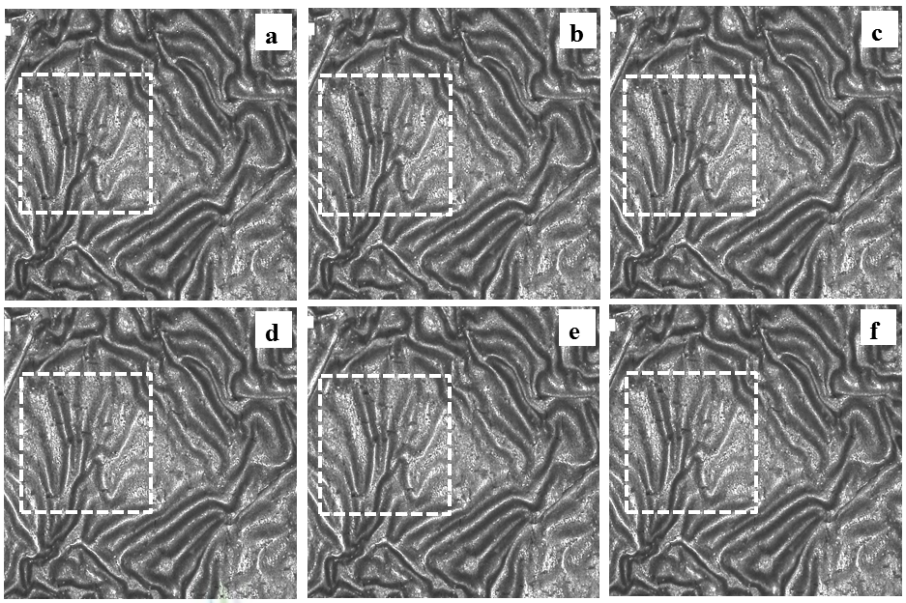

Figure 5-11 Micrographs of typical Ag nanoparticle film on PDMS having random micro ridges during stretching with in the low zone of applied strain (after the first full stretching cycle). (a) 0 % applied strain, (b) 0.6 % applied strain, (c) 1.2 % applied strain, (d) 1.8 % applied strain and (e) 2.4 % applied strain. Scale bar is 50 μm in all figures.

It can be noticed, that this particular effect actually renders a useful property of repeatability under a small zone of applied strain (up to 2.4%) to these films. Figure 5-12 shows this result where three test samples were first stretched up to complete rupture (open circuit) and then they were again stretched for total of three times under low zone of applied strain (up to 2.4%).

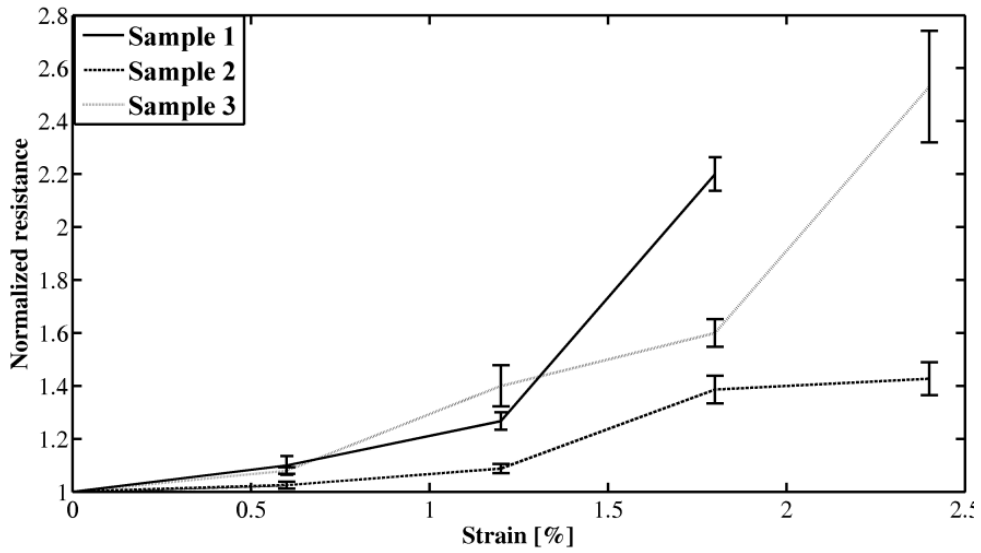

Figure 5-12 Variation of normalized resistance with strain under low zone of applied strain (after the first full stretching cycle). The error bars on each curve represents the standard deviation in the measured resistance at applied strain over three stretching cycles.

The result clearly demonstrate the fact that under low zone of applied strain and owing to the preserved crack morphology, the metal-polymer laminate was able to give repeated values of the resistance at a given value of applied strain. This useful effect can be utilized for the measurement of small strains and motion detection in applications like microelectromechanical systems.

5.2 Rod coated Ag films on micro trenched type ultra-low modulus PDMS

Rod coating is a cost effective, scalable and non-vacuum based thin film fabrication technique. The schematic of the rod coating process used in this study is shown in Figure 5-13.

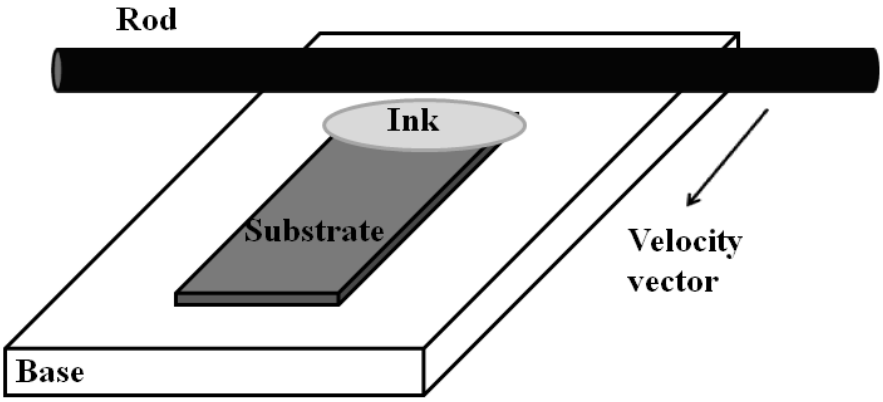

Figure 5-13 Schematic of the rod coating process.

Usually rod coating is for large area film fabrication however, substrate sizes of order of mm can also be used. A steel rod with wire wound on it is used to apply films on substrates like PET or PI sheets. In rod coating process controlled pressure and rod speed are important factors for achieving high quality films. The film thickness depends on the wire diameter and its spacing, the ink formulation and the substrate temperature (Liu & Yu 2011) and (Murphy et al. 2011). The entire process is scalable and can be made fully automatic as well.

Ag nanoparticles based ink for this metal-polymer laminate was synthesized by diluting the Ag nanopaste (PARU Corp. Korea) by adding ethylene glycol in it as a solvent. 30% concentration by weight of Ag nanopaste was diluted in ethylene glycol and the dispersion was thoroughly shaken before applying the films. First the back sides of the PDMS substrates were sprayed with KF96 lubricant (Shin-Etsu Chemicals, Japan). Spraying the lubricant was found to assist in easy removal of the samples containing the sintered films from the glass substrates and avoided pre cracking of the films. After this step the PDMS substrates were exposed to ultra-violet ozone (UVO) treatment for 10 minutes, it was observed that higher exposure times tend to generate cracks on the silica like layer that results from the UVO treatment of the ultra-low modulus PDMS (Berdichevsky et al. 2004). Total of two coats were applied in order to fabricate the films with an intermediate heating step of 100^{o}C for 15 minutes on a hot plate in ambient air. Each time a measured drop of ink having a volume of 2 μL was dropped on the PDMS substrates and a smooth steel rod having a diameter of 2.5 mm was gently pulled over the substrate with a velocity of 5 mm/s to apply the films. After

applying the final coat, the films were baked on the hot plate at 100^{o}C for 1 hour in ambient air. The samples were finally removed from the hot plate once the temperature reaches the ambient. Figure 5-14 shows different images of the as fabricated silver nanoparticles films on the rough ultra-low modulus PDMS having trench type roughness. It can be seen from Figure 5-14 that within the patterned region the substrate is fully covered with the Ag film such that the trenches are also nearly filled. In addition it can be seen that baking the film on a hot plate at 100^{o}C for 1 hour substantially causes the nanoparticles to sinter (see Figure 5-14(d)). Consequently, the as-fabricated films were found to be conductive immediately after the sintering process.

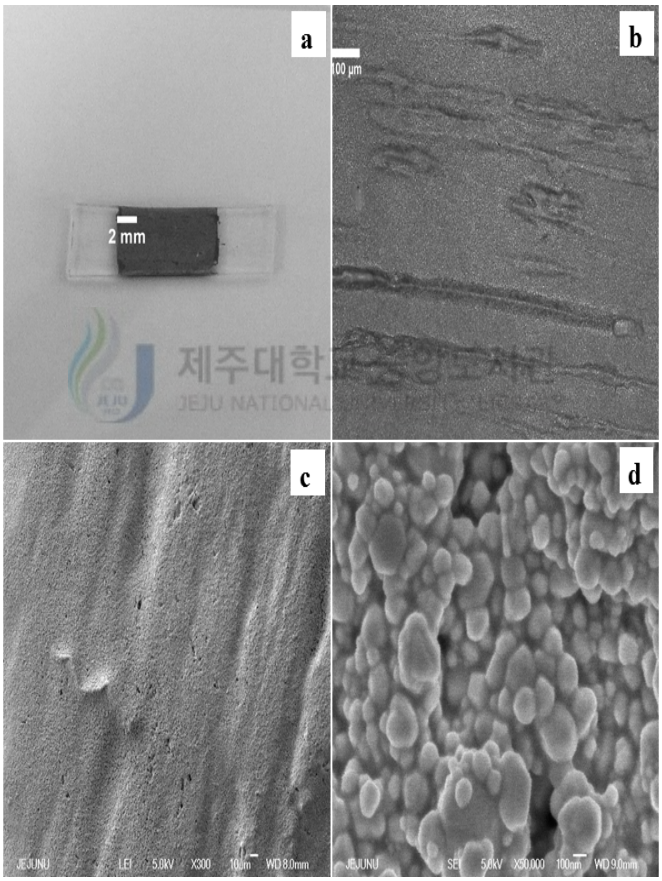

Figure 5-14 (a) Photographic image of the rod coated Ag film on ultra-low modulus PDMS having trench type roughness. (b) Micrograph of the rod coated Ag film on ultra-low modulus PDMS having trench type roughness. (c) and (d) SEM images of the rod coated Ag film on ultra-low modulus PDMS having trench type roughness. Scale bar in (b), (c) and (d) is 100 μm.

The film thickness was estimated from analysis of the SEM images and was found to be 7 μm on average. A typical SEM image depicting the film thickness is shown in Figure 5-15.

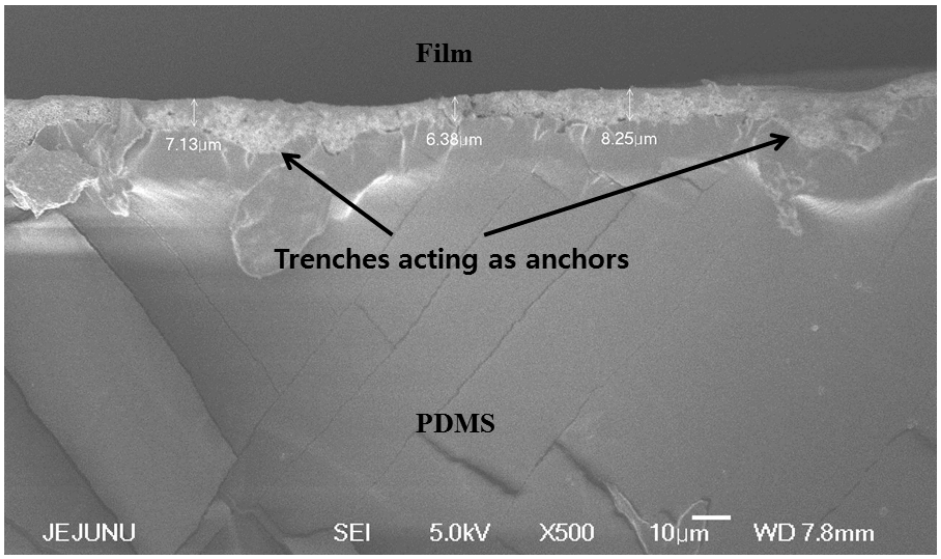

Figure 5-15 Typical SEM image showing the thickness of the rod coated Ag film on ultra-low modulus PDMS substrate having micro trench type roughness.

5.2.1 Micro trenched type roughness generation and characterization

In order to prepare ultra-low modulus PDMS substrates the cross linker was mixed with the base in concentration of 3% by weight (10:0.3 weight ratio) and the mixture was thoroughly stirred for 2 minutes. This mixture was then placed inside a vacuum chamber for 20 minutes in order to remove the air bubbles. Clear solution in amounts of 1 mL volume was then poured on PET covered glass substrates with the help of a syringe and the substrate was spin coated at 30 rpm for 30 seconds with a 1 second ramp in the beginning and end stages. These PDMS substrates were then baked at 100^{o}C for 3 hours inside a convection oven and finally brought to the room temperature inside the oven. This entire procedure is known to give a Young's modulus of 120-140 kPa for the PDMS substrates used in this study (Fuard et al. 2008). The samples were then cut into strips having dimensions of length 20 mm, breadth 5 mm and an average thickness of 622 μm using a sharp blade. A sand paper was used to generate the trench type roughness by gently applying strokes on one surface of the PDMS. The strokes were unidirectional i.e. only along the length of the substrate and were applied from top to bottom. These strokes were limited to 50 strokes per direction i.e. after applying

the strokes in one direction, the substrates were rotated by 180^{o} and another 50 strokes were applied. Figure 5-16 shows the SEM images of the rough PDMS substrate having random scratches on its surface. It can be seen from Figure 5-16 that these scratches actually form narrow trenches on the surface with an average width of 100 μm and an average depth of 11 μm. For estimating the average depth of trenches different SEM images were used.

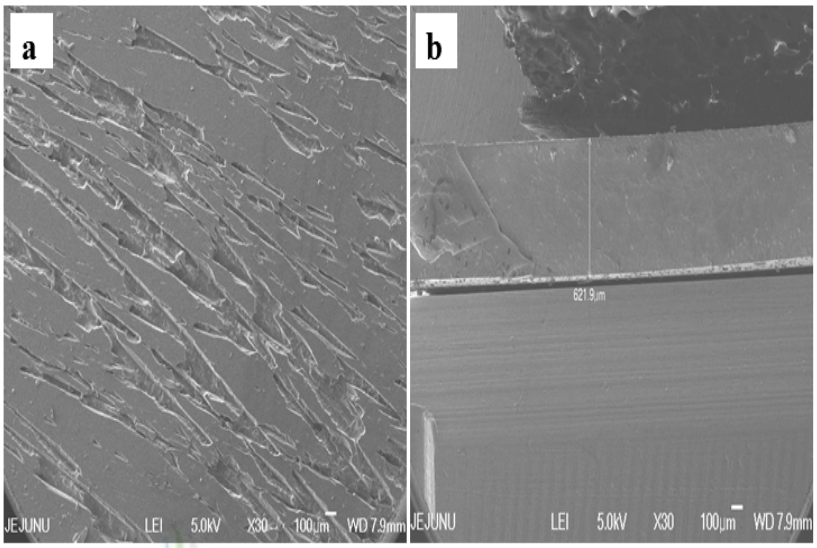

Figure 5-16 SEM images of ultra-low modulus PDMS substrate having micro trench type roughness. (a) Top view and (b) lateral view. Scale bar is 100 μm in both figures.

The roughness was characterized using high accuracy noncontact surface profiler Nanoview E-1000 (NanoSystems). An area (A_s) of 0.622×0.466 mm^2 was scanned on total of 10 substrates. Figure 5-17(a) represents one such typical image. In Figure 5-17(a) the average roughness excluding the trenches is shown and was found to be ($R_{a,u}$= 0.66 μm) while Figure 5-17(b) shows the image of the same area focusing the trenches only. The roughness within the trenches was found to remain much higher than the unscratched or untrenched regions and was equal to ($R_{a,t}$= 4.22 μm). Using these images in image analysis software the total area of trenches (A_t) was subtracted from the total scanned area (A_s) which gives the total area of the unscratched or untrenched regions (A_u). Finally, based on the average roughness values for the untrenched and trenched regions, and their respective areas, a cumulative area average roughness (R_{ca}) was calculated from the equation (R_{ca}= ($R_{a,u}$×A_u+$R_{a,t}$×A_t)/A_s) (Syed Murtuza Mehdi et al. 2014) and was found to be 2.29 μm for these ultra-low modulus PDMS substrates having trench type roughness patterns.

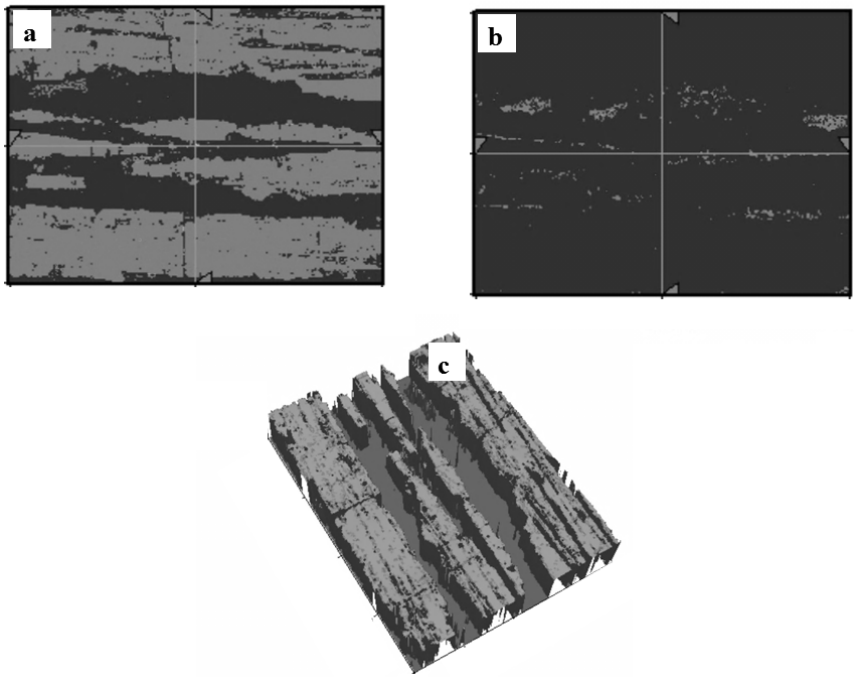

Figure 5-17 (a) Typical surface scan of an untrenched region having an area average roughness of 0.66 μm. (b) Typical surface scan of trenched region only having an area averaged roughness of 4.22 μm. (c) 3D scan of (a) where removed regions are the micro trenches. The scan area in each figure is 0.622×0.466 mm^2.

5.2.2 Stretchability of rod coated Ag films on micro trenched type ultra-low modulus PDMS

Figure 5-14 and Figure 5-15 indicates that the rod coated Ag films completely fills the micro trenches and further these trenches acts like anchor points which can enhance the adhesion between the films and the substrate during stretching. Also it is known that the presence of micro trenches provides sites for mechanical interlocking effect of nanoparticles and increases the adhesion (Joo 2009). Consequently, Figure 5-18 indicates that this metal-polymer laminate is able to achieve maximum stretchability (maximum strain before complete rupture) of approximately 25% on average untill the films suddenly ruptures by cracking as shown in Figure 5-19. It can also be noticed that the normalized resistance only minutely changes among different curves which is a desirable property for stretchable conductors and resistors.

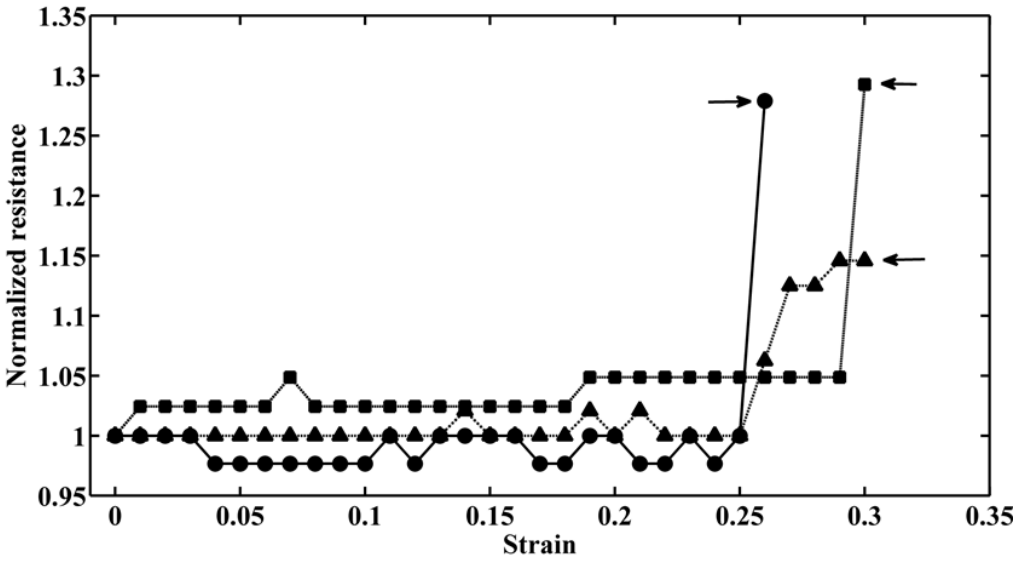

Figure 5-18. Variation of normalized resistance with axial strain for rod coated Ag films on ultra-low modulus PDMS having micro trench type roughness. Symbols represent three tested samples that were all prepared by following exactly the same experimental protocols whereas arrows indicate point of electrical failure (open circuit).

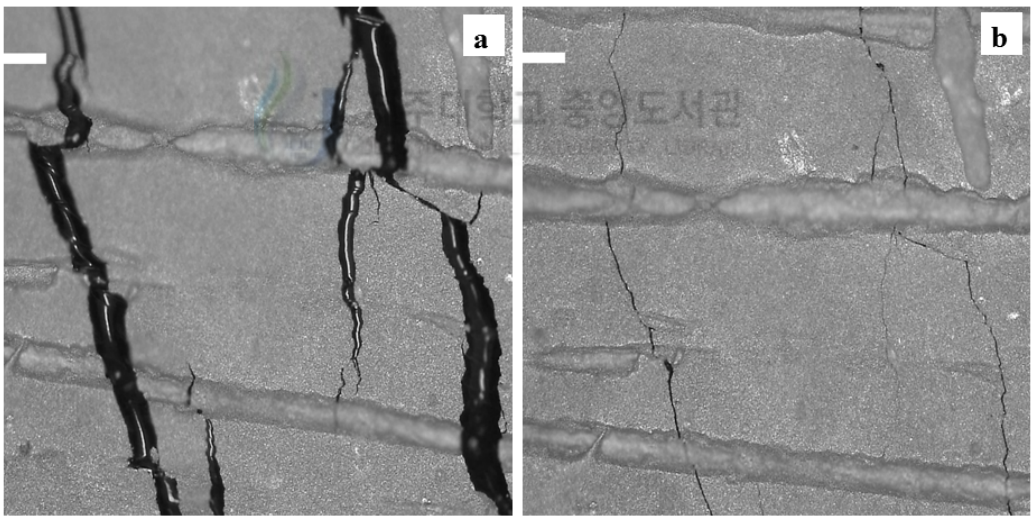

Figure 5-19 Typical micrographs of (a) cracked and (b) unstrained or relaxed Ag film on ultra-low modulus PDMS having trench type roughness. The scale bar in (a) and (b) is 100 μm.

From Figure 5-19 (b) it can be noticed that on complete removal of the strain the cracks width significantly reduces. This particular characteristic of the rod coated Ag films on ultra-low modulus PDMS having micro trench type roughness renders these films to regain their initial value of the resistance by 94% on average.

5.2.3 Flexibility of rod coated Ag films on micro trenched type ultra-low modulus PDMS

The rod coated Ag nanoparticles films on ultra-low modulus PDMS having trench type roughness were not only stretchable but were also found to remain functional when bent on curved surfaces. Figure 5-20 shows the variation of the normalized resistance of three tested samples with respect to different bending radii. It can be seen that the overall increase in the resistance of these films during bending was on average limited to 1.04 times their initial resistance which occurs at the smallest test radius of 5 mm. These films resulted immediately in an open circuit when bent at a radius of 4 mm. The approximate failure strain in bending for the as fabricated films can be estimated from equation (5.2) (Cho et al. 2011; Lipomi et al. 2012)

$$\varepsilon_b = (t_f + t_s)/2r \qquad (5\text{-}2)$$

Where ε_b is the bending strain, t_f is the film thickness, t_s is the substrate thickness and r is the radius of the rod and was found to be 7.86 %.

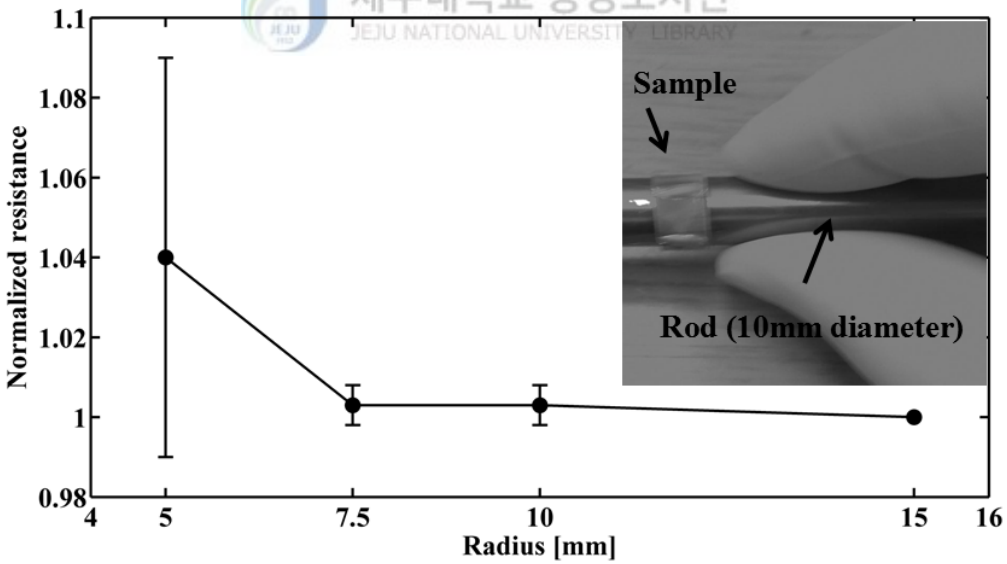

Figure 5-20 Variation of normalized resistance for rod coated Ag films on ultra-low modulus PDMS having trench type roughness with different bending radii. The inset shows the photographic image of the sample being bent on a rod.

These films also show functionality when repeatedly bent at a radius of approximately 6 to 8 mm up to 1000 times. Figure 5-21 depicts the resistive behavior of the as fabricated films at various bending cycles (data for three tested samples is shown). The average increase in the resistance at the end of the 1000^{th} cycle was only 1.07 times the initial value. These results render the as fabricated films to be exploited as flexible resistors in applications where the device must maintain its functionality during repeated conformal contacts with curved surfaces.

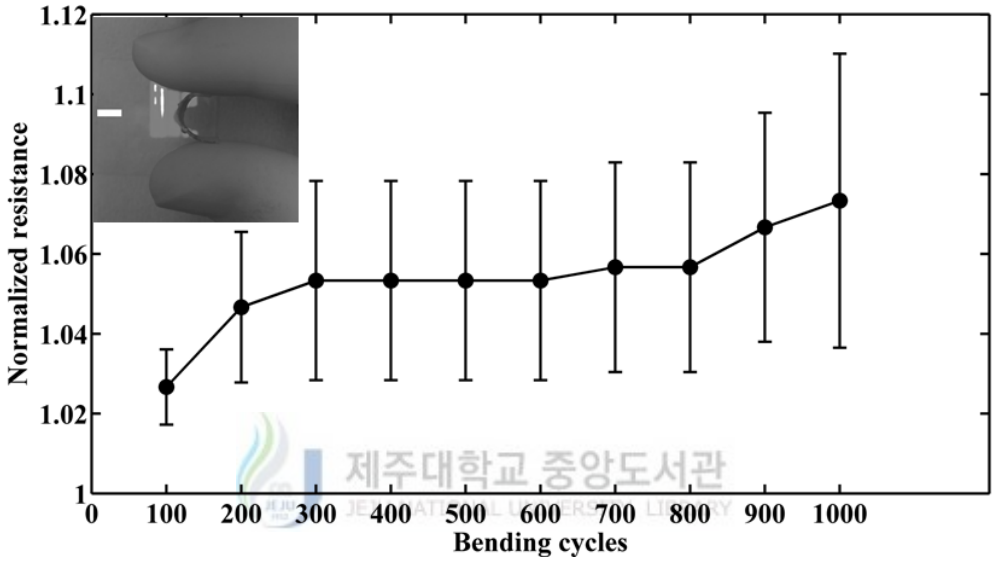

Figure 5-21 Variation of normalized resistance for rod coated Ag films on ultra-low modulus PDMS having micro trench type roughness with the number of bending cycles. The inset shows the photograph of a typical sample being bent. The scale bar is 10 mm.

5.3 Electrospray deposition (ESD) of Ag nanoparticles films on acid etched rough PDMS

Electrospray deposition (ESD) is a non-vacuum based and cost effective thin film fabrication technique. It has been widely used to deposit thin films of conductive as well as semiconducting materials which can be used as functional thin layers in numerous electronic devices (Duraisamy et al. 2013; Muhammad et al. 2012; Choi et al. 2010). In ESD high DC voltage typically in orders of kV is applied between a metallic nozzle and a ground substrate separated by an optimized distance, so called the standoff distance. The liquid ink is fed to the electrified nozzle through a syringe pump at a specified flow rate. As the liquid reaches the nozzle's outlet the electrostatic force field tends to atomize the liquid ink into a fine spray

containing charged droplets. These droplets are then deposited on the desired substrate that is kept below the spray nozzle for a specified time. After the deposition the material can be baked or annealed to form a continuous functional film. The schematic of the ESD experimental setup used in this study is shown in Figure 5-22 whereas the photograph of the ESD experiment is shown in Figure 5-23.

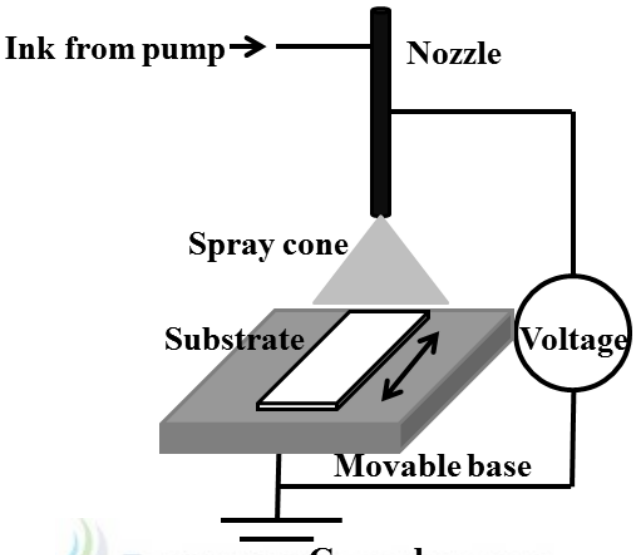

Figure 5-22 Schematic of the ESD experimental setup.

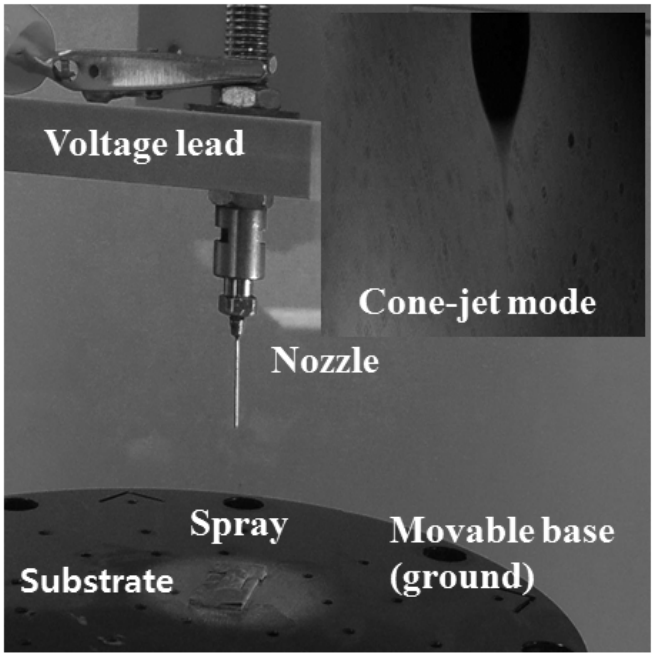

Figure 5-23 Photograph taken during the ESD of Ag films on ultra-low modulus PDMS. The inset shows the cone-jet mode of spray.

The Ag nanoparticle ink for the ESD process was prepared by adding 47 wt% of Ag nanopaste (PARU Co. Ltd. Korea) in ethylene glycol as a solvent. The solution was thoroughly shaken for 5 minutes. The viscosity was measured to be 42×10^{-3} Pa.s with the help of a rotating viscometer (Sekonic Corporation Japan). For preparing PDMS samples with Young's modulus of approximately 1 MPa 10 wt% of the cross linker was thoroughly mixed with the base and was degassed inside a vacuum chamber in order to remove all air bubbles. Clear PDMS solution was then poured on PET covered glass substrates in amounts of 1 mL volume and was spun at 30 rpm for 30 seconds on a spin coater with 1 second ramp in the beginning and end stages. These samples were annealed at 100 ^{o}C inside a convection oven for 35 minutes. In case of low modulus PDMS (120-140 kPa) 3 wt% of the cross linker was mixed with the base, other protocols remains the same except that the annealing was done at 100 ^{o}C for 3 hours in this case. Following these chemical and thermal protocols the required Young's modulus for the PDMS substrates can be achieve (Fuard et al. 2008). Finally the PDMS castings were cut into substrate sizes of desired dimensions by using a sharp blade cutter.

ESD parameters for the deposition of Ag nanoparticles based films on thin acid etched rough PDMS substrates were same for both the versions of the PDMS used. The important parameters were flow rate = $\dot{Q}$ = 200 μL/h, voltage = V = 9.3 kV, standoff distance = 15 to 20 mm and nozzle inside diameter = N_D = 310 μm. The entire deposition process was performed in two steps. In the first step the deposition was performed for 7 minutes and after that the samples were left in ambient condition for approximately 1 hour. In the second step the deposition was performed for 2 more minutes and finally the films were annealed at 100 ^{o}C inside a convection furnace to render themselves conductive. It is to be noted that prior to deposition the Ag nanoparticles ink was bath sonicated for 15 minutes. Figures 5-24(a) and 5-24(b) shows the ESD deposited Ag films on thin acid etched rough PDMS substrates having low and high values of modulus respectively, whereas Figures 5-24(c) and 5-24(d) show the micrograph image of the deposited films after sintering on the low and high modulus PDMS, respectively. As can be noticed from Figure 5-24(c) surface cracks exist on the films that were deposited on the low modulus PDMS. These cracks were due to the mismatch between the coefficient of thermal expansion of low modulus PDMS and the Ag films during the annealing step (Fang & Lo 2000). On the other hand the films deposited on the high modulus PDMS were found to remain crack free for the annealing conditions used in this study. This indicates that the post sintering film condition of ESD deposited Ag films on thin acid etched rough PDMS improves when the Young's modulus is increased. Also Figure 5-24(e) shows the typical film thickness of the ESD deposited Ag film which remains on average 5μm for both the high and low modulus PDMS.

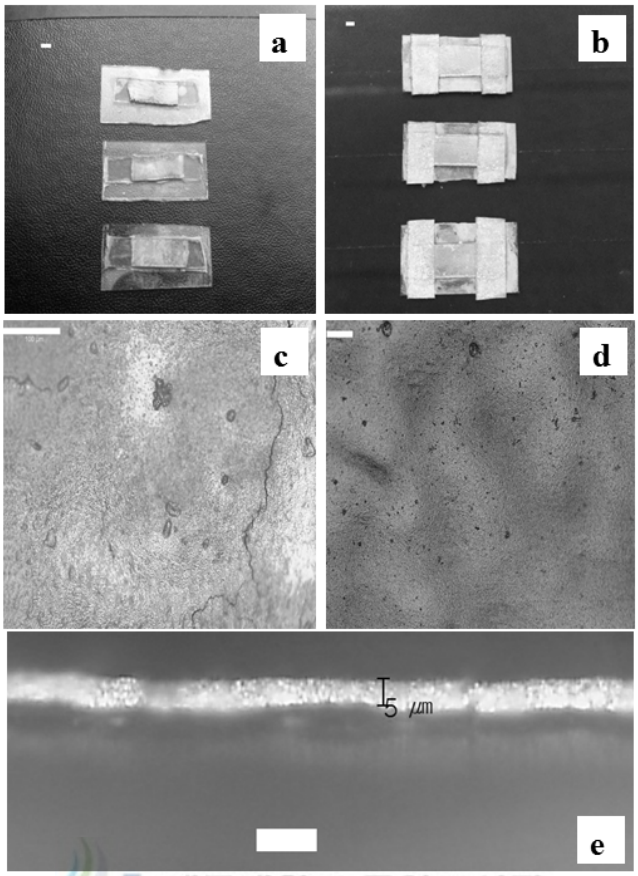

Figure 5-24 Photographs and Micrographs showing ESD deposited Ag films and the thickness of the PDMS substrate. (a) Photograph of the annealed ESD deposited Ag films on low modulus PDMS (initial micro crack is visible), (b) photograph of the annealed ESD deposited Ag films on high modulus PDMS, (c) micrograph of ESD deposited Ag film on low modulus PDMS, (d) micrograph of ESD deposited Ag film on high modulus PDMS and (e) typical thickness of the Ag film. Scale bar in (a) and (b) is 2 mm, in (c) and (d) is 100 μm and in (e) is 10 μm.

5.3.1 Acid etched type roughness generation and characterization

The roughness on the PDMS substrates was generated by using concentrated sulphuric acid (H_2SO_4) etching. The PDMS substrates were stick on to the glass substrates and were completely submerged inside the acid pool for the desired etching times. These substrates were then dipped in DI water for several minutes and bath sonicated in acetone for 15 minutes after which they were scrubbed with the help of a tissue paper and again bath sonicated in acetone for 15 minutes. Finally the substrates were dried by using dry compressed air. The effect of acid etching results in a chemical reaction that dissolves PDMS into smaller subunits consisting of oligomers with different numbers of dimethylsiloxane

subunits (Lee et al. 2003). The effect of acid etching was found to be different on the two versions of the PDMS used in this study. The cause of this difference is mainly attributed towards the amount of cross linker concentration and thus the presence of different numbers of Si-H groups in PDMS (Esteves et al. 2009). At first the etching time for low modulus PDMS was maintain at 10 minutes while that for high modulus was limited to 5 minutes only (higher exposure time resulted in complete decomposition of the high modulus PDMS in concentrated sulphuric acid). Secondly, there was a systematic reduction observed in the length width and thickness of the PDMS substrates after the acid etching was performed. The greatest reduction (on average 32%) was observed in the thickness direction for both the versions of the PDMS. Therefore in order to attain the desired substrate thickness the initial thickness of the PDMS must be properly designed or the etching times must be optimized. Thirdly, the acid etching was found to generate slightly different kinds of roughness patterns on low and high modulus PDMS, respectively. It can be noticed from Figure 5-25(b) that in case of high modulus PDMS, ridges or bumps were observed on the surface while these ridges were not found on the low modulus PDMS (see Figure 5-25(a)). Also it can be seen from Figures 5-25 (c) and 5-25(d) that the area averaged roughness for low modulus PDMS as measured by high accuracy noncontact surface profiler (NanoView E-1000 by Nanosystems) was found to be 2.89 μm while that for high modulus PDMS was 1.93 μm. Total of 15 samples for each type of PDMS were used to quantify the average roughness values. Also Figure 5-25(e) depicts the typical PDMS substrate thickness used in this study that was on average 400 μm.

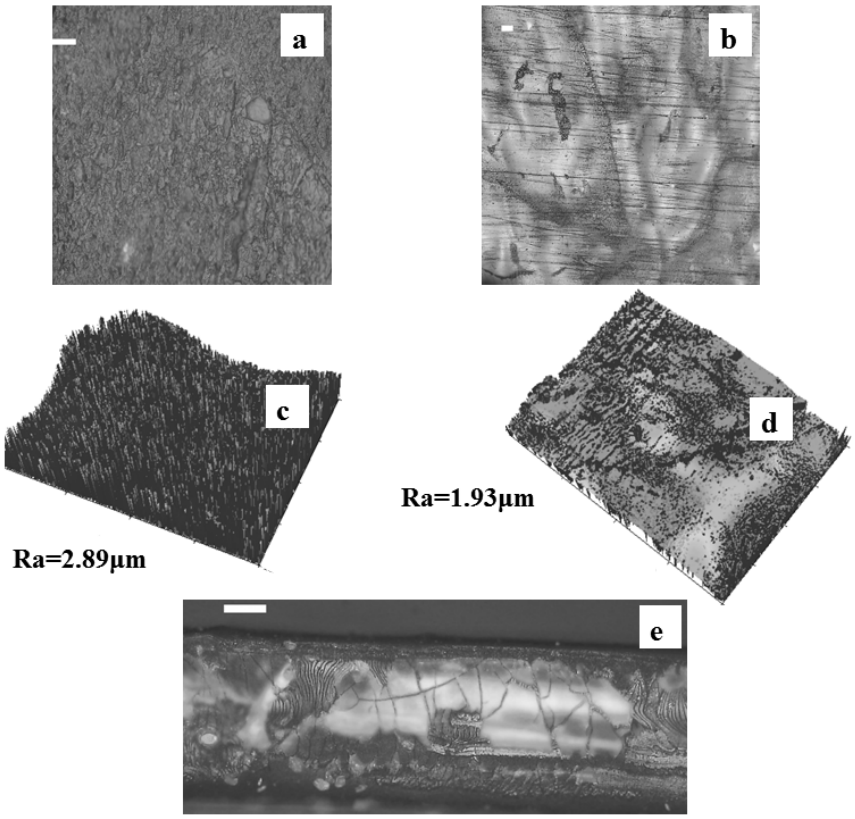

Figure 5-25 Micrographs and 3D optical surface scans showing the rough surfaces of the acid etched PDMS substrates and its typical thickness. (a) Micrograph of acid etched rough low modulus PDMS, (b) micrograph of acid etched rough high modulus PDMS (ridges or bumps are visible on its surface), (c) 3D optical surface scan of low modulus PDMS showing its area averaged roughness, (d) 3D optical surface scan of high modulus PDMS showing its area averaged roughness and (e) micrograph showing the typical thickness of the PDMS samples used in this study. Scale bar in (a) is 50 µm while in (b) and (e) is 100 µm. Scan area in (c) and (d) was kept same during all measurements.

5.3.2 Stretchability of ESD deposited Ag films on acid etched ultra-low modulus PDMS

Figure 5-26 show the variation of the normalized resistance with strain for the ESD deposited Ag films on thin, acid etched rough and low modulus PDMS substrates. It must be noticed that stretchability on very compliant and thin substrates is always difficult to achieve as compared to stiffer substrates (Li et al. 2004, Li & Suo 2006), however, the experimental result are encouraging and reveals that the as-fabricated films on thin and low modulus PDMS can attain an average stretchability of 5.6% before complete electrical failure occurs. The normalized resistance for these films reaches a value of 22.74 and eventually resulted in an open circuit after this point. This rather low value of the failure strain is primarily due to the very compliant nature of the PDMS (low modulus) and its low thickness and secondly

due to the presence of initial surface cracks on the films. However, it must be noted that low modulus substrate with thicknesses of order of micrometer can be useful in applications like epidermal electronics and biomedical implants.

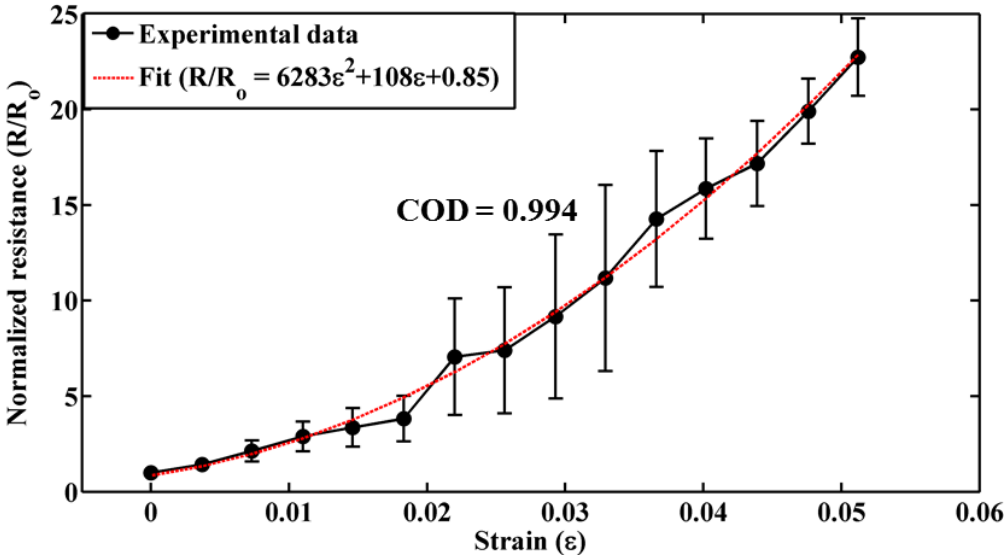

Figure 5-26 Variation of the normalized resistance as a function of axial strain for low modulus PDMS.

Figure 5-27(a) depicts that these ESD deposited Ag films tend to fail by cracking which is known to be a familiar characteristic of thin metallic films on polymer substrates (Niu et al. 2008; Lacour et al. 2003). It is to be noted that no additional precautions such as oxygen plasma treatment, ultra violet ozone exposures and intermediate metal layer depositions were performed to enhance the adhesion of the Ag film, therefore the stretchable behavior is solely due to the type of roughness imparted to the PDMS. After the removal of the strain, on average, the resistance increases by 1.15 times the initial value. This is evident from Figure 5-27(b) which highlights the fact that the cracks tend to close after the removal of the strain, making the films reversibly conductive with minute changes in their resistance.

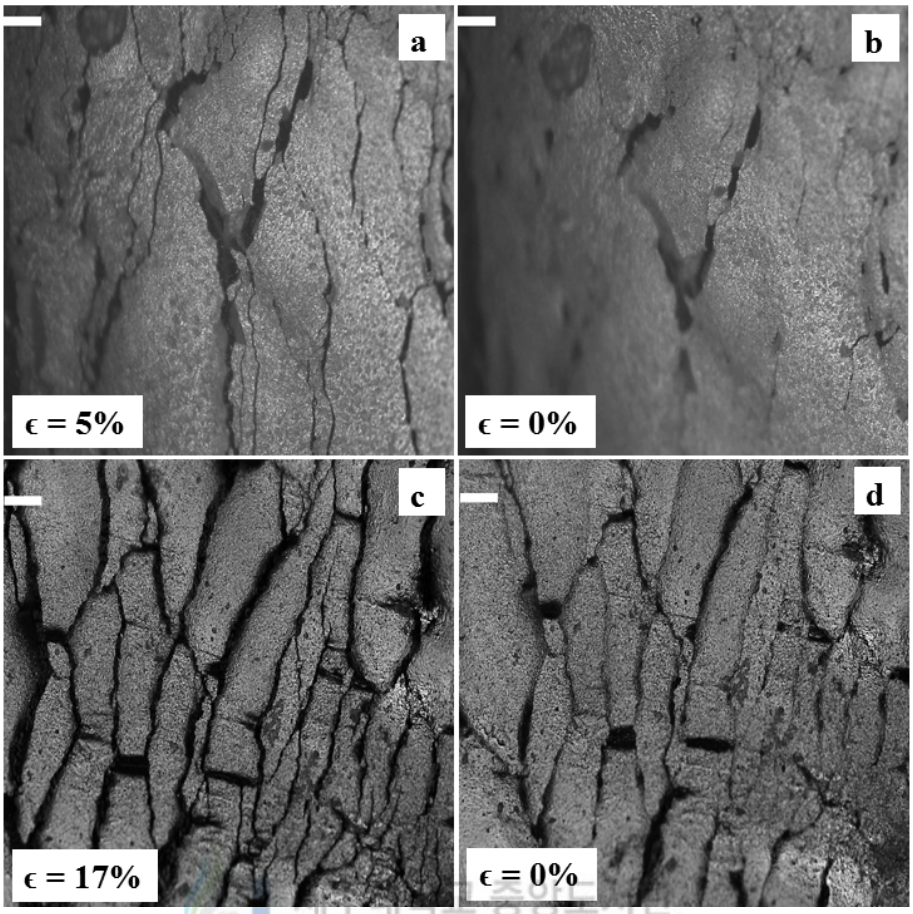

Figure 5-27 Micrographs of ESD deposited Ag films under strain. (a) Micrograph of ESD deposited Ag film on low modulus PDMS at complete rupture (electrical failure) and (b) when the strain was completely removed. (c) Micrograph of ESD deposited Ag film on high modulus PDMS at complete rupture (electrical failure) and (d) when the strain was completely removed. Scale bar is 100 μm in each figure.

If the curve given in Figure 5-26 is made to split in two linear segments and fitted with linear models then the average value of the piezoresistive coefficient (β) can be estimated by comparison to the equation of the type [$\Delta R/R_o = (1+\nu+\beta)\varepsilon$] where ΔR is the change in the resistance ($R-R_o$), R is the resistance at the applied strain, R_o is the initial resistance, ν is the Poisson's ratio of silver and ε is the applied axial strain (Lang et al. 2009). Following this procedure it was found out that the change in the normalized resistance for these ESD deposited Ag films depends 99% on the piezoresistive part rather than the geometric part. Keeping in view this fact, the variation of the normalized resistance as a function of applied strain was fitted with a second order polynomial model given by equation (5-3). Compared to

the simplified models available in the literature the curve fit model in Figure 5-26 was found to best fit the experimental data with a coefficient of determination (COD) of 0.994.

$$R/R_o = 6283\varepsilon^2 + 108\varepsilon + 0.85 \quad (5\text{-}3)$$

These preliminary results are encouraging and suggest that ESD deposited Ag films on thin and low modulus PDMS having acid etched roughness can be made stretchable with moderate increase in their resistances during stretching (it is to be noted that for the range of stretchability mentioned in this paper the change in resistance remains of the same order of magnitude as the initial resistances). Also high dependency on the piezoresistive part suggests changes in resistivity during stretching.

5.3.3 Stretchability of ESD deposited Ag films on acid etched rough high modulus PDMS

As compared to the stretchability of ESD deposited Ag films on thin and low modulus PDMS having acid etched roughness, the stretchability of ESD deposited films on high modulus PDMS was found to be 3 times higher i.e. 17%. Since all other parameters were same, the increase in stretchability is attributed towards high value of the modulus of PDMS which can better delocalize the strain field in the films, thereby increasing the rupture strain. Therefore, Figure 5-28 shows the variation of the normalized resistance as a function of applied strain for ESD deposited Ag films on thin and high modulus PDMS with acid etched roughness. Another favorable result for these films is that the normalized resistance only increases by 4.65 times the initial resistance during stretching.

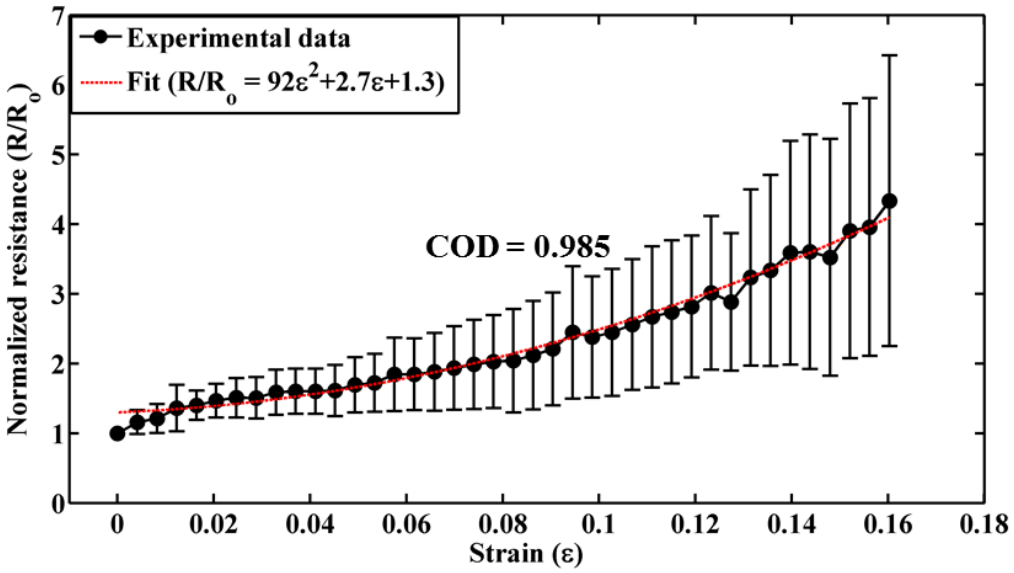

Figure 5-28 Variation of the normalized resistance as a function of axial strain for high modulus PDMS.

Figure 5-27 (c) and 5-27(d) indicates that these films also ruptures by cracking and the cracks tend to close after the removal of the strain, rendering the films reversibly conductive with an increase in the resistance that was only 1.8 times that of the initial resistance. A slightly higher increase in the resistance is due to the fact that these films tend to develop higher number of cracks owing to their high stretchability as compared to the films on low modulus PDMS. It must also be noted that multiple small cracks can divide the film into small islands (see Figure 5-27(c) and 5-27(d)) which can further enhance the stretchable behavior (Gutruf et al. 2013) of the ESD deposited Ag films on thin and high modulus PDMS with acid etched roughness. Fitting a linear model to the curve in Figure 5-28 and following the same procedure as mentioned earlier for the case of Ag films on low modulus PDMS it can be estimated that the variation in the normalized resistance depends 90% on the piezoresistive part. Therefore, a second order polynomial was again found to best fit the experimental data with coefficient of determination (COD) of 0.985 and is given by equation (5-4).

$$R/R_o = 92\varepsilon^2 + 2.7\varepsilon + 1.3 \quad (5\text{-}4)$$

6. Stretchable and Flexible Behaviors of PEDOT:PSS Films on Rough Polydimethylsiloxane Substrates

PEDOT:PSS is an intrinsically conductive polymer that has potential applicability in electronic devices like flexible solar cells, stretchable conductors, organic light emitting diodes, electromechanical actuators, and thermoelectric generators. PEDOT:PSS has also been found to remain chemically stable and soluble with many different solvents which can further improve its conductivity and hence its functionality making it a promising material for organic electronics. This chapter presents results for stretchable and flexible behaviors of PEDOTPSS films on rough PDMS substrates fabricated by non-vacuum based techniques.

6.1 Blade coated PEDOT:PSS films on micro ridged type PDMS

Figure 6-1 shows the simple schematic of the blade coating apparatus. Blade coating is a cost effective, scalable and non-vacuum based thin film fabrication technique that has been used for the fabrication of polymer solar cells, thin film batteries, organic thin film transistors and copper indium diselenide films for photovoltaic applications (Chang et al. 2009; Gaikwad et al. 2013; Pierre et al. 2014; Lee et al. 2010). In blade coating, the moving blade carries liquid into the gap between the free end of the blade and the substrate. Due to the moving blade the liquid is dragged towards the gap between the blade and the substrate increasing the hydrodynamic pressure near that region. Thus, adverse pressure gradient acts that induces a pressure-gradient flow component that opposes the viscous-drag driven flow component. In this way most of the liquid remains behind and only a fraction is allowed to pass through the gap between the blade and the substrate forming the final film (Pranckh & Scriven 1990).

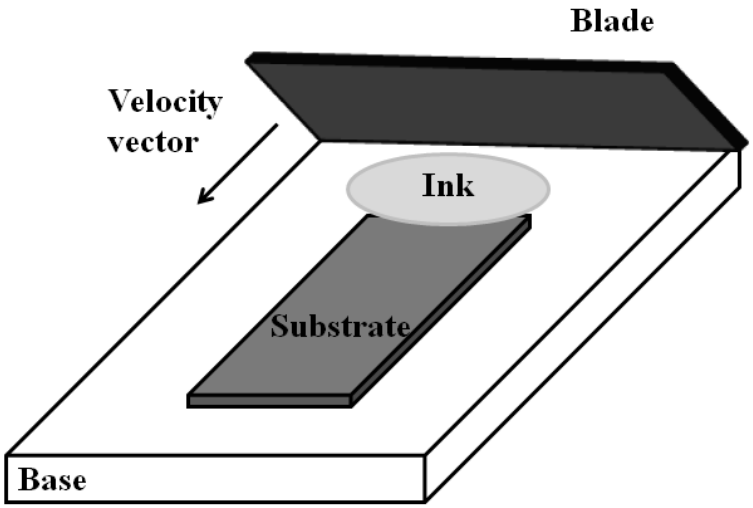

Figure 6-1 Schematic of the blade coating technique.

PEDOT:PSS paste was purchased from AGFA Materials (Japan) and was applied on the PDMS substrates using the miniaturized blade coating apparatus whose schematic is shown in Figure 6-1. The blade velocity was kept at 26 mm/sec for all samples prepared in this study. The PEDOT:PSS films were annealed at a temperature of 110^{o}C for 15 minutes inside a furnace (REF). Figure 6-2 shows the as fabricated PEDOT:PSS films on PDMS substrates having random micro ridges. Due to the presence of complex roughness patterns the film thickness was measured using gravimetric analysis (Trifigny et al. 2013). The mass of the PDMS substrates were measured with and without the films on a precision mass balance having a least count of 0.01mg and the thickness was estimated from the definition of the density. The average thickness was found to be 16 μm for these blade coated films.

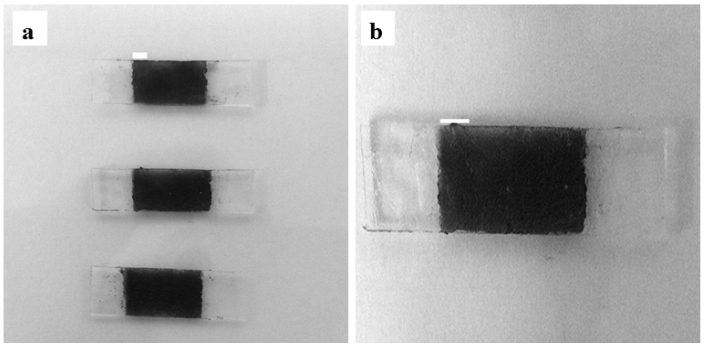

Figure 6-2 Photographs of the blade coated PETDOT:PSS films on PDMS substrates having random micro ridge type roughness. Scale bar in (a) and (b) is 2 mm.

The procedure for generating and characterization of the random micro ridges on the surface of the PDMS remains the same as explained in section 5.1.1 consequently, the roughness ratio for the PDMS samples in this study was once again found to be 0.3.

6.1.1 Stretchability of blade coated PEDOT:PSS films on micro ridged type PDMS

Figure 6-3 shows the variation in resistance as a function of axial strain for the as fabricated PEDOT:PSS films on PDMS substrate having random micro ridges for three tested samples. From this figure it can be seen that the films remain conductive even at an average strain of 78% but with an increase in the value of resistance that is on average 19 times higher than the initial resistance (unstretched condition).

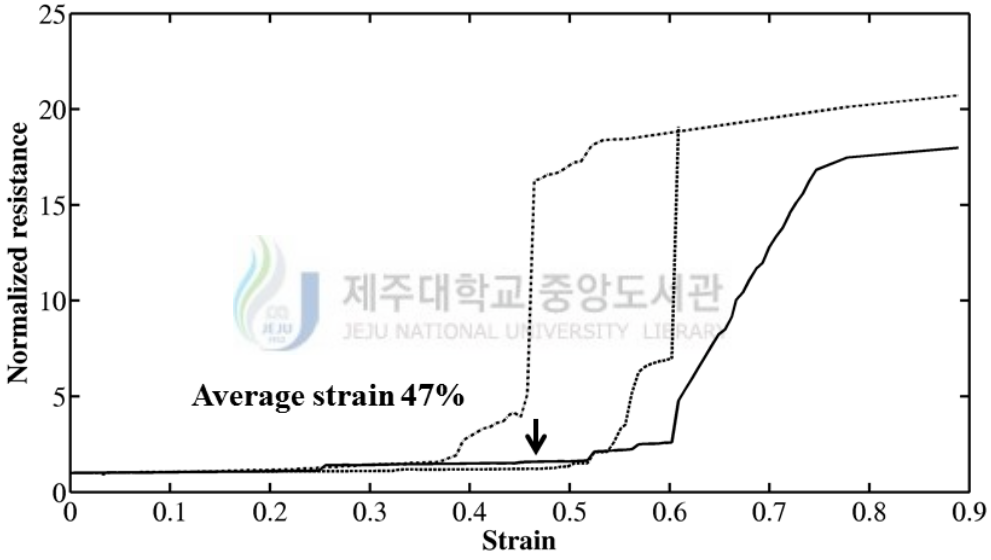

Figure 6-3 Normalized resistance vs strain for as fabricated PEDOT:PSS films on three different PDMS substrates having random micro ridges.

As shown in Figure 6-4 that the cracks can appear as a brittle fracture and are due to tensile stresses in the film which tends to split the films into two halves (Lang, Naujoks, et al. 2009). However, as mentioned earlier, the reason why these films remain conductive even after crack formation is the presence of random micro ridges on the surface of the PDMS substrate which tends to increase the adhesion, suppress the crack propagation and allows the films to remain conductive even after cracking by forming random interconnected bridges (links). This behavior indicates the usefulness of the random micro ridges on the PDMS surface and

could possibly open a doorway for further optimization in topographic designs of these interconnected micro features for various applications.

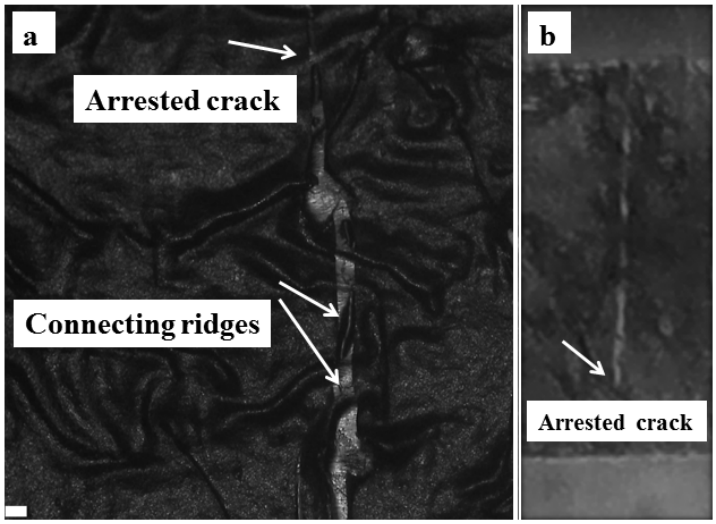

Figure 6-4 A typical crack propagation behavior of as fabricated PEDOT:PSS film on PDMS substrate having random micro ridges (a) Micrograph and (b) photographic image. Scale bar in (a) is 50 micrometer.

On the other hand, from Figure 6-3 it can be realized that on average up to 45% axial strain the increase in the value of the resistance as compared to the initial value remains below 1.5 therefore, this range can be considered as the useful stretchable range for these blade coated PEDOT:PSS films on PDMS substrates having random micro ridges. On this basis, Figure 6-5 shows the increase in the resistance of the films up to 35% axial strain only.

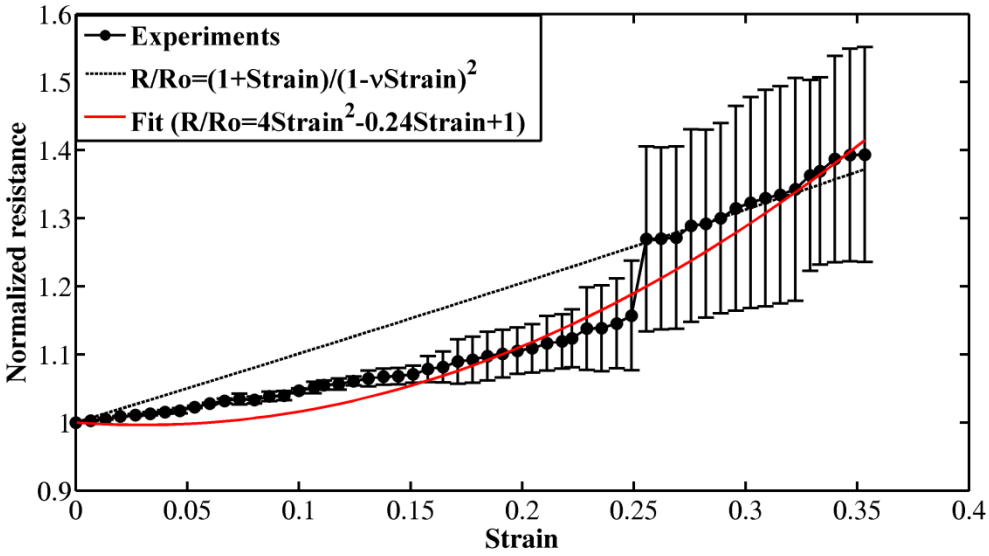

Figure 6-5 Average normalized resistance vs strain for as fabricated PEDOT:PSS films on PDMS having random micro ridges for three tested samples. Error bars show the standard deviation from the mean value of the normalized resistance at each value of strain.

The curve in Figure 6-5 represents an average taken over three tested samples. It can also be seen that a theoretical model (Mandlik et al. 2006) seems to fit this variation with a coefficient of determination of 0.74 while a proposed second degree polynomial given by equation (6-1) fits the experimental data points with much better value of the coefficient of determination of 0.96.

$$R/R_o = 4Strain^2 - 0.24Strain + 1 \quad (6\text{-}1)$$

A quantitative investigation into the resistive behavior of these films with respect to the applied strain suggests that the change in resistance actually depends on the geometric part more dominantly than the piezoresistive portion ($\beta = -0.22$) where β is the piezo component neglecting any dimensional changes along the thickness direction and can be calculated using Figure 6-5 and the Poisson ratio of PEDOT:PSS (Lang, Rust, et al. 2009). Consequently, these films breaks with a brittle crack formation near the critical value of the strain as mentioned earlier. This indicates that the morphological changes within the films remain minimal during stretching and contribute in a way that reduces the change in resistance as indicated by a negative sign untill cracking appears and begins to propagate. Finally it can be concluded that for the as-fabricated PEDOT:PSS films on PDMS having random micro

ridges the useful range of stretchability lies between 35 to 45%. This behavior suggests that the polymer-polymer laminate can be used in applications like stretchable electronics.

6.1.2 Resistive behavior of blade coated PEDOT:PSS films as a function of temperature on micro ridged type PDMS

There exist several experimental studies which have demonstrated the resistive behavior of PEDOT:PSS films on polymeric substrates as a function of temperature (Lam et al. 2006; Busu et al. 2009; Rannou & Nechtschein 1999), however the results seems to depend on factors such as temperature range and thickness of the film. Most studies have suggested decrease in the resistance of the PEDOT:PSS films between temperatures of 20 to 100^{o}C. On the other hand, Basu et al. 2009 has shown that the resistance of the micrometer thick films of PEDOT:PSS on polymeric substrate increases by increasing the temperature within 40 to 80^{o}C. In the present study the thickness remains in order of micrometers therefore, it was observed that on average the resistance increases by increasing the temperature between 20 to 80^{o}C. However, PEDOT:PSS being a polymer exhibits decrease in its resistance due to increased tunneling effect with increasing temperatures. The temperature range utilized in the present study could be increased due to high thermal stability of PDMS as a substrate material and therefore lie between 25 to 230^{o}C. Figure 6-6 depicts the resistive behaviors of three samples. It can be noticed that each sample shows increase in the resistance up to an average temperature of 80^{o}C and thereafter starts to decrease. This decrease in resistance indicates an increase in the intermolecular hopping which is due to thermally assisted tunneling effect (Schweizer 2005). It can be seen that for the as fabricated PEDOT:PSS films the tunneling effect can be triggered within 80 to 100^{o}C. Also in the temperature range of 25 to 100^{o}C the average increase in the resistance was only 1.14 times the initial resistance while on the other hand the resistance decreases by almost 2 times at the highest temperature during the experiment.

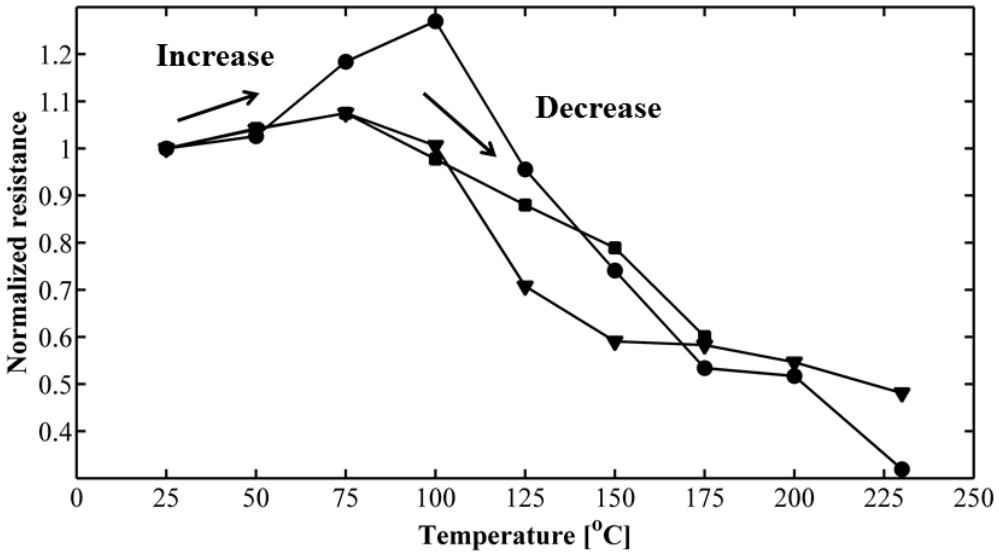

Figure 6-6 Normalized resistance vs temperature for PEDOT:PSS films on PDMS having random micro ridges for three tested samples.

It can also be seen from Figure 6-7 that even at a temperature of 230^{o}C no thermal degradations has taken place which indicates thermal stability of these PEDOT:PSS films on PDMS substrates having random micro ridges. This behavior is encouraging in the sense that the polymer-polymer laminate can be used as heating surface in microfluidics applications and also in thin film thermoelectric generators.

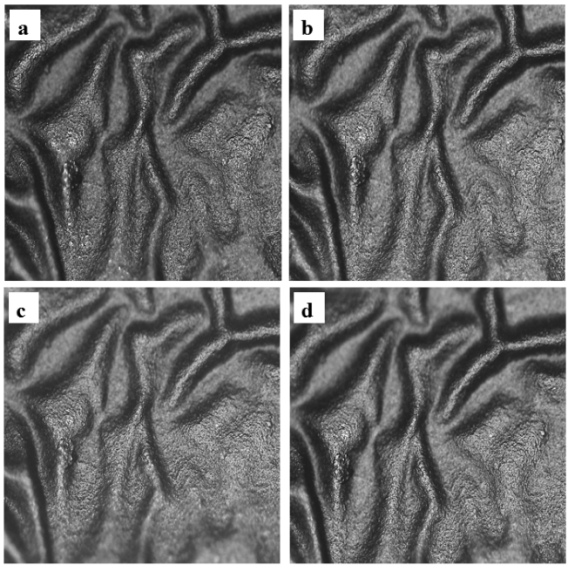

Figure 6-7 Micrographs of PEDOT:PSS film at different temperatures (a) 25^{o}C, (b) 150^{o}C, (c) 230^{o}C and (d) 25^{o}C.

6.1.3 Thermal actuation of blade coated PEDOT:PSS films on micro ridged type PDMS

Figure 6-8 shows the actuation behavior of the blade coated PEDOT:PSS films on PDMS substrate having random micro ridges. It can be seen that the as fabricated polymer-polymer laminate shows a good linear thermal actuation behavior. The actuations were in orders of millimeters with response time of 2.4 seconds per degree rise in temperature. When the sample was removed from the hot plate it fully recovered its initial horizontal position in less than a minute. The behavior suggests that the polymer-polymer laminate can also be used as a thermal actuator or thermal valve in microelectromechanical systems and microfluidics applications.

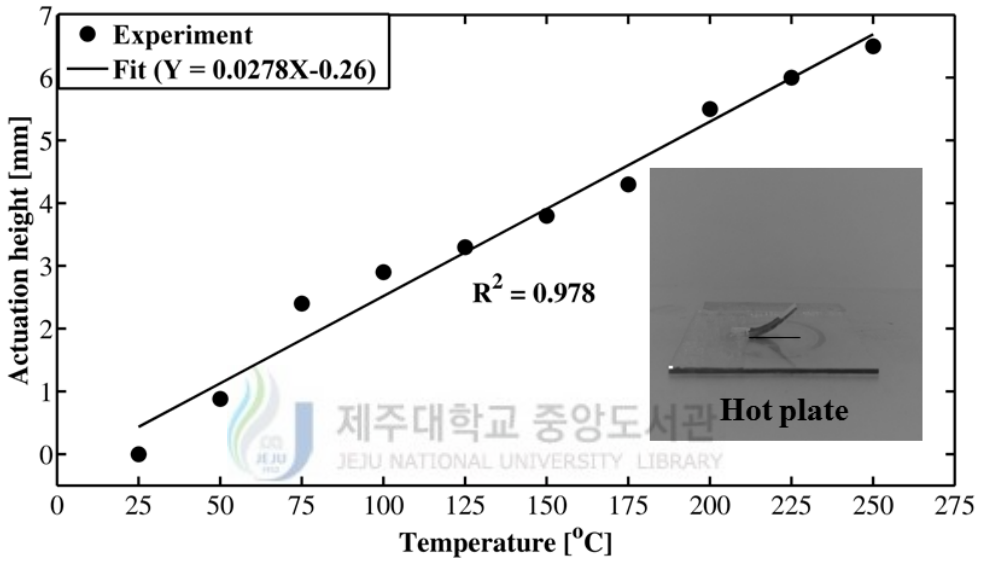

Figure 6-8 Thermal actuation behavior of a typical PEDOT:PSS film on PDMS substrate having random micro ridges. The inset shows a typical photographic image of the actuator. The scale bar is 1mm in the inset.

A linear fit given by equation (6-2) models this actuation behavior with a coefficient of determination of 0.978 as shown in Figure 6-8.

$$\text{Actuation(mm)} = 0.0278 \times \text{Temperature}(^{o}\text{C}) - 0.26 \qquad (6\text{-}2)$$

6.2 Rod coated PEDOT:PSS films on micro trenched type ultra-low modulus PDMS

The schematic of the rod coating technique is already shown in Figure 5-13. In this work the same setup was used for the rod coating of the PEDOT:PSS films on the ultra-low modulus PDMS substrates having micro trench type roughness. However, unlike section 6.1, in the present case the PEDOT:PSS ink was synthesized in a different way. 80% weight concentration of PEDOT: PSS paste from AGFA Materials (Japan) was thoroughly mixed with the mixture of solvents (IPA and DMSO). The DMSO was added in concentration of 8% by weight of the ink. DMSO was added in order to enhance the conductivity (Cruz-Cruz et al. 2010). The viscosity of the ink was measured by a viscometer (Sekonic Corp. Japan) and was found to be 0.051 Pa.s. The density of the ink was calculated by measuring the mass and the volume of the ink and was found to be 908 kg/m^3.

The synthesized PEDOT: PSS ink was deposited in volumes of 1.45 μL using a micro pipette on to the PDMS samples having trench type roughness patterns. A smooth steel rod of diameter 2.5 mm was gently pulled over the samples with an average velocity of 5 mm/s. The films were dried in ambient air on a hot plate at a temperature of 95^{o}C for 10 minutes. After the intermediate drying step another coat of ink (with volume of 1.45 μL) was rod coated and finally the films were baked at 95^{o}C for 20 minutes on a hot plate in ambient air. Figure 6-9 show the typical rod coated PEDOT:PSS films on ultra-low modulus PDMS having trench type roughness.

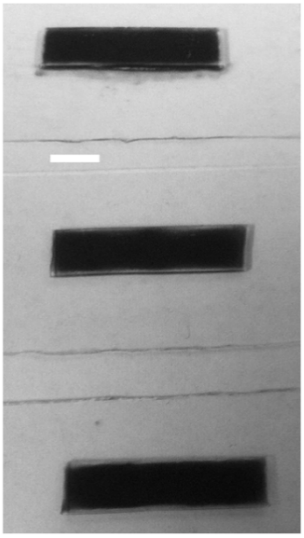

Figure 6-9 Photograph of rod coated PEDOT:PSS films on ultra-low modulus PDMS having trench type roughness. The scale bar is 5 mm and applies to each sample shown.

Also Figures 6-10(a)-(c) shows the morphology of the rod coated films at increasing magnification. It can be seen from the enclosed regions in Figure 6-10(a)-(c) that the rod coated PEDOT:PSS films exhibit no post baking morphological defects and the micro trenches have been substantially filled with the PEDOT:PSS film.

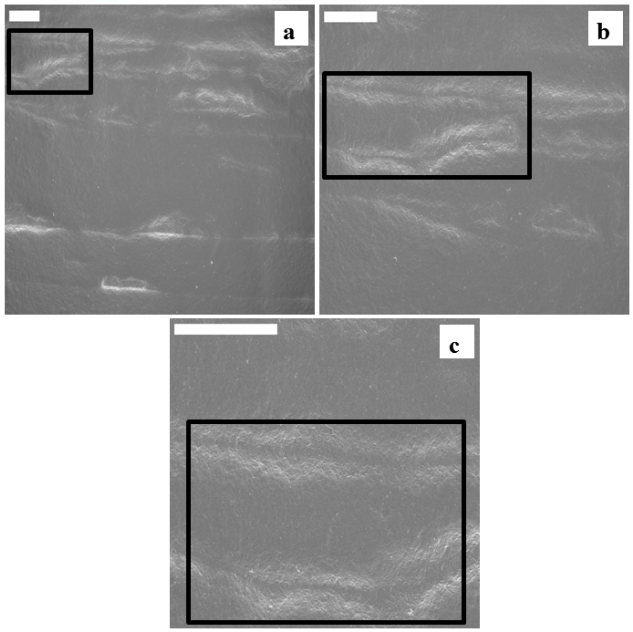

Figure 6-10 SEM images showing the micro trench being completely filled with the PEDOT:PSS film. (a) 300X, (b) 500X and (c) 1000X magnification. Scale bar is 100 μm in each panel.

From various lateral micrographs (see Figure 6-11) the average thickness of the rod coated PEDOT:PSS films on ultra-low modulus PDMS having trench type roughness was found to be 9 μm. Also from various SEM images, such as shown as Figure 6-11 The average depth of these micro trenches was found to be 16 μm.

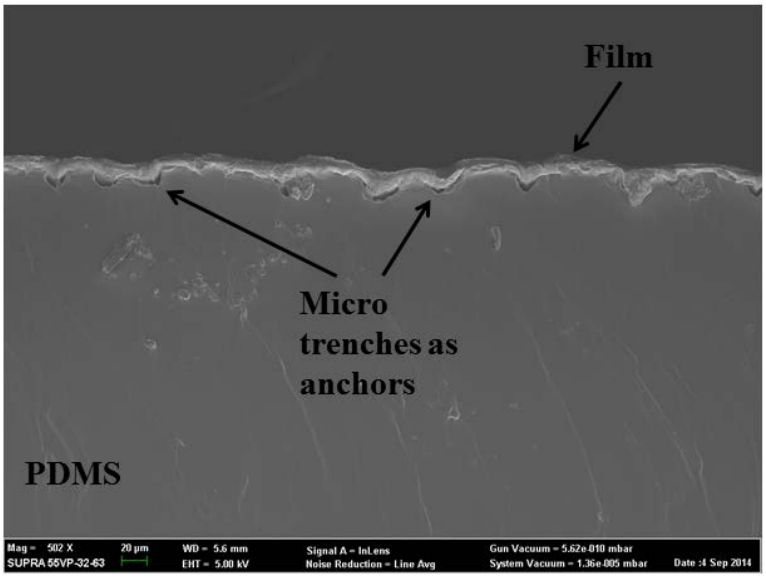

Figure 6-11 Lateral SEM image showing the film thickness and trenches acting as anchors. Scale bar is 20 μm.

It should be noted that in this work, the method of generating the micro trench type roughness patterns and their characterization remain exactly the same as described in section 5.2.1. Ultimately, the cumulative area averaged roughness for these PDMS substrates was found to be 2.29 μm.

6.2.1 Stretchability of rod coated PEDOT:PSS films on micro trenched type ultra-low modulus PDMS

Figure 6-12 shows the variation of the normalized resistance with the axial strain.

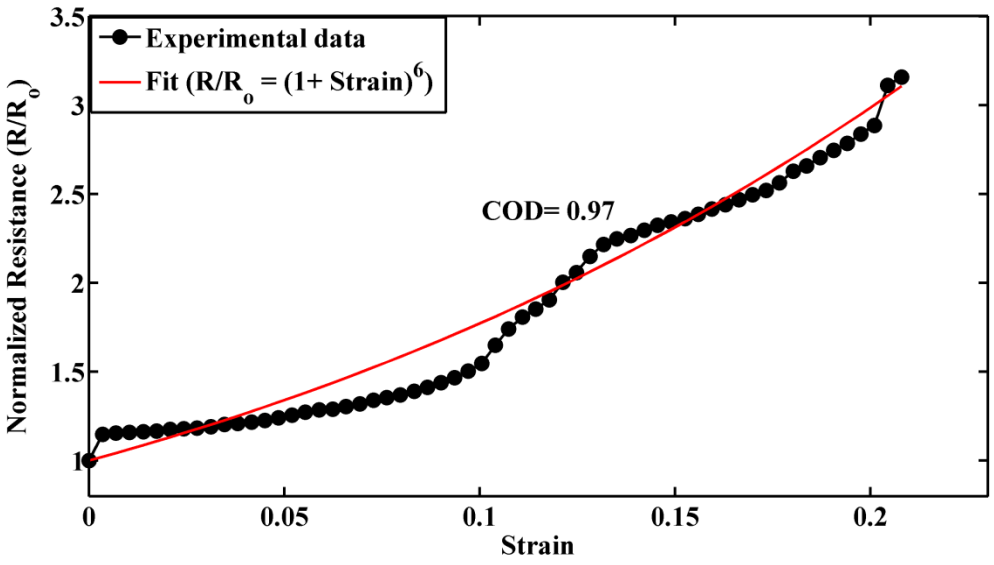

Figure 6-12 Variation of normalized resistance with the axial strain.

In Figure 6-12 it can be observed that on average the films remain electrically conductive around 23% strain after which the films were found to crack and delaminate on further application of strain as shown in Figure 6-13.

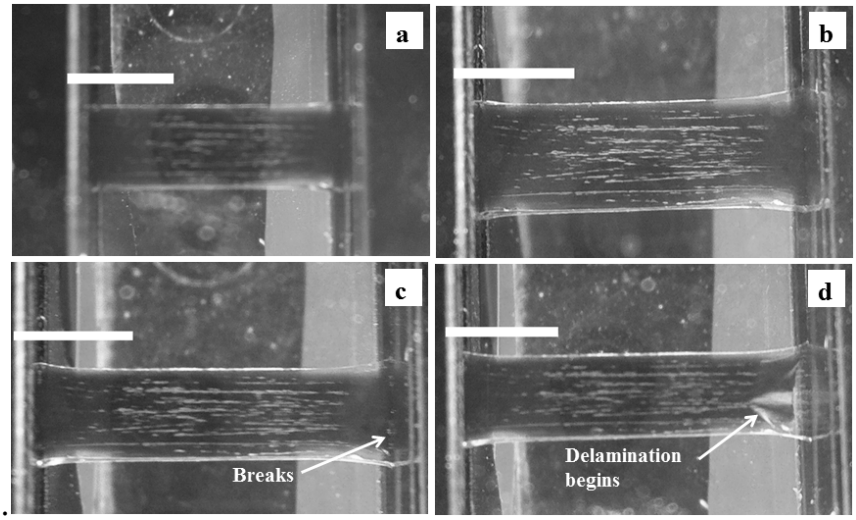

Figure 6-13 Photographs of the samples during tensile test. (a) 0% strain, (b) 11% strain, (c) 21% strain and (d) 25% strain. All scale bars are 5 mm.

The resistive behavior during stretching for these rod coated PEDOT:PSS films on ultra-low modulus PDMS substrates having micro trench type roughness patterns can be quantitatively expressed by equation (6-3) with a coefficient of determination of 0.97 as shown in Figure 6-12.

$$R/R_o=(1+Strain)^6 \quad (6\text{-}3)$$

It can also be seen in Figure 6-12 that the resistance of the as fabricated PEDOT:PSS films increases up to 3 times their initial resistance at complete failure. It is important to mention here, that even after utilizing an ultra-low modulus PDMS with sub millimeter thickness which is known to reduce the stretchability of thin films, the as fabricated PEDOT:PSS films were able to achieve 23% stretchability. It must also be noted that no extra substrate treatment such as oxygen plasma and/or ultra violet ozone treatment were used in this study. This behavior is due to two reasons. Firstly, this behavior can be attributed towards good wettability of the as synthesized PEDOT:PSS ink as shown in Figure 6-14 below.

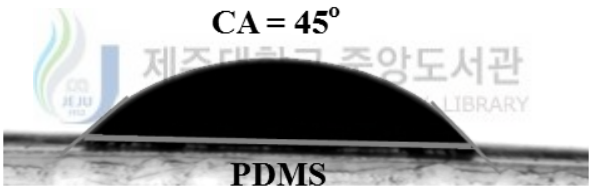

Figure 6-14 Wettability of the as synthesized PEDOT:PSS ink on ultra-low modulus PDMS having micro trench type roughness patterns.

Figure 6-14 clearly reveals that the as synthesized PEDOT:PSS ink has a good wettability (owing to the low contact angle of 45^o with the substrate) on the ultra-low modulus PDMS having micro trench type roughness patterns. Secondly, as it can be noticed from Figure 6-10 and Figure 6-11 that the micro trenches actually behaves as anchors which tends to keep the films in tact with the substrate during stretching. Consequently these films were able to achieve stretchability up to 23% (on average) without any additional substrate treatments. However, when the strain reaches the failure value (23%), the films eventually fail with a brittle crack propagating quickly through the entire film width (see Figure 6-13(c)). At this point, increasing axial strain causes the micro trenches to further contract due to the lateral strains in the PDMS substrate (Poisson's ratio ≈ 0.5) as shown in Figure 6-15.

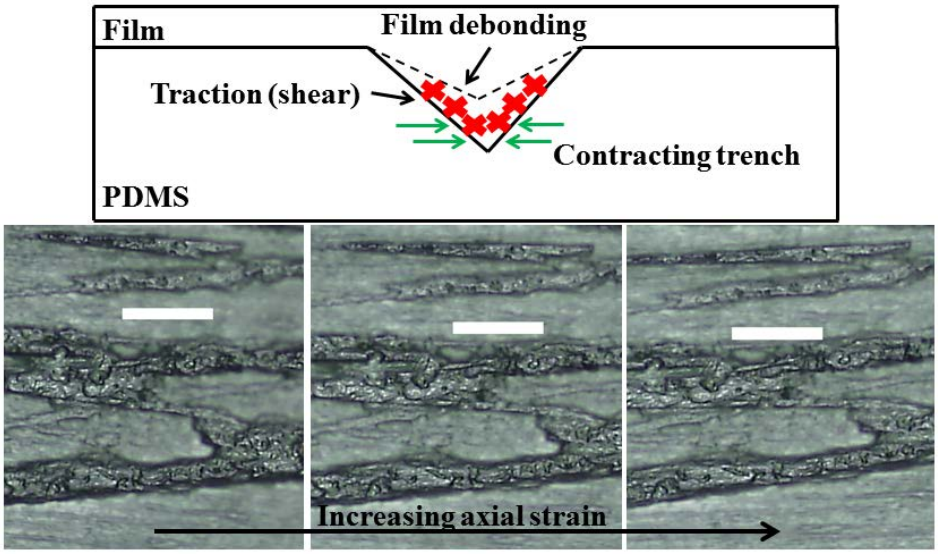

Figure 6-15 Schematic diagram of the failure mechanism of rod coated PEDOT:PSS films on sub millimeter thick ultra-low modulus PDMS substrates having micro trench type roughness patterns (Top). Micrographs showing contracting trenches at increasing strain (Bottom). Red cross represents the traction acting at the interface of the film and the surface of the trenches due to strain, dotted lines indicate the debonding of the film and green arrows represent the contraction of a typical micro trench. All scale bars are 100 μm.

This phenomenon also tends to generate the interface traction (shear) and eventually cause the films to locally debond from the micro trenches (Chiu et al. 1994) (see the schematic in Figure 6-15). Consequently, on further application of strain the films only debond from the substrate without cracking. Compared to the other research results available in the literature (Tait et al. 2013; Cairns & Crawford 2005) and (Cho et al. 2011), this particular behavior signifies the importance of the trench type roughness used in this study, which in spite of the low value of Young's modulus and substrate thickness was able to keep the films in tact up to 23% axial strain with only 3 times increase in the value of the resistance.

Neglecting the variation in thickness direction, the overall change in the resistance of the film during tension can be given by $\Delta R/R_o = (1+\nu+k)\,\varepsilon$ where ΔR is the change in resistance of the film, ν is the Poisson's ratio of PEDOT:PSS (= 0.34), k is the piezoresistive part and ε is the applied strain (Lang, Rust, et al. 2009). Fitting the experimental data given in Figure 6-12 with two separate linear models of the form $\Delta R/R_o = R/R_o - 1 = b\,\varepsilon$ (where b is the slope) and comparing with $\Delta R/R_o = (1+\nu+k)\,\varepsilon$ indicates that for the as-fabricated PEDOT:PSS films on ultra-low modulus PDMS having micro trench type roughness the

change in resistance with strain depends mostly (75%) on the piezoresistive part. This suggests that this polymer-polymer laminate also possess substantial piezoresistive sensing ability.

6.2.2 Flexibility of rod coated PEDOT:PSS films on micro trenched type ultra-low modulus PDMS

The rod coated PEDOT:PSS films on ultra-low modulus PDMS with trench type roughness were found to remain conductive when bent on rods of decreasing diameter. Unlike the case of stretching, the as fabricated polymer-polymer laminate do not exhibit any cracking or delamination during bending up till 4 mm of bending diameter (radius = 2 mm). The result for successive bending is shown in Figure 6-16.

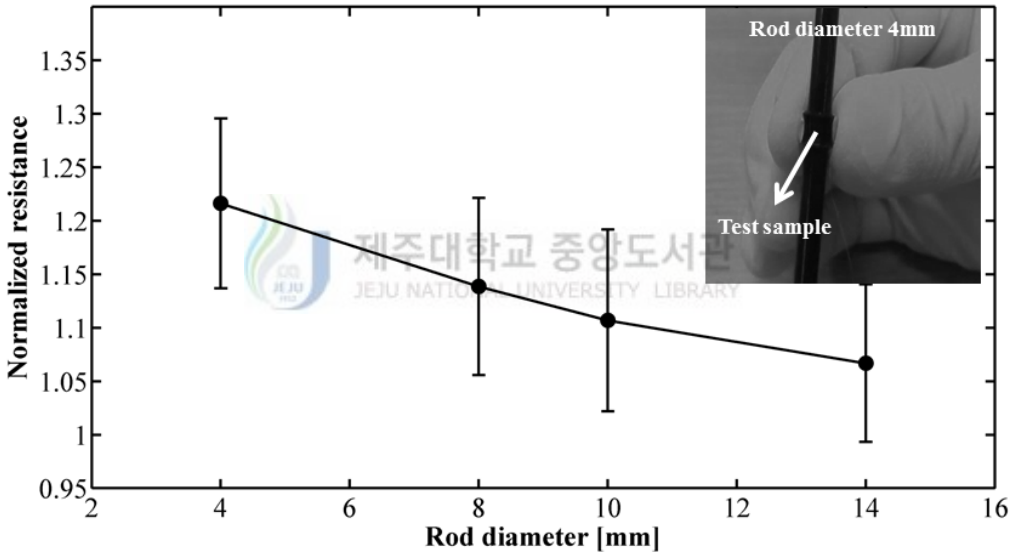

Figure 6-16 Variation of normalized resistance with bending diameters. The inset shows a typical test sample being bent on a rod of 4 mm diameter.

Figures 6-17(a)-(c) shows that the film remained conductive even when bent at 180^{o} (i.e. when both the flat edges in Figure 6-17(a) were forced to meet at a common point as shown in Figure 6-17(b)). Unlike the case of stretching, during bending no substantial contraction of the micro trenches was observed which helps in keeping the films in tact during extreme bendability.

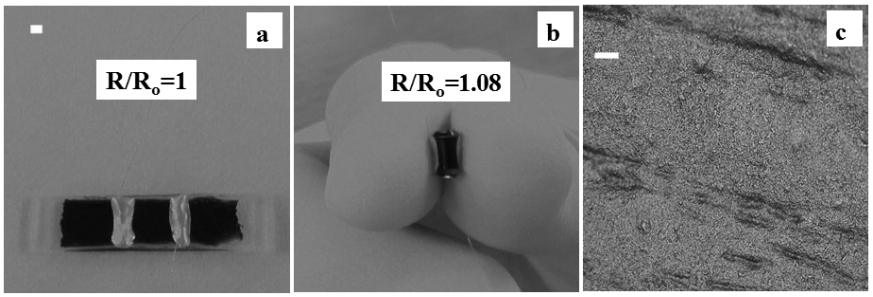

Figure 6-17 Extreme mechanical flexibility of the as fabricated PEDOT:PSS films. (a) Flat initial position. (b) When bent by 180^o. (c) Surface condition of the film after bending at 180^o. Scale bar in (a) is 1mm and in (c) is 100 μm.

Figure 6-17 (c) highlights this fact that even after such an extreme level of bending the morphological condition of the film was not defected. The average overall increase in the value of the normalized resistance for these films during bending was found to be only 1.12 times the initial resistance. An estimate of the bending strain induced at smallest bending diameter can be calculated by using equation (5-2) and was found to be 16%.

Finally, the films were also found to remain conductive when repeatedly bent for 1000 times at an approximate diameter of 4 mm. The result for the repeated bending is shown in Figure 6-18. After 1000 bending cycles the average increase in the normalized resistance was only 1.15 times the initial resistance. These results indicates extreme mechanical flexibility of the rod coated PEDOT:PSS films on ultra-low modulus PDMS having trench type roughness patterns and ultimately renders the polymer-polymer laminate potentially useful for numerous flexible electronics applications.

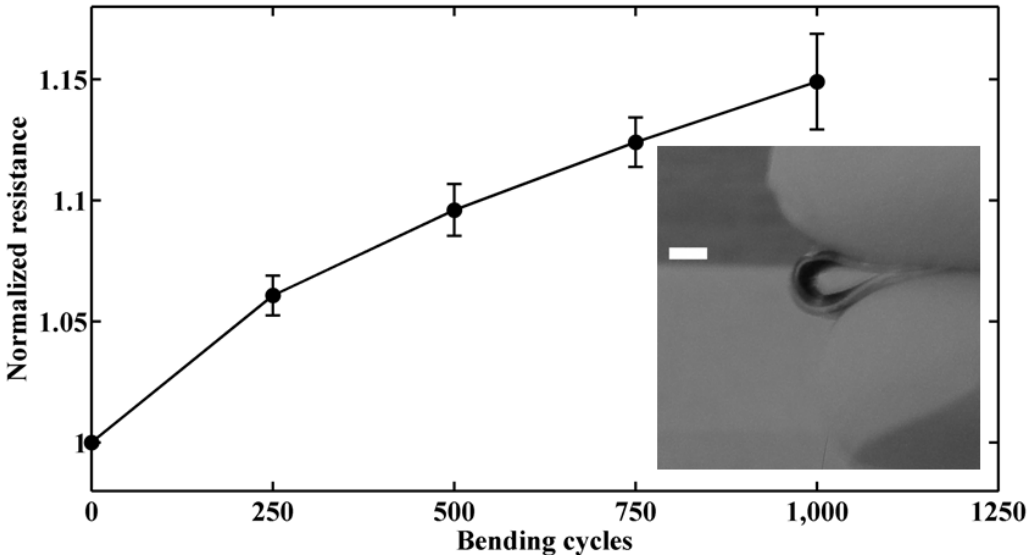

Figure 6-18 Variation of normalized resistance with the number of bending cycles. The inset shows a typical sample being tested at repeated bending. The scale bar is 5 mm.

7. Conclusions

7.1 Summary of the results

This work has investigated the stretchability and flexibility of Ag nanoparticles based films and PEDOT:PSS films on rough PDMS substrates. In each case the micro roughness features were generated in a different way and the films were fabricated using cost effective, scalable and non-vacuum based techniques such as spin coating, rod coating, blade coating and electrospray deposition (ESD). Both the conventional PDMS having Young's modulus of more or less 1 MPa and the ultra-low modulus PDMS having Young's modulus of 120-140 kPa was used. The summary of the research results is presented in Table 7-1 below.

Table 7-1 Maximum elongation (stretchability) of the fabricated films.

Scheme	Film Material	Film Thickness (µm)	Substrate/Treatment	Substrate Roughness (µm)	Roughness Type	Fabrication technique	Max Elongation (mm)	Max R/R_o
(1)	Ag nanoparticles	14	1 MPa PDMS/None	Roughness ratio = 0.31	Micro ridges	Spin coating	1.406	7
(2)	Ag nanoparticles	7	130 kPa PDMS/UVO	2.29	Micro trenches	Rod coating	1.37	1.05
(3)	Ag nanoparticles	5	130 kPa /None	2.89	Acid etched	ESD	0.25	4
(4)	PEDOT:PSS Paste	16	1MPa PDMS/None	Roughness ratio = 0.30	Micro ridges	Blade coating	1.766	1.5
(5)	PEDOT:PSS Ink	9	130 kPa/None	2.29	Micro trenches	Rod coating	3.33	3

In general, on the basis of the maximum elongation (stretchability) reached before complete electrical failure could be observed, rod coated PEDOT:PSS films on ultra-low modulus PDMS substrates having micro trench type roughness patterns (scheme 5) was found to exhibit the best results. In case of Ag nanoparticles on the ultra-low modulus PDMS, the maximum elongation was observed when the films were rod coated (scheme 2) on substrates having micro trench type roughness patterns. Among the Ag nanoparticles films the lowest increase in the value of the normalized resistance during stretching was also observed for this

particular case. The reason for this low variation of the normalized resistance is partly due to the presence of micro trenches that behaves as anchors during stretching and provide sites for mechanical interlocking effects for the nanoparticles and also due to the substrate treatment with ultra violet ozone which can further enhance the adhesion between the rod coated films and the ultra-low modulus PDMS during patterning. These results therefore, make scheme 2 a substantially useful option. Similarly, the maximum elongation before complete rupture for rod coated aqueous PEDOT:PSS ink on ultra-low modulus PDMS having micro trench type roughness patterns (scheme 5) was found to be 3.33 mm with only 3 times increase in the value of the normalized resistance which is another encouraging result for thin film on rough ultra-low modulus PDMS. The reason for this behavior is again the presence of micro trenches that acts as anchors and good wettability of the PEDOT:PSS aqueous ink on the sticky surface of the ultra-low modulus PDMS. It is to be noted that Ag nanoparticles films (scheme 2) and PEDOT:PSS films (scheme 5) on rough ultra-low modulus PDMS substrates were also found to remain mechanically flexible when bent on circular surfaces having minimum diameters of 10 mm and 4 mm respectively. In case of ESD deposited Ag nanoparticles films (scheme 3) the stretchability on ultra-low modulus PDMS was found to be the lowest however, the result was much improved when 1 MPa PDMS substrate was used. Relatively low value of stretchability for this scheme is due to several reasons which includes relatively low substrate thickness (approximately 400 μm) as compared to other schemes, substantial difference in the fabrication technique (deposition instead of patterning) and also due to the presence of post sintering cracks found on these films. Apart from these results, the change in resistance for the rod coated Ag and PEDOT:PSS films on the rough ultra-low modulus PDMS displays a strong dependence on the piezoresistive part during the applied strain. This particularly suggest that resistivity of the films fabricated through non-vacuum based techniques changes during stretching.

These intriguing results indicate that micrometer thick films of metals and also nonmetals fabricated by non-vacuum based techniques can have appreciable stretchability and flexibility on the ultra-low modulus rough PDMS substrates. These results also indicate that patterned films (schemes 2, 4 and 5) can perform better as compared to deposited films (schemes 1 and 3).

From application point of view, micrometer thick films of metals and nonmetals on PDMS can be potentially useful in application like heating elements for microfluidics and microelectromechanical systems (MEMS), thin film thermoelectric generators, piezoresistive and capacitive strain sensors and pressure sensors, electroactive actuators or artificial muscles, thin film fuel cells, MRI micro antennae, micro coils, filled interconnect groove (FIG), next generation computers and electronic gadgets and high power applications.

7.2 Future directions

With wide options available as solution based inks containing dispersed micro and/or nano structured materials, the research related with the roughness dependent performance of metallic and nonmetallic films on ultra-low modulus PDMS using non-vacuum based fabrication techniques remains an ongoing research area with potential applicability in stretchable and flexible electronics. Also the performance of large area films on rough ultra-low modulus PDMS substrates using non-vacuum based approaches could still be a challenging task. It is also anticipated that improvements based on the optimized designs of roughness patterns and other surface modification techniques can impart much better functionality to the fabricated films and can even tailor the films to fulfill specific tasks. Even though this work has focused its attention only on micrometer thick films on rough ultra-low modulus PDMS, behavior of nanometer thick films on these surfaces can be equally crucial. The performance of stretchable and flexible films on these surfaces with different scales of roughness patterns with respect to the film thickness can also be investigated and relatively compared, specially the roughness scales that can be completely buried in the films. Lastly with the use of more sophisticated instrumentation the reliability tests for stretching, bending and twisting also form a very important set of results for these laminates.

References

Akter T and Kim WS, Reversibly Stretchable Transparent Conductive Coatings of Spray-Deposited Silver Nanowires. *ACS Applied Materials and Interfaces* 4: 1855-1859 (2012).

Aricò AS, Bruce P, Scrosati B, Tarascon J-M and Schalkwijk WV, Nanostructured materials for advanced energy conversion and storage devices. *Nature Materials* 4: 366-377 (2005).

Baney RH, Thermal and Oxidative Behavior of Silicones. In Polymer Conference Series Wayne State University (1963).

Bayati R, Mishra YK, Naseri N and Nori S, Nanostructured Materials for Electronics and Photonics. *Journal of Nanomaterials* Article ID 725764 (2014).

Berdichevsky Y, Khandurina J, Guttman A and Lo Y-H, 2004. UV/ozone modification of poly(dimethylsiloxane) microfluidic channels. *Sensors and Actuators B: Chemical* 97: 402–408 (2004).

Bhattacharya S, Datta A, Jordon MB and Gangopadhyay S, Studies on surface wettability of poly(dimethyl) siloxane (PDMS) and glass under oxygen-plasma treatment and correlation with bond strength. *Journal of Microelectromechanical Systems* 14(3): 590–597 (2005).

Bossuyt F, Guenther J, Loher T, Seckel M, Sterken T and Vries J. de, Cyclic endurance reliability of stretchable electronic substrates. *Microelectronics Reliability* 51(3): 628–635 (2011).

Bossuyt F, Vervust T and Vanfleteren J, Stretchable Electronics Technology for Large Area Applications : Fabrication and Mechanical Characterization. *IEEE Transactions on Components, Packaging and Manufacturing Technology* 3(2): 229–235 (2013).

Bräuer B, Dietrich RTZ, Ruffer T and Salvan G, Deposition of thin films of a transition metal complex by spin coating. *Chemical Physics Letters* 432: 226–229 (2006).

Busu I, Svasta P, Bunea R and Bonfert D, DC and Thermal behavior of PEDOT:PSS thin films. In *15th International Symposium for Design and Technology of Electronics Packages (SIITME)*: 81–86 (2009).

Cai L, Li J, Luan P, Dong H, Zhao D, Zhang Q, Zhang X, Tu M, Zeng Q, Zhou W and Xie S, Highly Transparent and Conductive Stretchable Conductors Based on Hierarchical Reticulate Single-Walled Carbon Nanotube Architecture. *Advanced Functional Materials* 22(24): 5238–5244 (2012).

Cairns DR, Richard PW II, Sparacin DK, Sachsman SM, Paine DC and Crawford GP, Strain dependent electrical resistance of tin-doped indium oxide on polymer substrates. *Applied Physice Letters* 76: 1425-1427 (2000).

Cairns DR and Crawford GP, Electromechanical Properties of Transparent Conducting Substrates for Flexible Electronic Displays. *Proceedings of the IEEE*, 93(8):1451–1458 (2005).

Chang YH, Tseng SR, Chen CY, Meng HF, Chen EC, Horng SF and Hsu CS, Polymer solar cell by blade coating. *Organic Electronics* 10(5): 741–746 (2009).

Chiu SL, Leu J and Ho PS, 1994. Fracture of metal-polymer line structures. I. Semiflexible polyimide. *Journal of Applied Physics* 76(9): 5136-5142 (1994).

Cho CK, Hwang WJ, Eun K, Choa SH, Na SI and Kim HK, Mechanical flexibility of transparent PEDOT:PSS electrodes prepared by gravure printing for flexible organic solar cells. *Solar Energy Materials and Solar Cells* 95(12): 3269–3275 (2011).

Choi KH, Saleem K, Dang HW, Doh YH and Hong SJ, Electrohydrodynamic Spray Deposition of ZnO Nanoparticles. *Japanese Journal of Applied Physics* 49(5): 05EC08-6 (2010).

Choy KL, Chemical vapour deposition of coatings. Progress in Materials Science 48: 57–170 (2003).

Chung S, Lee J, Song H, Kim S and Jeong J, Inkjet-printed stretchable silver electrode on wave structured elastomeric substrate. *Applied Physics Letters* 98(15): 153110 (2011).

Cruz-Cruz I, Reyes-Reyes M, Aguilar-Frutis MA, Rodriguez AG, Lopez-Sandoval R, 2010. Study of the effect of DMSO concentration on the thickness of the PSS insulating barrier in PEDOT:PSS thin films. *Synthetic Metals* 160: 1501–1506 (2010).

Davis CS and Crosby AJ, Mechanics of wrinkled surface adhesion. *Soft Matter* 7(11): 5373-5381 (2011).

Duraisamy N, Muhammad NM, Hyun MT and Choi KH, Structural and electrical properties of P3HT:PCBM/PEDOT:PSS thin films deposited through electrohydrodynamic atomization technique. *Materials Letters* 92: 227–230 (2013).

Efimenko K, Wallace WE and Genzer J, Surface Modification of Sylgard-184 Poly(dimethyl siloxane) Networks by Ultraviolet and Ultraviolet/Ozone Treatment. *Journal of Colloid and Interface Science* 254(2): 306–315 (2002).

Esteves ACC, Brokken-Zijp J, Huinink HP, Reuvers NJW, Van MP and With G. de, Influence of cross-linker concentration on the cross-linking of PDMS and the network structures formed. *Polymer* 50(16): 3955–3966 (2009).

Fang SC, Huang CH, Chen IC, Liaw CF and Hurng WM, Preparation of YBCO superconductor thin film by spin-coating method with metal-organic precursors. *Journal of Materials Science* 29(1): 99–102 (1994).

Fang W and Lo C, On the thermal expansion coefficients of thin films. *Sensors and Actuators A: Physica*l 84: 310–314 (2000).

Flinn P, Principles and Applications of Wafer Curvature Techniques for Stress Measurements in Thin Films. *Materials Research Society Proceedings* 130: 41-51 (1989).

Florando J, Fujimoto H, Ma Q, Kraft O, Schwaiger R and Nix WD, Measurement of Thin Film Mechanical Properties by Microbeam Bending. *Materials Research Society Proceedings* 563: 231 (1999).

Fuard D, Tzvetkova-Chevolleau T, Decossas S, Tracqui P and Schiavone P, Optimization of poly-di-methyl-siloxane (PDMS) substrates for studying cellular adhesion and motility. *Microelectronic Engineering* 85: 1289–1293 (2008).

Gaikwad AM, Steingart DA, Ng TN, Schwartz DE, Whiting GL, et al., 2013. A flexible high potential printed battery for powering printed electronics. *Applied Physics Letter* 102(23): 233302.

Gonzalez M, Axisa F, Bulcke MV, Brosteaux D, Vandevelde B and Vanfleteren J, Design of metal interconnects for stretchable electronic circuits. *Microelectronics Reliability* 48(6): 825–832 (2008).

Gray DS, Tien J and Chen CS, High-Conductivity Elastomeric Electronics. *Advanced Materials* 16(5): 393–397 (2004).

Gutruf P, Shah CM, Walia S, Nili H, Zoolfakar AS, Karnutsch C, Kalantar-zadeh K, Sriram S and Bhaskaran M, Transparent functional oxide stretchable electronics: micro-tectonics enabled high strain electrodes. *NPG Asia Materials* 5(9) (2013).

Hamasha MM, Alzoubi K and Lu S, Behavior of Sputtered Indium–Tin–Oxide Thin Film on Poly-Ethylene Terephthalate Substrate Under Stretching. *Journal of Display Technology* 7(8): 426–433.

Han Y, Rogalsky AD, Zhao B and Kwon HJ, The Application of Digital Image Techniques to Determine the Large Stress – Strain Behaviors of Soft Materials. *Polymer Engineering and Science* 52 (4): 826-834 (2012).

Hay KM, Dragila MI and Liburdy J, Theoretical model for the wetting of a rough surface. *Journal of colloid and interface science* 325(2): 472–477.

Helmersson U, Lattemann M, Bohlmark J, Ehiasarian AP, Gudmundsson JT, et al., 2006. Ionized physical vapor deposition (IPVD): A review of technology and applications. *Thin Solid Films* 513: 1–24 (2006).

Hummelgård C, Gustavsson J, Cornell A, Olin H and Backstrom J, Spin coated titanium–ruthenium oxide thin films. *Thin Solid Films* 536: 74–80 (2013).

Hwang KS and Kim BH, Preparation of Highly Oriented LaNiO 3 Thin Films by Spin-Coating Technique. *Journal of Sol-Gel Science and Technology* 14: 203–207 (1999).

Joo SC, Adhesion Mechanisms of Nano-Particle Silver to Electronics Packaging Materials. PhD Thesis, Georgia Institute of Technology (2006).

Jung M, Noh J, Kim J, Kim D and Cho G, 2013. Roll to Plate Printed Stretchable Silver Electrode Using Single Walled Carbon Nanotube on Elastomeric Substrate. *Journal of Nanoscience and Nanotechnology* 13(8): 5620–5623.

Kim DH, Nanshu L, Ma R, Kim YS, Kim RH, Wang S, Wu J, Won SM, Tao H, Islam A, Yu KJ, Tae-il K, Chowdhury R, Ying M, Xu L, Li M, Chung HJ, Keum H, McCormick M, Liu P, Zhang YW, Omenetto FG, Huang Y, Coleman T and Rogers JA. Epidermal electronics. *Science* 333: 838–43 (2011).

Kim J, Jung W and Kim HS, In-plane strain of electro-active paper under electric fields. *Sensors and Actuators A: Physical* 140(2): 225–231 (2007).

Kim S, Won S, Sim GD, Park I and Lee SB, Tensile characteristics of metal nanoparticle films on flexible polymer substrates for printed electronics applications. *Nanotechnology*, 24(8): 085701 (2013).

Korshak VV, Heat -Resistant Polymers. Israel Program Science Translations (1971).

Ko W and Lin K, 2013. Highly Conductive, Transparent Flexible Films Based on Metal Nanoparticle-Carbon Nanotube Composites. *Journal of Nanomaterials* Article ID 505292 (2013).

Lacour SP and Wagner S, Stretchable gold conductors on elastomeric substrates. *Applied Physics Letters* 82(15): 2404-2406 (2003).

Lam L, McBride JW and Swingler J, The influence of thermal cycling and compressive force on the resistance of poly(3,4-ethylenedioxythiophene)/poly(4-styrenesulfonic acid)-coated surfaces. *Journal of Applied Polymer Science* 101(4): 2445–2452 (2006).

Lambricht N, Pardoen T and Yunus S, Giant stretchability of thin gold films on rough elastomeric substrates. *Acta Materialia* 61: 540–547 (2013).

Lang U, Naujoks N and Dual J, Mechanical characterization of PEDOT:PSS thin films. *Synthetic Metals* 159: 473–479 (2009)

Lang U, Rust P, Schoberle B and Dual Jurg, Piezoresistive properties of PEDOT:PSS. *Microelectronic Engineering* 86: 330–334 (2009).

Lee D, Choi Yand Yong K, Morphology and crystal phase evolution of doctor-blade coated CuInSe2 thin films. *Journal of Crystal Growth* 312: 3665–3669 (2010).

Lee I, Lee J, Ko SH and Kim TS, Reinforcing Ag nanoparticle thin films with very long Ag nanowires. *Nanotechnology* 24: 415704 (2013).

Lee J, Kim S, Lee J, Yang D, Park BC, Ryu S and Park I, 2014. A stretchable strain sensor based on a metal nanoparticle thin film for human motion detection. *Nanoscale* 6:11932–11939.

Lee JH, Lee KY, Gupta MK, Kim TY, Lee DY, Oh J, Ryu C, Yoo WJ, Kang CY, Yoon SJ, Yoo JB and Kim SW, Highly stretchable piezoelectric-pyroelectric hybrid nanogenerator. *Advanced materials* 26: 765–9 (2014).

Lee JN, Park C and Whitesides GM, Solvent Compatibility of Poly (dimethylsiloxane) -Based Microfluidic Devices. *Analytical Chemistry* 75(23): 6544–6554.

Lee MT, Lee D, Sherry A and Grigoropoulos CP, Rapid selective metal patterning on polydimethylsiloxane (PDMS) fabricated by capillarity-assisted laser direct write. *Journal of Micromechanics and Microengineering*, 21: 095018 (2011).

Li T, Huang ZY, Xi ZC, Lacour SP, Wagner S and Suo Z, 2005. Delocalizing strain in a thin metal film on a polymer substrate. *Mechanics of Materials* 37: 261–273 (2005).

Li T, Huang Z and Suo Z, Stretchability of thin metal films on elastomer substrates. *Applied Physics Letters* 85(16): 3435 (2004).

Li T and Suo Z, Deformability of thin metal films on elastomer substrates. *International Journal of Solids and Structures* 43: 2351–2363.

Lipomi DJ, Lee JA,Vosgueritchian M, Tee BCK, Bolander JA and Bao Z, Electronic Properties of Transparent Conductive Films of PEDOT:PSS on Stretchable Substrates. *Chemistry of Materials* 24: 373-382 (2012).

Lipomi DJ, Tee BCK, Vosgueritchian M and Bao Z, Stretchable organic solar cells. *Advanced materials* 23: 1771–1775.

Liu CH and Yu X, Silver nanowire-based transparent, flexible, and conductive thin film. *Nanoscale research letters* 6: 75 (2011).

Liu M, Sun J, Sun Y, Bock C and Chen Q, Thickness-dependent mechanical properties of polydimethylsiloxane membranes. *Journal of Micromechanics and Microengineering* 19: 035028 (2009).

Lu N, Wang X, Suo Z and Vlassak JJ, Metal films on polymer substrates stretched beyond 50%. *Applied Physics Letters* 91: 221909 (2007).

Lu N, Suo, Z and Vlassak JJ, The effect of film thickness on the failure strain of polymer-supported metal films. *Acta Materialia* 58: 1679–1687 (2010).

Mandlik P, Lacour SP, Li JW, Chou SY, and Wagner S, Fully Elastic Interconnects on Nanopatterned Elastomeric Substrates. *IEEE Electron Device Letters*, 27(8): 650–652 (2006).

Mata A, Fleischman AJ and Roy S, 2005. Characterization of Polydimethylsiloxane (PDMS) Properties for Biomedical Micro/Nanosystems. *Biomedical Microdevices* 7(4): 281–293 (2005).

Mehdi M, Cho KH and Choi KH, Versatile poly(3,4-ethylenedioxythiophene) poly(styrenesulfonate) films on polydimethylsiloxane substrates having random micro ridges: Study of resistive behaviors of a polymer-polymer laminate. *Journal of Applied Polymer Science* 132(1): 41235 (2015).

Mehdi SM, Jo J, Doh YH, Dang HW and Choi KH, Stretchable and flexible resistive behavior of poly(3,4-ethylenedioxythiophene):Poly(styrenesulfonate) thin film on ultra-low modulus polydimethylsiloxane with trench-type roughness. *Journal of Polymer Science Part B: Polymer Physics*. DOI: 10.1002/polb.23615

Mehdi SM, Cho KH and Choi KH Stretchability and resistive behavior of silver (Ag) nanoparticle films on polydimethylsiloxane (PDMS) with random micro ridges. *Journal of Materials Science: Materials in Electronics* 25(8): 3375–3382 (2014).

Muhammad NM, Naeem AM, Duraisamy N, Kim DS and Choi KH, Fabrication of high quality zinc-oxide layers through electrohydrodynamic atomization. *Thin Solid Films* 520: 1751–1756.

Murphy CE, Yang L, Ray S, Yu L, Knox S and Stingelin N, Wire-bar coating of semiconducting polythiophene/insulating polyethylene blend thin films for organic transistors. *Journal of Applied Physics* 110(9): 093523 (2011).

Niu RM, Liu G, Ding XD and Sun J, Ductility of metal thin films in flexible electronics. *Science in China Series E: Technological Sciences* 51(11): 1971–1979 (2008).

Niu RM, Liu G, Ding XD and Sun J et al., 2007. Thickness dependent critical strain in submicron Cu films adherent to polymer substrate. *Applied Physics Letters* 90(16): 161907 (2007).

Niu Z, Dong H, Zhu B, Li J, Hng HH, Zhou W, Chen X and Xie S, Highly stretchable, integrated supercapacitors based on single-walled carbon nanotube films with continuous reticulate architecture. *Advanced materials* 25: 1058–1064 (2013).

Noh YJ, Kim SS, Kim TW and Na SI, Effect of sheet resistance of Ag-nanowire-based electrodes on cell-performances of ITO-free organic solar cells. *Semiconductor Science and Technology*, 28: 125008 (2013).

Norkhairunnisa M, Azizan A, Mariatti M, Ismail H and Sim LC, Thermal stability and electrical behavior of polydimethylsiloxane nanocomposites with carbon nanotubes and carbon black fillers. *Journal of Composite Materials* 46(8): 903–910 (2011).

Oliver WC and Pharr GM, Measurement of hardness and elastic modulus by instrumented indentation: Advances in understanding and refinements to methodology. *Journal of Materials Research* 19(1): 3-20 (2004).

Pierre A, Sadeghi M, Payne MM, Facchetti A, Anthony JE and Arias AC, All-Printed Flexible Organic Transistors Enabled by Surface Tension-Guided Blade Coating. *Advanced materials* 26: 5722–5727 (2014).

Polmanteer KE, New Developments in Silicone Elastomers. *Journal of Elastoplast* 2: 165-194 (1979).

Pranckh FR and Scriven LE, Elastohydrodynamics of Blade Coating. AIChE Journal 36(4): 587-597 (1990).

Rannou P and Nechtschein M, Ageing of Poly(3,4-ethylenedioxythiophene): Kinetics of conductivity decay and lifespan. *Synthetic Metals* 101: 474 (1999).

Renault PO, Villain P, Coupeau C, Goudeau P and Badawi KF, Damage mode tensile testing of thin gold films on polyimide substrates by X-ray diffraction and atomic force microscopy. *Thin Solid Films* 424: 267–273.

Rhein, Thermally Stable Elastomers: A Review. NWC Technical Publication 6372: 1-39 (1983).

Robinson AP, Minev I, Graz IM and Lacour SP, Microstructured silicone substrate for printable and stretchable metallic films. *Langmuir : the ACS journal of surfaces and colloids* 27(8): 4279–84 (2011).

Rogers JA, Someya T and Huang Y, Materials and Mechanics for Stretchable Electronics. *Science* 327: 1603–1607 (2010).

Schoonman J, Nanostructured materials in solid state ionics. *Solid State Ionics* 135: 5–19 (2000).

Schweizer TM, Electrical characterization and investigation of the piezoresistive effect of PEDOT: PSS thin films. MSc Thesis, Georgia Institute of Technology (2005).

Someya T, Stretchable Electronics. ISBN 978-3-527-32978-6-Wiley-VCH, Weinheim.

Tait JG, Worfolk BJ, Maloney SA, Hauger TC, Elias AL, Buriak JM and Harris KD, Spray coated high-conductivity PEDOT:PSS transparent electrodes for stretchable and mechanically-robust organic solar cells. *Solar Energy Materials and Solar Cells* 110: 98–106 (2013).

Tokuno T, Nogi M, Jiu J and Suganuma K, Hybrid transparent electrodes of silver nanowires and carbon nanotubes : a low-temperature solution process. *Nanoscale Research Letters* 7: 281 (2012).

Trifigny N, Kelly FM, Cochrane C, Boussu F, Koncar V and Soulat D, 2013. PEDOT:PSS-Based Piezo-Resistive Sensors Applied to Reinforcement Glass Fibres for in Situ Measurement during the Composite Material Weaving Process. *Sensors* 13: 10749–10764 (2013).

Vickers JA, Caulum MM and Henry CS Generation of Hydrophilic Poly(dimethylsiloxane) for High-Performance Microchip Electrophoresis. *Analytical chemistry* 78(21): 7446–7452 (2006).

Wang S, Li M, Wu J, Kim DH, Lu N, Su Y, Kang Z, Huang Y and Rogers JA, Mechanics of Epidermal Electronics. *Journal of Applied Mechanics* 79: 031022 (2012).

Wei K and Zhao Y, Fast and Versatile Fabrication of PDMS Nano Wrinkling Structures. In 16th International Conference on Miniaturized Systems for Chemistry and Life Sciences: 665–667 (2012).

White MS, Kaltenbrunner M, Glowacki ED, Gutnichenko K, Kettlgruber G, Graz I, Aazou S, Ulbricht C, Egbe DAM, Miron MC, Major Z, Scharber MC, Sekitani T, Someya T, Bauer S and Sariciftci NS, Ultrathin, highly flexible and stretchable PLEDs. *Nature Photonics* 7: 811–816 (2013).

Wu H, Kustra S, Gates EM and Bettinger CJ, Topographic substrates as strain relief features in stretchable organic thin film transistors. *Organic Electronics* 14: 1636–1642 (2013).

Xiang Y, Chen X and Vlassak JJ, The plane-strain bulge test for thin films. *Journal of Materials Research* 20(9): 2360–2370 (2005).

Xu S, Zhang Y, Cho J, Lee J, Huang X, Jia L, Fan JA, Su Y, Su J, Zhang H, Cheng H, Lu B, Yu C, Chuang C, Kim T, Song T, Shigeta K, Kang S, Dagdeviren C, Petrov I, Braun PV, Huang Y, Paik U and Rogers JA, Stretchable batteries with self-similar serpentine interconnects and integrated wireless recharging systems. *Nature communications* 4: 1543 (2013).

Xu W, Yang JS and Lu TJ, Ductility of thin copper films on rough polymer substrates. *Materials and Design* 32: 154–161 (2011).

Yan C, Cho JH and Ahn JH, Graphene-based flexible and stretchable thin film transistors. *Nanoscale* 4: 4870–4882 (2012).